A Study of Two Problems in Nonlinear Dynamics Using the Method of Multiple Scales

A Thesis
Submitted For the Degree of
Doctor of Philosophy
in the Faculty of Engineering

by

Basireddy Sandeep Reddy

Department of Mechanical Engineering
Indian Institute of Science
BANGALORE – 560 012

August 2015

DEDICATED TO

my wife Anusha, brother Siddharth, parents

and

all my friends

CERTIFICATE

I hereby certify that the content embodied in this thesis titled **A Study of Two Problems in Nonlinear Dynamics Using the Method of Multiple Scales** has been carried out by *Mr. Basireddy Sandeep Reddy* at the Indian Institute of Science, Bangalore under my supervision and that it has not been submitted elsewhere for the award of any degree or diploma.

Ashitava Ghosal
Research Supervisor
Professor, Department of Mechanical Engineering, IISc Bangalore

DECLARATION

I hereby declare that the content embodied in this thesis titled **A Study of Two Problems in Nonlinear Dynamics Using the Method of Multiple Scales** is the research carried out by me in the Department of Mechanical Engineering, Indian Institute of Science, Bangalore, India, under the supervision of Prof. Ashitava Ghosal, Department of Mechanical Engineering, IISc. In keeping with the general practice in reporting scientific observations, due acknowledgment has been made wherever the work described is based on the findings of other investigations.

Basireddy Sandeep Reddy

Acknowledgements

I would first like to express my deepest gratitude to the Department of Mechanical Engineering, Indian Institute of Science for all the help during this research work. I would like to acknowledge and thank my advisor Prof. Ashitava Ghosal for his guidance, help and encouragement. His technical expertise in the field of nonlinear dynamics and robotics has helped me through critical junctures throughout the period of my research work. I also would like to thank Prof. Ghosal for making available high performance computing and other facilities in the lab which has enabled me to complete this research work much faster than it would have taken otherwise. I would like to thank my lab mates, Ashith, Midhun, Aditya, Bharat, Ravi Teja, Puneet, Ashwin, Anirudh for their support.

Abstract

This thesis deals with the study of two problems in the area of nonlinear dynamics using the method of multiple scales. Accordingly, it consists of two parts.

In the first part of the thesis, we explore the asymptotic stability of a planar two-degree-of-freedom robot with two rotary (R) joints following a desired trajectory under feedback control. Although such robots have been extensively studied and there exists stability and other results for position control, there are no analytical results for asymptotic stability when the end of the robot or its joints are made to follow a time dependent trajectory. The nonlinear dynamics of a 2R planar robot, under a proportional plus derivative (PD) and a model based computed torque control, is studied. The method of multiple scales is applied to the two nonlinear second-order ordinary differential equations which describes the dynamics of the feedback controlled 2R robot. Amplitude modulation equations, as a set of four first-order equations, are derived. At a fixed point, the Routh-Hurwitz criterion is used to obtain positive values of proportional and derivative gains at which the controller is asymptotically stable or indeterminate. For the model based control, a parameter representing model mismatch is incorporated and again controller gains are obtained, for a chosen mismatch parameter value, where the controller results in asymptotic stability or is indeterminate. From numerical simulations with gain values in the indeterminate region, it is shown that for some values and ranges of the gains, the nonlinear dynamical equations are chaotic and hence the 2R robot cannot follow the desired trajectory and be asymptotically stable.

The second part of the thesis deals with the study of the nonlinear dynamics of a rotating flexible link, modeled as a one dimensional beam, undergoing large deformation and with geometric nonlinearities. The partial differential equation of motion is discretized using a finite element approach to yield four nonlinear, non-autonomous and coupled ordinary

differential equations. The equations are non-dimensionalized using two characteristic velocities – the speed of sound in the material and a speed associated with the transverse bending vibration of the beam. The method of multiple scales is used to perform a detailed study of the system. A set of four autonomous equations of the first-order are derived considering primary resonance of the external excitation with one of the natural frequencies of the model and one-to-one internal resonance between two different natural frequencies of the model. Numerical simulations show that for certain ranges of values of these characteristic velocities, the slow flow equations can exhibit chaotic motions. The numerical simulations and the results are related to a rotating wind turbine blade and the approach can be used for the study of the nonlinear dynamics of a single link flexible manipulator.

The second part of the thesis also deals with the synchronization of chaos in the equations of motion of the flexible beam. A nonlinear control scheme via active nonlinear control and Lyapunov stability theory is proposed to synchronize the chaotic system. The proposed controller ensures that the error between the controlled and the original system asymptotically go to zero. A numerical example using parameters of a rotating power generating wind turbine blade is used to illustrate the theoretical approach.

Contents

List of Tables

List of Figures

Chapter 1

Introduction

Calling the subject "nonlinear dynamics" is like calling zoology nonelephant studies –
Stanislaus Ulam

This thesis deals with the study of two problems in the area of nonlinear dynamics. The common theme in both the problems is that they involve equations of motion, which for particular values of parameters of the physical system lead to chaos. In the first problem, we deal with a planar two-degree-of-freedom robot, moving on a horizontal plane under feedback control and modeled by nonlinear ordinary differential equations (ODEs). We identify regions and values of controller gains where the motion is not asymptotically stable and the robot equations can exhibit chaos. For such gains the robot is not asymptotically stable for trajectory following task and these results gives us more insight into unsolved problem of trajectory following and robustness of feedback control of nonlinear robots. In the second problem, a rotating flexible link, modeled as a beam undergoing large deformation and with geometric nonlinearities is studied. The partial differential equation of the rotating beam is discretized using a finite element method and parameter values are identified for which the nonlinear ordinary equations exhibit chaos. In the last part of the thesis, a control method to synchronize the chaotic oscillations of the rotating flexible link is presented.

The two problems mentioned above are studied using the method of multiple scales (MMS). There exists significant amount of literature on use of MMS for two- and three-dimensional nonlinear dynamical systems. The literature on nonlinear systems modeled with four ODEs are less and in this work, we present use of MMS on such systems.

Extensive numerical simulations have been performed to illustrate the theory developed and some of the analytical conditions developed in this thesis.

As this thesis deals with chaotic systems, we begin this Chapter with a brief introduction to chaotic systems and the tools that are used to identify chaos. Then we present in brief the classical method of multiple scales and give a brief description of both the problems with a review of existing literature on these problems. We end this Chapter with the contributions of this work and an outline of the thesis.

1.1 Chaotic Systems

Chaos is described as complex behavior of seemingly simple deterministic systems where the time evolution of such system are sensitive to small changes in the initial conditions and parameter values. Initially nearby trajectories deviate considerably with time and this makes future prediction of the system impossible. A key element in all chaotic systems is nonlinearity and chaos is exhibited only by nonlinear systems.

Almost all natural systems are nonlinear and chaos has been observed in systems ranging from chemical, biological, mechanical, electrical, communication and is thought to exist even in economic and financial systems [1–7]. Mathematical models of nonlinear systems in the form of ordinary, partial differential equations or iterative maps contain nonlinear terms and many of them exhibit chaos. In mechanical systems, among others, the nonlinearities arise from Coriolis, centripetal and gravity terms in equations of motion of a multi-body system, nonlinear constitutive stress-strain relationships in deformable objects, various kinds of friction between contacting bodies and large deformations in flexible objects modeled as beams, plates and shells [8–15]. In this thesis, we look at two kinds of nonlinearities. The planar two-degree-of-freedom robot contains nonlinear Coriolis and centripetal term in its equation of motion and, in addition, it contains nonlinear terms arising out of the use of model-based control for trajectory following. In the second problem of the rotating flexible link, the nonlinearity comes from large deformation which leads to a nonlinear stiffness term in the ordinary differential equations used to model the system.

Perhaps the most well-known nonlinear system which exhibits chaos is the second-order Duffing's equation [16] with a cubic stiffness term. The Duffing's equation is given by

$$\ddot{x} + \gamma\dot{x} + k_0 x + k_1 x^3 = f\sin(\Omega t) \tag{1.1}$$

where t denotes time and is the independent variable, x is the dependent variable, γ is the damping co-efficient, $k_0 x + k_1 x^3$ represents the cubic stiffness, and f, Ω are the amplitude and frequency of the external forcing, respectively.

The above equation is a second-order nonlinear ordinary differential equation which is known to exhibit chaos for certain range of γ and for certain values of Ω and f. To analyze the system, the second-order equation is written as two first-order ODE's and numerically simulated. For chosen values, $k_0 = -0.5$, $k_1 = 0.5$, $\gamma = 0.1$, $f = 0.24$ and $\Omega = 1$, the equation (1.1) was simulated in Matlab *R2012b* [17] and $x(t)$ as a function of t was obtained. Figure 1.1 shows the plot of $x(t)$ with respect to time for two initial conditions. The blue (solid) line represents the plot of $x(t)$ for initial condition $(0, 0)$, while the green (dotted) line represents the plot of $x(t)$ for the initial condition $(0, 0.01)$. As it can be seen that the two trajectories, although very close initially, diverge significantly with time. This sensitivity to initial conditions is the well known characteristic of chaos.

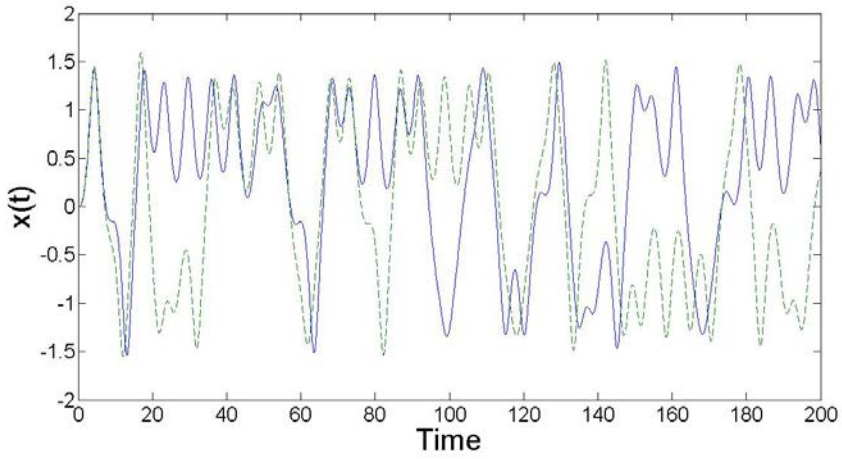

Figure 1.1: Time response of the Duffing's equation when simulated with two initial conditions $(0, 0)$ and $(0, 0.01)$

There exists several other examples of two first-order ODEs which exhibit chaos –

some of the well-known ones are the Brusselator [18], Van-der pol's equation [19] and the Morse oscillator [20]. Chaos was also shown in a two-dimensional system, obtained after reduction of variables from a three-dimensional system [21]. There are also examples of chaos found in three dimensional systems, the most well known of which are – the Rossler system [22], the Chua circuit [23] and the three dimensional Volterra equations [24]. Another very well-known system of equations which exhibits chaos is the set of three first-order ODEs known as the Lorenz system [25]. The system is given by

$$\begin{aligned} \dot{x} &= \sigma(y - x) \\ \dot{y} &= x(r - z) - y \\ \dot{z} &= xy - bz \end{aligned} \tag{1.2}$$

where x, y, z are the state variables of the system and σ, r, b are constant system parameters. The above system given by equations (1.2) are dissipative in nature and can be verified geometrically, i.e., the rate of change of the volume enclosed by the system (x, y, z) is related to the divergence of the vector field of the flow (see for example, reference [26], page 216). We can observe this by considering the divergence of the vector field V given by equation (1.2) as

$$\mathrm{div}(V) = \frac{\partial}{\partial x}(\dot{x}) + \frac{\partial}{\partial y}(\dot{y}) + \frac{\partial}{\partial z}(\dot{z}) = -(\sigma + b + 1) \tag{1.3}$$

If $\sigma + b + 1 > 0$, then $div\ (V) < 0$ and the system is dissipative. In a dissipative system, the trajectories settles down to a region in state space known as an attractor. This type of attractor is known as a strange attractor. It maybe mentioned that the size and location of the attractor is sensitive to initial conditions. In the case of the Lorenz system, for particular values of system parameters, $\sigma = 10$, $b = 8/3$, $r = 28$, the equations show chaotic behavior. A detailed examination of the Lorenz system is given in reference [27].

Chaos exists in two- and three-dimensional systems and many studies exist in literature, as indicated above, that demonstrate the phenomenon. There are, however, very few studies which deal with four or more first-order ODEs. One well known study is that of strange attractors in the four-dimensional Volterra equations for more than three competing species [28]. The Hopf bifurcations in the Volterra equations were also

shown to undergo successive period-doubling cascades [29]. In another study, dynamical properties of orbits of a four-dimensional nonlinear circuit were observed on an oscilloscope [30]. Numerical analysis of the system also showed chaos. A system consisting of a second-order lag element and two first-order lag elements with piecewise linear static feedback were shown to exhibit chaotic behavior [31].

Tests for Chaos

The core features of a chaotic systems are

- Boundedness in state space,
- Aperiodicity, and
- Determinism, but sensitive dependence on initial conditions.

To determine if a system is chaotic or not is based on the above mentioned features. The tools that are used are the well-known time series data, phase plots, bifurcation plots, Poincaré maps and Lyapunov exponents. The algorithms for computing all the tools mentioned for analyzing chaos are well-known and are available in standard references (see, for example, [32]).

We can numerically verify that the system is bounded in state space by examining whether the output of the system is enclosed within finite limits. This can be done by considering the phase plots which are plots of the various state variables with respect to one another. For example, in the Duffing's system given by equation (1.1), the phase plot of $\dot{x}$ versus x, for the values used to obtain the time series plots in figure 1.1, is shown in figure 1.2. It can be seen that both the state variables, $\dot{x}$ and x, are bounded.

The periodic (or aperiodic) nature of a system can be ascertained in two ways. One well-known way is to compute what is known as a Poincaré map [32]. For the flow of any system[1] $\underline{x}(t)$, the first step is to construct a surface S (also known as Poincaré surface) as shown schematically in figure 1.3. Next, the points at which the flow of the system intersects the surface are computed (points P_0, P_1... in figure 1.3). Periodicity requires that the flow intersects the Poincaré surface S repeatedly at the same point. If the flow

[1]The flow of a system is defined as as the time evolution of the state $\underline{x}$ with respect to time.

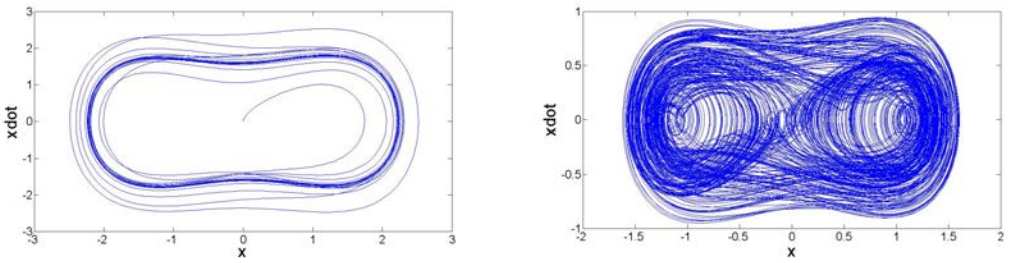

Figure 1.2: Phase plots for the Duffing's system – (a) $f = 0.5$ – non-chaotic, (b) $f = 0.24$ – chaotic

intersects the surface S at the same point, i.e., there will be only one point P_0 on the Poincaré map at which the flow intersects repeatedly, then the system is periodic with period one. If it intersects the surface S at two points, it is periodic with period two and so on. If the flow intersects the surface S at altogether different points, then it implies that it is aperiodic. Thus, the Poincaré map converts a continuous time system into a discrete map $P_{n+1} = f_p(P_n)$, explaining the periodic (or aperiodic) nature of the flow. It also reduces the state space dimension of the flow by one. The Poincaré map for the Duffing's system is shown in figure 1.4.

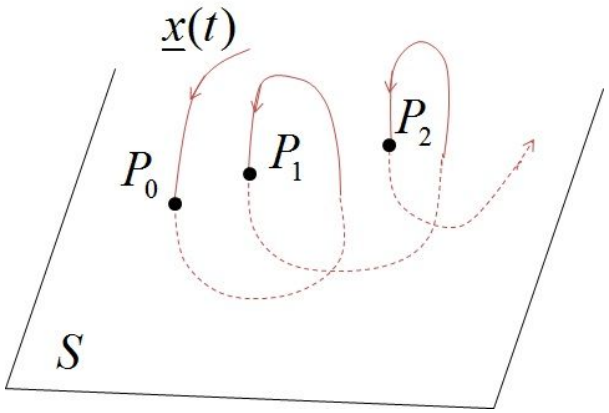

Figure 1.3: Poincaré surface cutting the state space orbits giving a discrete map $P_{n+1} = f_p(P_n)$

Another way of computing the aperiodic nature of any nonlinear system is to compute what are known as bifurcation plots. For particular values of any system parameter, the system shows periodic behavior, i.e., it oscillates around n points in state space (period n). For some particular value of system parameter, the system may begin to oscillate around a greater number of points, i.e., it's period increases. If the increase in the period of the system happens continuously, the system will eventually have a period of infinity

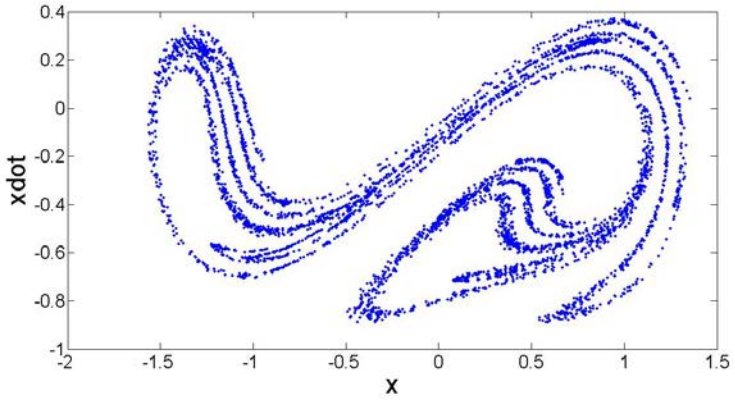

Figure 1.4: Poincaré map for the Duffing's equation at $k_0 = -0.5$, $k_1 = 0.5$, $\gamma = 0.1$, $f = 0.24$ and $\Omega = 1$

- it becomes aperiodic. The bifurcation plot shows an increase in the period by period-doubling cascades, until the system becomes aperiodic, implying chaos. A method for computing bifurcation values is given by Tsumoto et al. [33]. The bifurcation plot of the Duffing's equation is shown in figure 1.5.

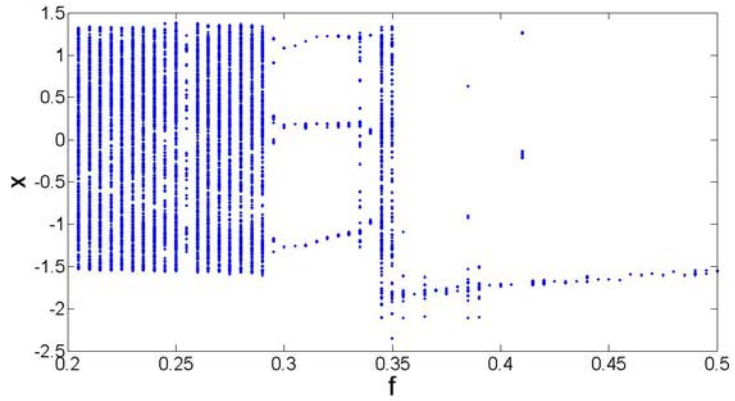

Figure 1.5: Bifurcation plot for the Duffing's equation at $k_0 = -0.5$, $k_1 = 0.5$, $\gamma = 0.1$ and $\Omega = 1$

The most definitive way of verifying chaos is to determine it's sensitivity to initial conditions. A measure of sensitivity to initial conditions lies in measuring the divergence of trajectories for two initial conditions a small distance apart. For this end, plots of time series data are used. As shown in figure 1.1, the same Duffing's system when simulated with two different initial conditions very close to each other, the behaviors diverge

radically. The divergence of trajectories is quantified by computing the well-known Lyapunov exponents [34]. The concept of Lyapunov exponent is described by figure 1.6.

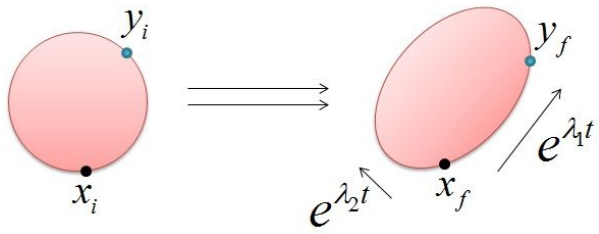

Figure 1.6: A measure of the average rate of divergence of neighboring trajectories

Consider two trajectories starting at two initial conditions x_i and y_i inside of an n dimensional sphere (n equals the dimensions in state space of the system). After a period of time the trajectories end up as x_f and y_f. The distance between the two trajectories can be measured by the alteration of the sphere along n dimensions in state space. The rate of divergence along the i^{th} dimension is given by λ_i (as shown in figure 1.6), where λ_i is called the Lyapunov exponent. For chaos to occur, there must be divergence along at least one dimension in state space, and hence there must be at least one positive Lyapunov exponent. For the Duffing's system, the spectra of Lyapunov exponents is shown in figure 1.7. As one of the exponents is positive at $f = 0.24$, the Duffing's system is chaotic at $f = 0.24$.

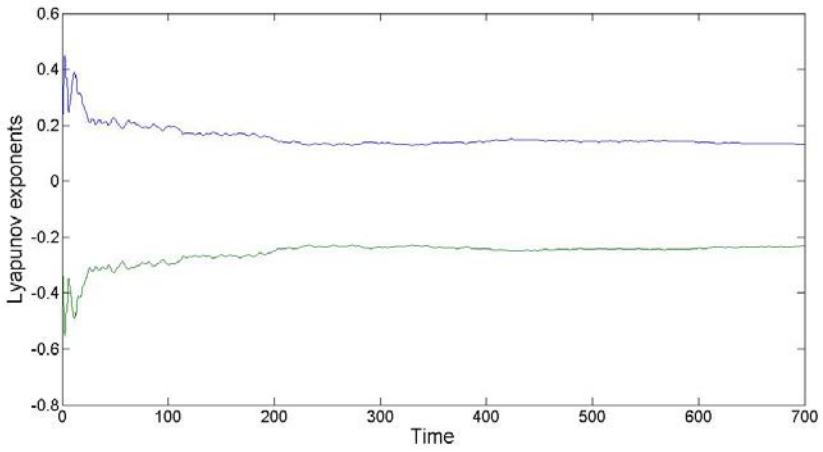

Figure 1.7: Spectra of Lyapunov exponents for the Duffing's system at $f = 0.24$

In this thesis, we use Lyapunov exponents, phase plots and Poincaré maps for analyzing chaos. The algorithms for computing the above mentioned tools are available in reference [32]. We use MATLAB *R*2012*b* [17] for numerical simulation of the Lyapunov exponents and other diagnostic tools for chaos.

1.2 Method of Multiple Scales

The method of multiple scales (MMS) is a singular perturbation method used to study systems involving distinct phenomena at different time scales [35, 36]. We again use the Duffing's system described above to illustrate MMS, it's relevance for this work and our motivation for using it – details about MMS is available in several textbooks (see, for example, [38]).

We start by re-writing the Duffing's equation in the form

$$\ddot{x} + \epsilon\gamma\dot{x} + k_0 x + \epsilon k_1 x^3 = \epsilon f \sin(\Omega t) \tag{1.4}$$

where the description of all the terms in equation (1.4) are given in section 1.1 below equation (1.1). In the above equation, there are two phenomena operating at different time scales. The inertial effect given by $\ddot{x}$ operates at a faster time scale, while the damping effect given by $\gamma\dot{x}$ operates at a slower time scale. To study both phenomena at different time scales, we order the equation (1.4) at different orders of time scale ϵ (as shown), where the time scales are defined as $T_0 = t$, $T_1 = \epsilon t$. The inertial effects operate at faster time scale T_0, whereas the damping and forcing effects operate at slower time scale T_1. The derivatives are treated as

$$\frac{d}{dt} = D_0 + \epsilon D_1 + ..., \qquad \frac{d^2}{dt^2} = D_0^2 + \epsilon(2D_0D_1 + D_1^2) + ... \tag{1.5}$$

where D_0 and D_1 are derivatives with respect to time scales T_0 and T_1 respectively. The solution to the equation (1.4) is expanded in a power series of ϵ as

$$X(T_0, T_1) = X_0(T_0, T_1) + \epsilon X_1(T_0, T_1) + ... \tag{1.6}$$

where X_0 and X_1 are first-order or $O(1)$ quantities.

Now we substitute equations (1.5, 1.6) into equation (1.4) and compute the solution $X(T_0, T_1)$ by equating the terms in equation (1.4) at different orders of ϵ.

Order ϵ^0

$$D_0^2 X_0 + k_0 X_0 = 0 \tag{1.7}$$

where the dependencies of X_0 on the independent variables is suppressed.

The solution to equation (1.7) is given by

$$X_0(T_0, T_1) = A(T_1)e^{i\omega T_0} + \bar{A}(T_1)e^{-i\omega T_0} \tag{1.8}$$

where A is the amplitude and ω is the natural frequency of oscillations, respectively. At the first-order of ϵ, using equation (1.8), we have

Order ϵ

$$\begin{aligned} D_0^2 X_1 + k_0 X_1 &= -2D_0 D_1 X_0 - \gamma D_0 X_0 - k_1 X_0^3 + f\frac{(e^{i\Omega T_0} - e^{-i\Omega T_0})}{2i} \\ &= \left(-2A'(i\omega) - \gamma A(i\omega) - 3k_1 A^2 \bar{A}\right) e^{i\omega T_0} - if\frac{e^{i\Omega T_0} - e^{-i\Omega T_0}}{2} + c.c. + N.S.T. \end{aligned} \tag{1.9}$$

where *c.c.* and *N.S.T.* stand for complex conjugate and non-secular terms, respectively.

It can be observed from equation (1.9), that the homogeneous part has a solution proportional to $e^{i\omega T_0}$. If the non-homogeneous part of equation (1.9) also has a term proportional to $e^{i\omega T_0}$, then it gives rise to *terms* in the solution X_1 which make it unbounded. Boundedness, in this context, implies that the solution of equation (1.4) is within finite limits. These terms (proportional to $e^{i\omega T_0}$) are called *secular terms*. In order to keep the solution bounded, and hence stable, these terms have to be eliminated.

In equation (1.9), it can be observed that the non-homogeneous part does have terms proportional to $e^{i\omega T_0}$ and hence, they must be eliminated by equating these terms to zero. Further it can also be observed that if the forcing frequency $\Omega = \omega$, then resonance

occurs and even the forcing terms on the right-hand side become proportional to $e^{i\omega T_0}$, and again it gives rise to secular terms in the solution. To address the issue of resonance, we introduce what is known as a detuning parameter

$$\Omega = \omega + \epsilon\sigma \tag{1.10}$$

Substituting equation (1.10) into equation (1.9), we get

$$D_0^2 X_1 + k_0 X_1 = \left(-2A'(i\omega) - \gamma A(i\omega) - 3k_1 A^2 \bar{A} - i\frac{f}{2} e^{i\sigma T_1} \right) e^{i\omega T_0} + c.c. + N.S.T. \tag{1.11}$$

Equating the terms in the above equation (1.11) which are proportional to $e^{i\omega T_0}$ to zero, we have

$$-2A'(i\omega) - \gamma A(i\omega) - 3k_1 A^2 \bar{A} - i\frac{f}{2} e^{i\sigma T_1} = 0 \tag{1.12}$$

If equation (1.12) is not satisfied, then the solution X_1 is not bounded. Rewriting in polar co-ordinates $A = ae^{ib}$, we have

$$a' = -\frac{1}{2}\gamma a - \frac{F}{4\omega}\cos(\gamma), \quad b' = \frac{3k_1}{2\omega}a^2 - \frac{1}{a}\frac{F}{4\omega}\sin(\gamma), \quad \gamma = \sigma T_1 - b \tag{1.13}$$

Transforming the above equation using Cartesian co-ordinates $x = A\cos(\gamma)$, $y = A\sin(\gamma)$, we have

$$\begin{aligned} x' &= -\frac{1}{2}\gamma x - y\left(\sigma - \frac{3k_1}{2\omega}(x^2 + y^2)\right) - \frac{F}{4\omega} \\ y' &= -\frac{1}{2}\gamma y + x\left(\sigma - \frac{3k_1}{2\omega}(x^2 + y^2)\right) \end{aligned} \tag{1.14}$$

Equations (1.14) are known as the slow flow equations (also known as solvability conditions). The significance of these equations is that in the absence of their satisfaction, the solution to the Duffing's system cannot be bounded. The central idea in the application of the MMS is the computation of slow flow equations to ensure boundedness of solutions. An analysis of the slow flow equations reveal how different system parameters (in this case k_0, k_1, γ ,σ, f) affect the nature of the final solution $X_0(T_0, T_1)$ of the original equation (1.4). In this thesis, we use the MMS to study two systems, namely the 2R planar robot and a flexible rotating beam and derive slow flow equations for

each. We then analyze the slow equations to study how given system parameters affect the original system of equations of the 2R planar robot and the flexible beam respectively.

A vast amount of literature exists on the application of MMS. In the book by Nayfeh and Mook [38], the authors use MMS to address several problems related to the topic of vibrations, which include free, forced, parametrically excited vibrations of single and multi-degree-of-freedom systems as well as continuous systems. In a review article, Cartmell et al. [39] discuss the applicability of MMS to weakly nonlinear dynamical systems. The authors discuss the aspects of MMS such as non-dimensionalization, time scaling, inclusion and exclusion of higher-order nonlinearities, and problems in handling secular terms.

El-Bassiouny [40] uses MMS to show that when a nonlinear system (with cubic, quartic and quintic nonlinearities) is subject to excitation centered at a frequency higher than its own natural frequency, the system averages the excitation. Cao et al. [41] describe how MMS can be used to transform a parametrically and externally excited string-beam coupled system into a averaged equation to study it's global bifurcations and chaotic dynamics. Jinchen et al. [42] study the nonlinear response of a two-degree-of-freedom nonlinear oscillating system to parametric excitation, by using MMS to derive four first-order autonomous ODEs describing the modulation of the amplitudes and phases. Apart from the above mentioned works, there are several review articles on the applications of MMS in the areas of machining dynamics [43], rotordynamics [44, 45], delayed systems [46, 47], strong nonlinear oscillations [48, 49] and fractional-order systems [50].

Most of the above mentioned works deal with two and three first-order ODEs. There are very few works dealing four or more first-order ODEs. Some of the well-known studies involving four ODEs are Nayfeh et al. [51] where the motions near the Hopf bifurcations of a non-conservative four dimensional autonomous system were studied. Using the method of multiple scales [35], the Hopf bifurcation problem was reduced to two differential equations for the amplitude and phase of the bifurcating cyclic solutions, and the stability of constant solutions to those equations determined the nature of bifurcation. In the work by Kumawat et al. [52], a parametric study of reduced order model of boiling water reactors, modeled by four first-order differential equations, has been performed by using the multiple scales method, and the authors report sub-critical

bifurcations at a particular value of fuel temperature. However, with a decrease in the fuel temperature coefficient of reactivity the bifurcation turns to supercritical implying global stability of the steady state operation in the linear stability regime.

One of the reasons why systems involving four ODEs may not have been studied is because of multiple ways in which resonance (internal or external) would happen. In the Duffing's system, with a single second-order ODE (equation (1.4)), the application of MMS lead to equation (1.9) in which we have only one natural frequency and one external forcing frequency. Hence, there is only one possible resonance between the single natural frequency and the single forcing frequency (as shown in equation (1.10)) and we get two first-order ODEs (slow flow equations given by equation (1.14)). However, if the original system had two or more second-order ODEs (the 2R planar robot described in section 1.3 being one such example), with more than one forcing frequency, then we could have multiple natural frequencies with multiple forcing frequencies. In such cases, one can get multiple possible resonance conditions leading to four or more first-order ODEs. Analysing four and more ODEs is significantly more difficult than simple system of two ODEs.

In this thesis both the 2R planar robot and the flexible rotating beam yield slow flow equations as four first-order ODEs.

1.3 Problems Studied in the Thesis

In this thesis, we have used the method of multiple scales to study two problems. In this section, we state and discuss the two problems studied.

1.3.1 Asymptotic Stability of a Feedback Controlled 2R Planar Robot

Figure 1.8 shows the schematic of a two-degree-of-freedom planar robot. It consists of two rotary (R) joints actuated by two DC servo motors which can generate torques Γ_1 and Γ_2 respectively. The tip of the robot, point (x, y), traces a trajectory as the R joints are rotated and this trajectory is a function of time. The equations of motion of the 2R

planar robot are available in standard textbooks on robotics (see, for example, [53]). They are a set of two nonlinear ODEs of the form

$$[I_1 + I_2 + m_2 l_1^2 + m_1 r_1^2 + 2m_2 l_1 r_2 \cos(\theta_2)]\ddot{\theta}_1 + [m_2 r_2^2 + I_2 + m_2 l_1 r_2 \cos(\theta_2)]\ddot{\theta}_2$$
$$- m_2 l_1 r_2 \sin(\theta_2)[2\dot{\theta}_1 + \dot{\theta}_2]\dot{\theta}_2 = \Gamma_1 \tag{1.15}$$
$$[m_2 r_2^2 + I_2 + m_2 l_1 r_2 \cos(\theta_2)]\ddot{\theta}_1 + [m_2 r_2^2 + I_2]\ddot{\theta}_2 + m_2 l_1 r_2 \sin(\theta_2)\dot{\theta}_1^2 = \Gamma_2 \tag{1.16}$$

which is often written in a compact form (using matrices) as

$$[M(\Theta)]\ddot{\Theta} + [C(\Theta, \dot{\Theta})] = \Gamma$$

In the above equations, m_j, l_j, I_j, r_j $(j = 1, 2)$ are the masses, lengths, inertia and position of center of mass of link j respectively. The matrix $[M]$ is the well-known mass matrix (in this case of dimension 2×2) and $[C]$ is the 2×1 vector of centripetal and Coriolis terms. The symbol Θ denotes the vector of joint angles (θ_1, θ_2) and Γ is the 2×1 vector of joint torques (Γ_1, Γ_2). To trace a desired trajectory, feedback control is used. A typical robot controller implementing a proportional plus derivative (PD) control scheme is given by

$$\Gamma_1 = \ddot{\theta}_{d_1} + K_{v_1}\dot{e}_1 + K_{p_1}e_1$$
$$\Gamma_2 = \ddot{\theta}_{d_2} + K_{v_2}\dot{e}_2 + K_{p_2}e_2 \tag{1.17}$$

where K_{p_i} and K_{v_i} are the controller gains, $e_i = \theta_{d_i}$ - θ_i is the servo error, $\dot{e}_i$ is the derivative of the servo error and θ_{d_i} is the desired trajectory to be traced.

Asymptotic stability, in this context, implies that the state trajectory of the robot given by solving equation (1.15) tracks the desired trajectory, i.e. e_i as defined above tends to zero. The PD control scheme has been proven to be asymptotically stable for any positive derivative gain ($K_{v_i} > 0$) when the first and the second derivative of the desired trajectory are equal to zero [54], i.e., for set point control ($\dot{\theta}_d = \ddot{\theta}_d = 0$). For the case of trajectory following with $\dot{\theta}_d \neq \ddot{\theta}_d \neq 0$, there exist numerical studies where the ranges of proportional and derivative gains for which the system is chaotic [55, 56] has been obtained, and for these values of gains, the planar 2R robot does not track the desired trajectory and is thus asymptotically stable. To the best of our knowledge, there are no theoretical development related to asymptotic stability during trajectory following. In

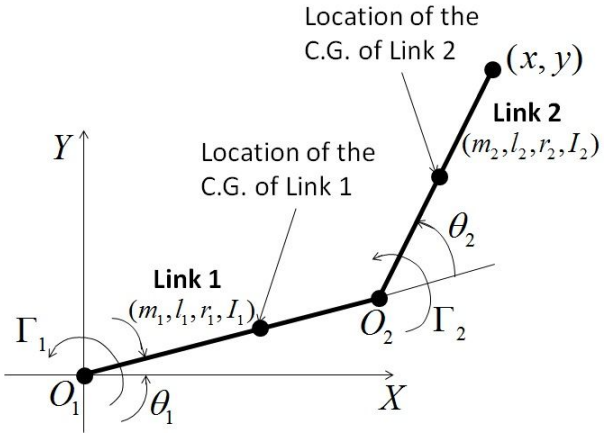

Figure 1.8: A 2R planar robot

Chapter 2, we propose an analytical approach to derive the ranges of proportional and derivative gains for which the PD controlled 2R planar robot is asymptotically stable. Since the equations of motion of the PD controlled 2R planar robot are non-autonomous (due to the time dependent forcing terms on the right-hand side of the equations for trajectory tracking), there will be no fixed point to the entire system. Hence, we use the method of multiple scales (MMS) to convert these equations into autonomous equations (slow flow equations), to evaluate fixed points and find the stability around those fixed points.

After non-dimensionalizing equation (1.15), a procedure described in Chapter 3, we apply the method of multiple scales, and derive the slow flow equations, as a set of four first-order equations. These equations are known as the solvability conditions, i.e., the conditions needed to be satisfied for the equation to have a bounded solution. We then compute the fixed points of those equations. At one particular fixed point, we use the Routh-Hurwitz criterion [57,58] to obtain the values of proportional and derivative gains at which the controller is asymptotically stable or indeterminate. We show that for certain values of gains, some of the indeterminate points in the (K_p, K_v) space are chaotic and hence the planar 2R robot is not asymptotically stable at these gain values.

Apart from the PD control scheme, a well-known robot control scheme uses the dynamic model of a robot [55]. This scheme is called the model-based or computed torque control scheme. In its realistic form, the knowledge of model parameters of the

robot are uncertain. We characterize the uncertainty in the model of the robot by a mismatch parameter e. The estimated mass matrix $\hat{M}(\Theta)$ and the estimated Coriolis and centripetal torques vector $\hat{C}(\Theta, \dot{\Theta})$ are computed by perturbing the robot parameters as

$$\hat{m}_i = (1+e)m_i, \quad \hat{r}_i = (1+e)r_i, \quad \hat{I}_i = (1+e)I_i, \quad \hat{l}_i = (1+e)l_i \tag{1.18}$$

where $e > 0$ implies an overestimated model and $e < 0$ implies an underestimated model. Since the mass cannot be negative $-1 < e < \infty$. The computed joint torque, also called feedback linearization, control scheme is given

$$\Gamma = [\hat{M}(\Theta)]\Gamma_p + [\hat{C}(\Theta, \dot{\Theta})] \tag{1.19}$$

where Γ_p is the servo portion of the control scheme as given by equation (1.17).

In this thesis, as with the PD control scheme, we study the effects of mismatch parameter e in the model-based control scheme at certain ranges of K_p and K_v on the asymptotic stability of the 2R planar robot. After applying MMS to derive the slow flow equations, we use the Routh-Hurwitz criterion to compute the values of proportional and derivative gains in (K_p, K_v) space at which the planar 2R robot is asymptotically stable. Chapter 2 deals with the study of asymptotic stability of planar 2R robot under feedback control.

1.3.2 Chaotic Dynamics of a Rotating Flexible Link

Figure 1.9 shows the schematic of a rotating flexible link undergoing large deformation. The flexible link is modeled as a beam with four generalized co-ordinates, one rigid and three flexible. The vector of flexible variables is given by $Q_f = (u_{2i}, v_{2i}, \phi_{2i})^T$ and the vector of rigid and flexible variables is given by $Q = (\theta_1, u_{2i}, v_{2i}, \phi_{2i})^T$. The partial differential equation of motion can be discretized using a finite element approach to yield four nonlinear, non-autonomous and coupled ordinary differential equations [59]. The equations can be non-dimensionalized using two characteristic velocities – the speed of sound in the material and a speed associated with the transverse bending vibration of

the beam [60]. The equations are given by

$$[\mathcal{M}(Q_f)]\ \{Q^{''}\} + \left(\mathcal{K} + \Delta\mathcal{K}(Q_f, \frac{U_a}{U_g})\right)\{Q\} + \mathcal{C}\{Q'\} + \{\mathcal{H}(Q, Q')\} = \frac{\{\tau\}}{\rho A L U_g^2} \tag{1.20}$$

where $(\cdot)', (\cdot)''$ represent the first and the second derivative with respect to non-dimensional time T, $\mathcal{M}$ is the 4×4 non-dimensional mass matrix, $\mathcal{K}$ and $\Delta\mathcal{K}$ are the 4×4 non-dimensional conventional and geometric stiffness matrices respectively, $\mathcal{H}$ is the 4×1 vector of non-dimensional centripetal and Coriolis terms, $\{\tau\} = [F\sin(\frac{\Omega L}{U_g}T), 0, 0, 0]^T$ with F and Ω denoting the amplitude and the frequency of forcing term respectively. In the above equation, $\mathcal{C}\{Q'\}$ represents an added Rayleigh damping term of the form $\alpha[\mathcal{M}] + \beta[\mathcal{K}]$, U_a is the speed of sound and U_g is a characteristic speed associated with bending vibration.

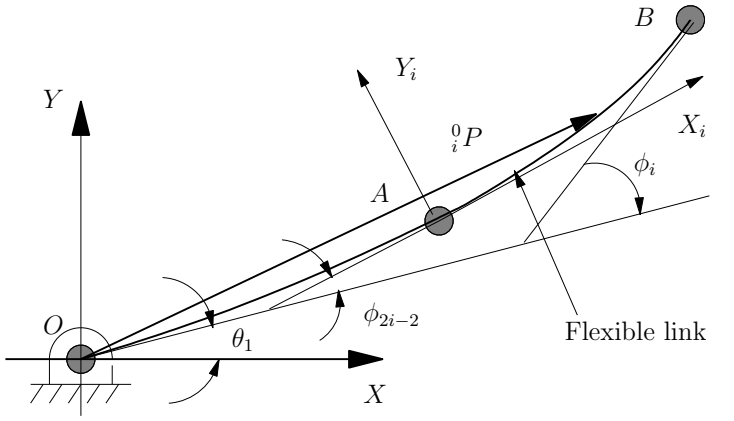

(a) Flexible rotating beam

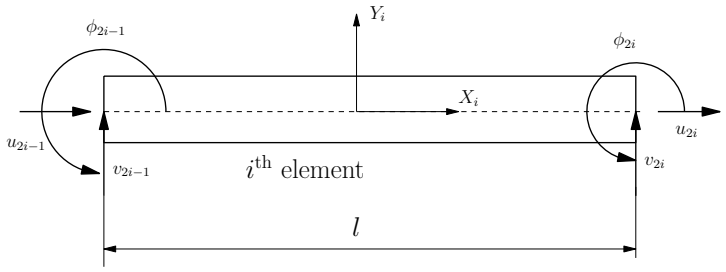

(b) Planar beam element

Figure 1.9: Schematic of a rotating flexible beam and an i^{th} element

The method of multiple scales is used to perform a detailed study of the above system. A set of four autonomous equations of the first-order are derived considering primary

resonances of the external excitation with one of the natural frequencies and one-to-one internal resonances between the natural frequencies of the equations. Numerical simulations show that for certain ranges of values of these characteristic velocities, the slow flow equations can exhibit chaos. The numerical simulations and the results are related to a rotating wind turbine blade and the approach can also be used for the study of the nonlinear dynamics of a single link flexible manipulator. The study of this problem of nonlinear dynamics of rotating flexible beam undergoing large deformation is the content of Chapter 3.

1.3.3 Synchronization of Chaos in a Rotating Flexible Link

Many natural systems are nonlinear and often exhibit chaos. Controlling chaos systems has thus received a significant amount of attention and many approaches [61–68] have been proposed. An approach of chaos control, called chaos synchronization, has received increased attention recently after the work of Pecora et al. [69, 70]. In chaos synchronization, a *drive-response* system is considered. A chaotic system with one given set of initial conditions is known as the drive system and another identical system with a different set of initial conditions is known as the response system. In the absence of a controller, the drive and response systems will diverge due to the property of sensitivity to initial conditions. The central idea of synchronization is to design a controller such that the response system asymptotically tracks the drive system.

A number of approaches have been proposed for synchronizing chaotic systems such as back-stepping design [71], adaptive control [72], and sliding mode control [73]. In this thesis, we use active nonlinear control and Lyapunov stability theory to design a controller for chaos synchronization. The example of a power generating wind turbine blade described in Chapter 3 is used to illustrate the theoretical development.

At the end of the studies of these problems, we present some conclusions and scope for extending this work in Chapter 5.

1.4 Contributions of the Thesis

This thesis deals with the study two problems in nonlinear dynamics using MMS. The main contributions of this thesis are as follows.

- In the study of the 2R planar robot, the lack of analytical criteria for asymptotic stability in trajectory tracking is highlighted. Two well-known controllers, namely a PD and a model-based controllers, are studied. A first and a partially successful attempt in developing an analytical procedure to derive the ranges of proportional and derivative gains (K_p and K_v), for both types of controllers, at which the 2R robot is asymptotically stable is presented.

- The chaotic motions in the equations of a damped and undamped flexible rotating beam, undergoing large deformation, are studied. The method of multiple scales is used to derive the slow flow equations of the rotating beam and nature of chaos is determined for the undamped and damped equations. Numerical simulation of the original nonlinear equations are presented which are consistent with the results obtained from the slow flow equations.

- The problem of negating the sensitivity to initial conditions in chaotic systems is addressed using the concept of chaos synchronization. A active nonlinear controller developed, using Lyapunov stability theory to synchronize the chaotic slow flow equations, is obtained for both the damped and the undamped rotating beam systems. Numerical results demonstrate the control of chaos for the rotating beam system.

Chapter 2

Asymptotic Stability of a Feedback Controlled 2R Planar Robot

The stability of dynamical systems is an important area of study in nonlinear dynamics. Stability is generally verified via the Lyapunov stability theory [74], where it is considered about an equilibrium point. There are generally two concepts of stability which are largely used when studying dynamical systems, namely simple/marginal stability and asymptotic stability. A stable equilibrium point is one where a trajectory of the system beginning in a small neighbourhood of that point stay in a larger bounded neighborhood of the equilibrium point. An equilibrium point is said to be asymptotically stable if in addition to being stable, the trajectories approach the equilibrium point as time tends to infinity. Asymptotic stability is a much stronger condition than simple stability. These concepts of stability are used in autonomous systems.

In addition to the above, in robotics typical tasks involve the robot tracking a desired trajectory which is generally dependent on time. In such cases, the system is no longer autonomous as it has a time dependent forcing input. In such cases, stability is measured with respect to the error between the desired trajectory and the system/state trajectory. If the error is bounded, yet doesn't go to zero, then the controller is said to be simply stable. However if the error, apart from being bounded, asymptotically goes to zero, then the controller is said to be asymptotically stable and the robot tracks the

desired trajectory. For a robot, controllers cannot simply stable, but must be asymptotically stable[1] and extensive research has been done to design and implement controllers and asymptotic stability of controllers has been demonstrated by numerical simulation. References [75, 76] demonstrate asymptotic stability of robot manipulators using PID control, whereas Jose and Wen [77] demonstrates asymptotic stability for a robot manipulator based on PD control. Asymptotic stability has also been shown for planar multi-link flexible manipulators [78] and for a robot manipulator using adaptive fuzzy control [79]. Asymptotic stability has also been demonstrated experimentally for PID control of robot manipulators [80,81], PD control of closed chain mechanical systems [82] and Lyapunov-based control of robot and mass-spring system undergoing an impact collision [83]. It has also been shown theoretically, using Lyapunov stability, that a robot is asymptotically stable when the desired velocity is zero (or set point control) [54] and for a trajectory with non-zero velocity and acceleration [84] when the controller gains are greater than zero.

In nonlinear dynamical systems, a phenomena called chaos exists (see Chapter 1). In chaos, the states and trajectories of the system are bounded. However, due to the sensitive dependence on initial conditions and for particular values of the parameters of the system, the trajectory of the nonlinear dynamical system diverge and becomes unpredictable in time. Chaos can also exist in a nonlinear robotic systems and there exist literature on chaos in robots [85–92]. In the presence of chaos, the state trajectory *does not* track the desired trajectory and the error between the state and the desired trajectory, although bounded, does not asymptotically go to zero. In such a case, the robot controller cannot be said to be asymptotically stable. In this Chapter, we study a simple 2R planar robot, under feedback control following a desired trajectory, and obtain values of controller gains for which the robot equations show chaos and asymptotic stability. Two well-known controllers, namely a proportional plus derivative and a model based computed torque controller are studied. Before studying the 2R planar robot, we give a brief and formal introduction to the concepts of stability. More details on the various definitions of stability are available in various textbooks (see, for example, [74]).

[1]The formal definitions of stability and asymptotic stability with respect to an equilibrium point as well as tracking are given in section 2.1.

2.1 Concepts of Stability

For linear systems, clear theoretical concepts and techniques to determine stability and instability exist. However, in a nonlinear system, the concept of stability is more complex. In the following, we define various concepts of stability for a nonlinear system of the form $\dot{x} = f(x)$, where $x(t) \subset \Re^n$. We have used the notations and definitions as given in Slotine and Li [74].

Definition 1: *Equilibrium Point* – A state X_e is said to be an equilibrium state (point) of a nonlinear system, $\dot{x} = f(x)$, if $f(X_e) = 0$.

Figure 2.1 schematically shows an equilibrium point X_e. Now consider two spheres of radius R and r around X_e.

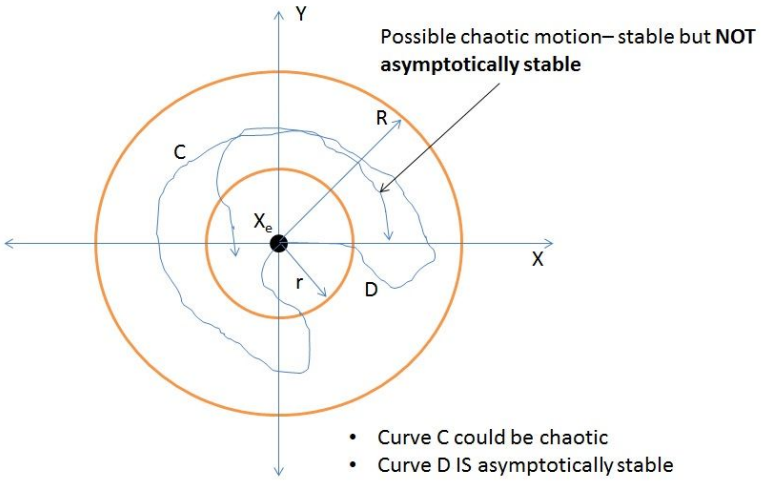

Figure 2.1: Concepts of stability and asymptotic stability

Definition 2: *Simple/Marginal Stability* – The equilibrium point X_e is said to be *simply stable* in the sense of Lyapunov if for any $R > 0$, there exists $r > 0$ such that if $||x(0)|| < r$, then $||x(t)|| < R$ for $t > 0$. Otherwise X_e is unstable.

Simple stability implies that if we perturb the initial conditions of the system in a small region around equilibrium point X_e given by the sphere of radius r, then the final state of the system will be *bounded* and will lie inside the sphere of radius R. However,

the system which is stable may not return to it's equilibrium point. If the trajectories return to its equilibrium point, then the system is said to be asymptotically stable. Formally,

Definition 3: The equilibrium point X_e is said to be *asymptotically stable* if it is stable, and if, in addition, there exists some $r > 0$ such that $||x(0)|| < r$ implies that $x(t) \longrightarrow X_e$ as $t \longrightarrow \infty$.

In a stable system, the trajectories can wander in bounded state space between the larger and the smaller spheres in figure 2.1. The curve C, in figure 2.1, is an illustration of a stable trajectory. The curve D illustrates asymptotically stability as it approaches the equilibrium point X_e with increasing time. Asymptotic stability is much stronger condition and often stability is sufficient. The trajectories of a nonlinear systems, as illustrated by the forced Duffing's equation in Chapter 1, can be bounded and stable but need not be asymptotically stable and can demonstrate chaos.

In control systems dealing with trajectory tracking, the concept of stability is defined slightly differently [93]. Consider a system given by $\dot{x} = f(x, u)$, where $u(t)$ is the control law.

Definition 4: *Tracking stability* – A controller is said to be stable if we design $u(t)$, such that the the error $e(t)$ between the desired trajectory $(x_d(t))$ and the state trajectory $(x(t))$ remains bounded.

For a stable tracking controller, the error $e(t) = x_d(t) - x(t)$ must remain bounded, although it may *not* go to zero. In such a situation, the state trajectory *does not* track the desired trajectory, although the error between them is within reasonable bounds, and under certain conditions, the phenomena of chaos could exist. Now considering asymptotic stability, we have

Definition 5: *Asymptotic tracking stability* – A controller is said to be asymptotically stable if we design $u(t)$, such that the the error $e(t)$ between the desired trajectory $(x_d(t))$ and the state trajectory $(x(t))$ goes to zero as $t \longrightarrow \infty$.

For an asymptotically stable controller, the state trajectory tracks the desired trajectory and, in this case, chaos *cannot* exist. In trajectory tracking problems, it is asymptotic stability that is sought to be achieved.

In this chapter, we study the dynamics of a planar 2R robot under feedback control and following a desired trajectory. It has been shown in literature [55, 56], using numerical simulations, that for some values of the controller gains, the system of equations modeling the feedback control of a planar 2R robot can exhibit chaos and hence is not asymptotically stable. In this work, we apply the method of multiple scales (MMS) to the 2R robot equations, derive the slow flow equations and finally obtain conditions for chaos and asymptotic stability as defined above.

2.2 Modeling of the 2R Planar Robot

The schematic of a two-degree-of-freedom planar 2R robot, shown in Chapter 1, is reproduced in figure 2.2 below for convenience. The motion of the robot is in the horizontal plane and there is no effect of gravity. The robot has two links of length l_1 and l_2, respectively. The robot is driven by two motors, one each at the joints, providing a torque of Γ_1 and Γ_2 and the rotation caused at both the rotary joints are denoted by θ_1 and θ_2.

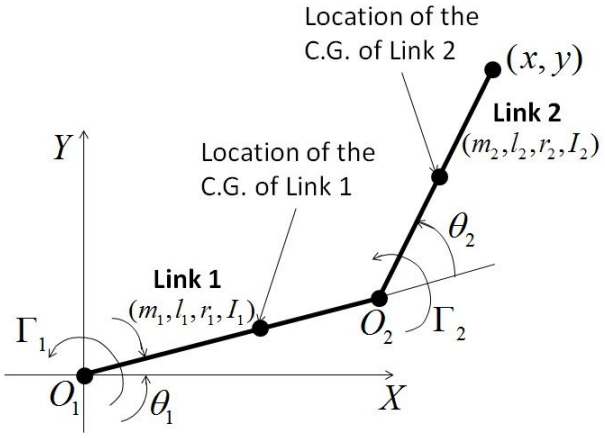

Figure 2.2: A 2R planar robot

The dynamic equations of motion of the 2R planar robot can be derived using the Lagrangian formulation and are given in equation (1.15). They can be rewritten in a

more compact form as

$$\begin{aligned}
&[A + B + 2C\cos(\theta_2)]\ddot{\theta_1} + [B + C\cos(\theta_2)]\ddot{\theta_2} - C\sin(\theta_2)[2\dot{\theta_1} + \dot{\theta_2}]\dot{\theta_2} = \Gamma_1 \\
&[B + C\cos(\theta_2)]\ddot{\theta_1} + B\ddot{\theta_2} + C\sin(\theta_2)\dot{\theta_1}^2 = \Gamma_2
\end{aligned} \tag{2.1}$$

where

$$A = m_1 r_1^2 + I_1 + m_2 l_1^2, \qquad B = m_2 r_2^2 + I_2, \qquad C = m_2 l_1 r_2 \tag{2.2}$$

and m_j, l_j, I_j, r_j $(j = 1, 2)$ are the masses, lengths, inertia and position of center of mass of link j, respectively. For trajectory tracking, we assume that the robot has to trace a desired periodic trajectory

$$\theta_{d_i} = A_{f_i}\sin(\Omega t), \qquad \text{for } i = 1, 2 \tag{2.3}$$

where θ_{d_i} is the desired trajectory, A_{f_i} is the amplitude of forcing and Ω is the forcing frequency.

The number of parameters in the above equations can be reduced by non-dimensionalization as follows:

- We define the non-dimensional time τ as Ωt. In terms of τ, we can write

$$\begin{aligned}
\frac{d\theta_j}{dt} &= \frac{d\theta_j}{d\tau}.\frac{d\tau}{dt} = \Omega\frac{d\theta_j}{d\tau} = \Omega\theta_j' \\
\frac{d^2\theta_j}{dt^2} &= \Omega^2\frac{d\theta_j}{d\tau} = \Omega^2\theta_j''
\end{aligned} \tag{2.4}$$

  where "$'$" represents derivative with respect to τ.

- Next we introduce the following non-dimensional variables [56]

$$P_1 = \frac{m_1 r_1^2 + I_1}{m_2 r_2^2 + I_2}, \qquad P_2 = \frac{m_1 l_1^2}{m_2 r_2^2 + I_2}, \qquad P_3 = \frac{r_2}{l_1} \tag{2.5}$$

Using equations (2.4) and (2.5) in equation (2.1) and dividing both sides of equation (2.1) by $(m_2 r_2^2 + I_2)$, the non-dimensionalized equations of motion of a 2R planar robot can

be written as

$$[P_1 + 1 + P_2 + 2P_2P_3\cos(\theta_2)]\theta_1'' + [1 + P_2P_3\cos(\theta_2)]\theta_1'' - P_2P_3\sin(\theta_2)[2\theta_1' + \theta_2']\theta_2' = \Gamma_{1n}$$
$$[1 + P_2P_3\cos(\theta_2)]\theta_1'' + \theta_2'' + P_2P_3\sin(\theta_2)\theta_1'^2 = \Gamma_{2n} \quad (2.6)$$

where Γ_{1n}, Γ_{2n} are the non-dimensional torques whose expressions depend on the controller used. We have considered two well-known controllers, namely the PD and model based controllers, and these are described next.

2.2.1 PD Control of a 2R Planar Robot

In order to trace a desired trajectory, we consider a PD control scheme, where the joint torques in equation (2.1) are computed as

$$\Gamma_1 = \ddot{\theta}_{d_1} + K_v\dot{e_1} + K_pe_1$$
$$\Gamma_2 = \ddot{\theta}_{d_2} + K_v\dot{e_2} + K_pe_2 \quad (2.7)$$

where $e_i = \theta_{d_i}$ - θ_i is the servo error, $\dot{e}_i$ is the derivative of the servo error, θ_{d_i} is the desired trajectory to be traced, and K_p and K_v are the proportional and derivative gains, respectively. It may be noted that we have assumed K_p and K_v are same for both the motors for simplicity and, in an actual robot they need not be same.

In non-dimensional form, using equation (2.4), the above equations can be written as

$$\Gamma_{1n} = S_n{\theta_{d_1}}'' + K_{vn}e_1' + K_{pn}e_1$$
$$\Gamma_{2n} = S_n{\theta_{d_2}}'' + K_{vn}e_1' + K_{pn}e_2 \quad (2.8)$$

where $S_n = \dfrac{1}{(m_2r_2^2 + I_2)}$, $K_{pn} = \dfrac{K_p}{\Omega^2(m_2r_2^2 + I_2)}$ and $K_{vn} = \dfrac{K_v}{\Omega(m_2r_2^2 + I_2)}$.

For the desired trajectory of the joints, $\theta_{d_i} = A_{f_i}\sin(\Omega t)$, $i = 1, 2$, the non-dimensional form is given by $\theta_{d_i} = A_{f_i}\sin(\tau)$. Using this non-dimensional form of the desired trajectory in equation (2.8) and substituting the resulting equation into equation (2.6), the non-dimensional equations of motion of the planar 2R robot with a PD controller are

given by

$$\begin{bmatrix} P_1+1+P_2+2P_2P_3\cos(\theta_2) & 1+P_2P_3\cos(\theta_2) \\ 1+P_2P_3\cos(\theta_2) & 1 \end{bmatrix} \begin{bmatrix} \theta_1'' \\ \theta_2'' \end{bmatrix} + \begin{bmatrix} -P_2P_3\sin(\theta_2)[2\theta_1'+\theta_2']\theta_2' \\ P_2P_3\sin(\theta_2)\theta_1'^2 \end{bmatrix}$$
$$= \begin{bmatrix} -A_{f_1}S_n\sin\tau + K_{pn}(A_{f_1}\sin\tau-\theta_1)+K_{vn}(A_{f_1}\cos\tau-\theta_1') \\ -A_{f_2}S_n\sin\tau + K_{pn}(A_{f_2}\sin\tau-\theta_2)+K_{vn}(A_{f_2}\cos\tau-\theta_2') \end{bmatrix} \tag{2.9}$$

The nonlinear system given by equations (2.9) is known to be asymptotically stable for all K_p, $K_v > 0$, when $\theta_{d_i}' = \theta_{d_i}'' = 0$. The proof of asymptotic stability (using the dimensional form of the equations) is available in several textbooks (see, for example, Ghosal [53]) and we present a brief discussion for the sake of completeness. In the absence of gravity, the non-dimensional equations are given as

$$\left[M_n(\Theta)\right]\Theta'' + \left[C_n(\Theta,\Theta')\right] = \Gamma_n \tag{2.10}$$

where $[M_n(\Theta)]$ represents the positive definite mass matrix, $[C_n(\Theta,\Theta')]$ represents the Coriolis terms and Θ is a 2×1 matrix of the joint variables (θ_1,θ_2). For the set point problem, $\Theta_d = 0$, $\Theta_d' = 0$, $\Theta_d'' = 0$, and the PD control in equation (2.8) reduces to

$$\Gamma_n = -\left[K_{pn}\right]\Theta - \left[K_{vn}\right]\dot{\Theta} \tag{2.11}$$

where the matrices $\left[K_{pn}\right]$ and $\left[K_{vn}\right]$ are diagonal 2×2 matrices and K_{pn}, K_{vn} denote non-dimensional gains. The Lyapunov second method [74] can be used to determine asymptotic stability and we consider a candidate Lyapunov function

$$V(\Theta,\Theta') = \frac{1}{2}\Theta'^T\left[M_n(\Theta)\right]\Theta' + \frac{1}{2}\Theta^T\left[K_{pn}\right]\Theta \tag{2.12}$$

It can be seen from equation (2.12), that $V(\Theta,\Theta')$ is positive definite. Evaluating $V'(\Theta,\Theta')$, we have

$$V'(\Theta,\Theta') = \Theta'^T\left[M_n(\Theta)\right]\Theta'' + \frac{1}{2}\Theta'^T\left[M'_n(\Theta)\right]\Theta' + \Theta'^T\left[K_{pn}\right]\Theta$$
$$= -\Theta'^T\left[K_{vn}\right]\Theta' + \frac{1}{2}\Theta'^T\{\left[M'_n(\Theta)\right] - 2\left[C_n(\Theta,\Theta')\right]\}\Theta' \tag{2.13}$$

where $\left[M'_n\right]$ denotes the derivative of the mass matrix $\left[M_n\right]$ with respect to non-dimensional time. Since ($\left[M'_n(\Theta)\right]$ -2 $\left[C_n(\Theta,\Theta')\right]$) is skew symmetric (see reference [53]), the second quadratic form is zero, and we get

$$V'(\Theta,\Theta') = -\Theta'^T \left[K_{vn}\right] \Theta' \tag{2.14}$$

From equation (2.14), as we can see that $V'(\Theta,\Theta')$ can be zero even for a nonzero Θ, $V'(\Theta,\Theta')$ is negative semi-definite and we cannot conclude asymptotic stability. Asymptotic stability can be shown however, by LaSalle's invariance principle [94], where the largest invariant set is a single point and hence the equilibrium point $(\Theta,\Theta') = 0$ is asymptotically stable.

In the above, we assumed that $\Theta'_d = \Theta''_d = 0$ and hence for the set point problem the planar 2R robot driven by a PD controller is asymptotically stable. However, when we consider a tracking problem $\Theta'_d \neq 0$, $\Theta''_d \neq 0$, asymptotic stability is not proven. We attempt to investigate the asymptotic stability of PD control for trajectory tracking in this Chapter and derive a partial analytical approach for obtaining values of gains for which the PD controller is asymptotically stable.

2.2.2 Model Based Control of a 2R Planar Robot

Another control scheme used in trajectory following in robots is the well-known model based computed torque control scheme where the dynamic model is used. We consider the case when the parameters of the dynamic model are not known exactly. We characterize the uncertainty in the dynamic model of the robot by a mismatch parameter e and the robot parameters are computed as

$$\hat{m}_i = (1+e)m_i, \quad \hat{r}_i = (1+e)r_i, \quad \hat{I}_i = (1+e)I_i, \quad \hat{l}_i = (1+e)l_i \tag{2.15}$$

where the $\hat{(\cdot)}$ quantities are the estimates. If $e > 0$ then it implies an overestimated model and $e < 0$ implies an underestimated model. From the above equation we can compute the estimated mass matrix $\hat{M}(\Theta)$ and the estimated vector of Coriolis and centripetal terms $\hat{C}(\Theta,\dot{\Theta})$ from equation (2.1). The computed torque using the estimates are given

by

$$\Gamma = \left[\hat{M}(\Theta)\right]\Gamma_p + \left[\hat{C}(\Theta,\dot{\Theta})\right] \tag{2.16}$$

where Γ_p is given by equation (2.7), with $S_n = 1$, $K_{pn} = \dfrac{K_p}{\Omega^2}$ and $K_{vn} = \dfrac{K_v}{\Omega}$.

To non-dimensionalize the equations of motion with the model based controller, we use three non-dimensional parameters in addition to those defined in equation (2.5) as

$$\alpha_1 = \frac{\hat{m}_1\hat{r}_1^2 + \hat{I}_1 + \hat{m}_2\hat{r}_2^2 + \hat{I}_2 + \hat{m}_2\hat{l}_1^2}{m_2r_2^2 + I_2}, \qquad \alpha_2 = \frac{\hat{m}_2\hat{l}_1\hat{r}_2}{m_2r_2^2 + I_2}, \qquad \alpha_3 = \frac{\hat{m}_2\hat{r}_2^2 + \hat{I}_2}{m_2r_2^2 + I_2} \tag{2.17}$$

Substituting the computed torque given by equation (2.16) into equation (2.1) and using the non-dimensional parameters given by equations (2.5, 2.17) and also using equation (2.4), the non-dimensional equations of motion of the 2R robot driven by a model based computed torque controller are given by

$$\begin{bmatrix} P_1 + 1 + P_2 + 2P_2P_3\cos(\theta_2) & 1 + P_2P_3\cos(\theta_2) \\ 1 + P_2P_3\cos(\theta_2) & 1 \end{bmatrix} \begin{bmatrix} \theta_1'' \\ \theta_2'' \end{bmatrix} + \begin{bmatrix} -P_2P_3\sin(\theta_2)[2\theta_1' + \theta_2']\theta_2' \\ P_2P_3\sin(\theta_2)\theta_1'^2 \end{bmatrix}$$

$$= \begin{bmatrix} \alpha_1(\theta_{d_1}'' + K_{pn}(\theta_{d_1} - \theta_1) + K_{vn}(\theta_{d_1}' - \theta_1')) + \alpha_2(-\sin(\theta_2)[2\theta_1' + \theta_2']\theta_2' \\ +\cos(\theta_2)(2\theta_{d_1}'' + \theta_{d_2}'' + K_{pn}(2\theta_{d_1} - 2\theta_1 + \theta_{d_2} - \theta_2) \\ +K_{vn}(2\theta_{d_1}' - 2\theta_1' + \theta_{d_2}' - \theta_2'))) \\ +\alpha_3(\theta_{d_2}'' + K_{pn}(\theta_{d_2} - \theta_2) + K_{vn}(\theta_{d_2}' - \theta_2')) \\ \\ \alpha_2(\cos(\theta_2)(\theta_{d_1}'' + K_{pn}(\theta_{d_1} - \theta_1) + K_{vn}(\theta_{d_1}' - \theta_1') + \theta_2\theta_1'^2) \\ +\alpha_3(\theta_{d_1}'' + \theta_{d_2}'' + K_{pn}(\theta_{d_1} - \theta_1 + \theta_{d_2} - \theta_2) + K_{vn}(\theta_{d_1}' - \theta_1' + \theta_{d_2}' - \theta_2')) \end{bmatrix} \tag{2.18}$$

The model based control, given by equation (2.18), was studied in literature [55, 56] for the effects of the mismatch parameter e on the ranges of controller gains K_p and K_v for which the 2R robot traces a desired trajectory (trajectory tracking problem). It was found by numerical studies that when the robot parameters are heavily underestimated ($e < -0.5$), for particular values of controller gains K_p and K_v, the robot equations demonstrated chaos. This implies that for the said values of K_p and K_v, the robot does not track the desired trajectory and is *not* asymptotically stable. The ranges were determined, by brute force numerical search based method, by computing the Lyapunov

exponents of the system for different values of K_p and K_v with mismatch parameter e. In reference [55,56], chaos was also reported for low values of K_v ($0 < K_v < 3$ for PD control for a particular value of forcing frequency $\Omega = 2$rad/s and $0 < K_v < 8$ for model based control for a particular value of mismatch parameter $e = -0.9$) and mid-range or higher values of K_p ($34 < K_p < 95$ for PD control for $\Omega = 2$rad/s and $20 < K_p < 100$ for model based control for $e = -0.9$). Again as in the case of the PD controller, no analytical criteria for such results exists. In this Chapter, we present an analytical approach to obtain the ranges of K_p, K_v and e for which the trajectory following planar 2R robot exhibits chaos.

2.3 The Method of Multiple Scales

In this section, we apply the method of multiple scales to the equations of a 2R robot driven by PD and model based controllers. The method of multiple scales and it's application was discussed in Chapter 1 for the Duffing's system, where the slow flow equations were computed. We apply the same procedure to derive the slow flow equations for the 2R robot driven by both PD and model based controllers. The uniform expansion for the solutions to the equations (2.9, 2.18) is of the form

$$\begin{aligned}\theta_1(\tau;\epsilon) &= \epsilon\theta_{10}(T_0,T_1,T_2) + \epsilon^2\theta_{11}(T_0,T_1,T_2) + \epsilon^3\theta_{12}(T_0,T_1,T_2)\\ \theta_2(\tau;\epsilon) &= \epsilon\theta_{20}(T_0,T_1,T_2) + \epsilon^2\theta_{21}(T_0,T_1,T_2) + \epsilon^3\theta_{22}(T_0,T_1,T_2)\end{aligned} \tag{2.19}$$

where, ϵ is a small dimensionless measure of the variables θ_1, θ_2. T_0 (same as τ) is the fast scale associated with changes occurring at the forcing frequencies Ω and the natural frequencies ω_n, and $T_1 = \epsilon\tau$ and $T_2 = \epsilon^2\tau$ are the slow scales associated with the modulations of the amplitudes and phases due to nonlinearities. The derivatives are treated as

$$\frac{d}{dt} = D_0 + \epsilon D_1 + \epsilon^2 D_2 + ..., \qquad \frac{d^2}{dt^2} = D_0^2 + \epsilon(2D_0D_1) + \epsilon^2(2D_0D_2 + D_1^2) + ... \tag{2.20}$$

First we apply MMS to the PD controller and then to the model based computed torque controller.

Application of MMS to PD control

The equation of motion of a 2R planar robot driven by PD control is given by equation (2.9). Before we apply MMS, we must resolve two problems. First, an examination of equation (2.9) reveals the presence of trigonometric functions in the form of $\cos(\theta_2)$ and $\sin(\theta_2)$. We observe that it is not possible to apply MMS to sine and cosine terms. To resolve this, we rewrite these trigonometric terms by using Taylor's theorem as

$$\cos(\theta_2) = 1 - \frac{\theta_2^2}{2!}, \qquad \sin(\theta_2) = \theta_2 - \frac{\theta_2^3}{3!} \approx \theta_2 \tag{2.21}$$

The reason why we neglect the cubic term for the expansion of $\sin(\theta_2)$ is because the highest order of expansion according to equation (2.19) is three. An examination of $\sin(\theta_2)$ in equation (2.9) reveals that it is coupled with a quadratic term. When the expansion given by equation (2.19) is performed, $\sin(\theta_2)$ coupled with the quadratic term gives a cubic term (order three). If the cubic term in equation (2.21) had been considered, then coupled with the quadratic term would have given a fifth-order term – higher than highest order of expansion we consider in equation (2.19).

Secondly, we need to decide how the terms have to be ordered according to various time scales, as described in Chapter 1 for the Duffing's equation. We order the inertial terms (constant terms in the mass matrix as shown in equation (2.9)), stiffness terms (K_p) and the forcing terms ($A_{f_i}\sin(\tau)$) at time scale $T_0 = \tau$, i.e., the faster time scale. We order the dissipative terms (K_v) at time scale $T_2 = \epsilon^2\tau$, which is the slower time scale. The nonlinearities due to the cubic terms in the equations automatically appear at time scale T_2. Lastly, equation (2.9) also has the terms $\sin(\tau)$ and $\cos(\tau)$. We rewrite them as $\sin(\tau) = \dfrac{e^{i\tau} - e^{-i\tau}}{2i}$ and $\cos(\tau) = \dfrac{e^{i\tau} + e^{-i\tau}}{2}$.

The equations of motion of the 2R planar robot driven by PD control with the ordering and other modifications described above can be written as

$$\begin{aligned}
&[P_1 + 1 + P_2 + 2P_2P_3\left(1 - \frac{\theta_2^2}{2}\right)]\theta_1'' + [1 + P_2P_3\left(1 - \frac{\theta_2^2}{2}\right)]\theta_1'' - P_2P_3\theta_2[2\theta_1' + \theta_2']\theta_2' \\
&= -K_{pn}\theta_1 - \epsilon^2 K_{vn}\theta_1' + \epsilon A_{f_1}((iE_1 + E_2)e^{i\tau} + (-iE_1 + E_2)e^{-i\tau}) \\
&[1 + P_2P_3\left(1 - \frac{\theta_2^2}{2}\right)]\theta_1'' + \theta_2'' + P_2P_3\theta_2\theta_1'^2 = -K_{pn}\theta_2 - \epsilon^2 K_{vn}\theta_2'
\end{aligned} \tag{2.22}$$

$$+ \epsilon A_{f_2}((iE_1 + E_2)e^{i\tau} + (-iE_1 + E_2)e^{-i\tau})$$

where $E_1 = (S_n - K_{pn})/2$ and $E_2 = (K_{vn}/2)$.

Equating coefficients of like powers of ϵ, we obtain

Order ϵ

$$\begin{aligned}
&(P_1 + 1 + P_2 + 2P_2P_3)D_0^2\theta_{10} + (1 + P_2P_3)D_0^2\theta_{20} + K_{pn}\theta_{10} = \\
&A_{f_1}((iE_1 + E_2)e^{i\tau} + (-iE_1 + E_2)e^{-i\tau}) \\
&(1 + P_2P_3)D_0^2\theta_{10} + D_0^2\theta_{20} + K_{pn}\theta_{20} = A_{f_2}((iE_1 + E_2)e^{i\tau} + (-iE_1 + E_2)e^{-i\tau})
\end{aligned} \tag{2.23}$$

where $D_n^2 = (\partial^2/\partial T_n^2)$. The solution of equations (2.23) is of the form

$$\begin{aligned}
\theta_{10} &= A_1e^{i\omega_1T_0} + A_2e^{i\omega_2T_0} + F_1(iE_1 + E_2)e^{iT_0} + F_1(-iE_1 + E2)e^{-iT_0} + c.c. \\
\theta_{20} &= c_{21}A_1e^{i\omega_1T_0} + c_{22}A_2e^{i\omega_2T_0} + F_2(iE_1 + E_2)e^{iT_0} + F_2(-iE_1 + E2)e^{-iT_0} + c.c.
\end{aligned} \tag{2.24}$$

where ω_1 and ω_2 are the natural frequencies of the system, $c.c$ stands for complex conjugate and the derivation of all terms in equation (2.24) is given in Appendix A. The above equation is used in computing terms at order ϵ^2 shown next.

Order ϵ^2

$$\begin{aligned}
&(P_1 + 1 + P_2 + 2P_2P_3)D_0^2\theta_{11} + (1 + P_2P_3)D_0^2\theta_{21} + K_{pn}\theta_{11} = \\
&-2(P_1 + 1 + P_2 + 2P_2P_3)D_0D_1\theta_{10} - 2(1 + P_2P_3)D_0D_1\theta_{20} \\
&(1 + P_2P_3)D_0^2\theta_{11} + D_0^2\theta_{21} + K_{pn}\theta_{21} = -2(1 + P_2P_3)D_0D_1\theta_{10} - 2D_0D_1\theta_{20}
\end{aligned} \tag{2.25}$$

In the above equation on the right-hand side, the non-secular terms are zero. Equating the secular terms on the right-hand side to zero would give $A_1(T_1)$ and $A_2(T_1)$. Hence, substituting equation (2.24) into the right-hand side of equation (2.25) and equating the secular terms to zero, we get

$$\begin{aligned}
&-2(P_1 + 1 + P_2 + 2P_2P_3)\frac{\partial A_1}{\partial T_1} - 2(1 + P_2P_3)\frac{\partial A_2}{\partial T_1} = 0 \\
&-2(1 + P_2P_3)\frac{\partial A_1}{\partial T_1} - 2\frac{\partial A_2}{\partial T_1} = 0
\end{aligned} \tag{2.26}$$

Solving equation (2.26), we get

$$\frac{\partial A_1}{\partial T_1} = 0, \qquad \frac{\partial A_2}{\partial T_1} = 0 \tag{2.27}$$

From equation (2.27), we have A_1=$A_1(T_0, T_2)$ and A_2=$A_2(T_0, T_2)$. Now at order ϵ^3, we have

Order ϵ^3

$$\begin{aligned}
&(P_1 + 1 + P_2 + 2P_2P_3)D_0^2\theta_{12} + (1 + P_2P_3)D_0^2\theta_{22} + K_{pn}\theta_{12} = \\
&P_2P_3(D_0^2\theta_{10}\theta_{20}^2 + D_0^2\theta_{20}\frac{\theta_{20}^2}{2} + \theta_{20}(2D_0\theta_{10} + D_0\theta_{20})D_0\theta_{20})) - K_{vn}D_0\theta_{10} \\
&(1 + P_2P_3)D_0^2\theta_{12} + D_0^2\theta_{22} + K_{pn}\theta_{22} = \\
&P_2P_3(D_0^2\theta_{10}\frac{\theta_{20}^2}{2} - \theta_{20}(D_0\theta_{10})^2) - K_{vn}D_0\theta_{20}
\end{aligned} \tag{2.28}$$

Equation (2.28) represents the third-order approximation for the 2R planar robot system. Now, we must separate the secular terms (as defined in Chapter 1 for the Duffing's system) in equation (2.28), to determine the solvability conditions (or the slow flow equations). We do this by introducing a detuning parameter, as described for the Duffing's system in Chapter 1, and we can write

$$\Omega = \omega_2 + \epsilon\sigma_1 \tag{2.29}$$

We rewrite equation (2.29) as follows:

$$3\Omega = \omega_1 + 3\epsilon\sigma_1, \quad \Omega = \left(\frac{\omega_1 - \omega_2}{2}\right) + \epsilon\sigma_1 \tag{2.30}$$

To determine the solvability conditions, we seek a particular solution free of secular terms corresponding to the terms proportional to $e^{i\omega_n T_0}$, in the form

$$\begin{aligned}
\theta_{12} &= \sum_{i=1}^{2} S_i(T_1)e^{i\omega_i T_0} \\
\theta_{22} &= \sum_{i=1}^{2} Q_i(T_1)e^{i\omega_i T_0}
\end{aligned} \tag{2.31}$$

Substituting equation (2.24) and equation (2.30) into the right-hand side of equation (2.28) and substituting equation (2.31) into the left-hand side of equation (2.28), and equating the coefficients of the powers of $e^{i\omega_1 T_0}$ and $e^{i\omega_2 T_0}$, we can determine the solvability conditions, thus eliminating the secular terms. Considering, after the above mentioned substitution into the equation (2.28) at powers $e^{i\omega_1 T_0}$ and $e^{i\omega_2 T_0}$, we get
At $e^{i\omega_1 T_0}$

$$\begin{bmatrix} K_{pn} - (P_1 + 1 + P_2 + 2P_2P_3)\omega_1^2 & -(1 + P_2P_3)\omega_1^2 \\ -(1 + P_2P_3)\omega_1^2 & K_{pn} - \omega_1^2 \end{bmatrix} \begin{bmatrix} S_1 \\ Q_1 \end{bmatrix} = \begin{bmatrix} Z_1 \\ Z_2 \end{bmatrix} \tag{2.32}$$

At $e^{i\omega_2 T_0}$

$$\begin{bmatrix} K_{pn} - (P_1 + 1 + P_2 + 2P_2P_3)\omega_2^2 & -(1 + P_2P_3)\omega_2^2 \\ -(1 + P_2P_3)\omega_2^2 & K_{pn} - \omega_2^2 \end{bmatrix} \begin{bmatrix} S_2 \\ Q_2 \end{bmatrix} = \begin{bmatrix} W_1 \\ W_2 \end{bmatrix} \tag{2.33}$$

where Z_1, Z_2, W_1 and W_2 are of the form

$$\begin{aligned}
Z_1 &= A_1^{'}(i\omega_1)R_{11} + A_1(R_{121}i + R_{122} + R_{123}A_1^2 + R_{124}A_2^2) \\
&\quad + A_2R_{13}(iE_1 + E2)e^{2i\sigma_1 T_1} + R_{14}(iE_1 + E2)^3 e^{3i\sigma_1 T_1} \\
Z_2 &= A_1^{'}(i\omega_1)R_{21} + A_1(R_{221}i + R_{222} + R_{223}A_1^2 + R_{224}A_2^2) \\
&\quad + A_2R_{23}(iE_1 + E2)e^{2i\sigma_1 T_1} + R_{24}(iE_1 + E2)^3 e^{3i\sigma_1 T_1} \\
W_1 &= A_2^{'}(i\omega_2)S_{11} + A_2(S_{121}i + S_{122} + S_{123}A_1^2 + S_{124}A_2^2) + A_1S_{13}(iE_1 + E2)e^{-2i\sigma_1 T_1} \\
W_2 &= A_2^{'}(i\omega_2)S_{21} + A_2(S_{221}i + S_{222} + S_{223}A_1^2 + S_{224}A_2^2) + A_1S_{23}(iE_1 + E2)e^{-2i\sigma_1 T_1}
\end{aligned} \tag{2.34}$$

The terms R_{11}, S_{11}..... are given in Appendix A.

Equations (2.32) and (2.33) are a system of two non-homogeneous equations for S_n, Q_n. The homogeneous parts have a non-trivial solution since the determinant of both the co-efficient matrices in equations (2.32-2.33) is equal to zero. Hence, the solvability conditions can be determined by
At $e^{i\omega_1 T_0}$

$$\begin{vmatrix} Z_1 & -(1 + P_2P_3)\omega_1^2 \\ Z_2 & K_{pn} - \omega_1^2 \end{vmatrix} = 0 \tag{2.35}$$

which gives

$$Z_1(K_{pn} - \omega_1^2) + Z_2(1 + P_2P_3)\omega_1^2 = 0 \tag{2.36}$$

At $e^{i\omega_2 T_0}$

$$\begin{vmatrix} W_1 & -(1 + P_2P_3)\omega_2^2 \\ W_2 & K_{pn} - \omega_2^2 \end{vmatrix} = 0 \tag{2.37}$$

which gives

$$W_1(K_{pn} - \omega_2^2) + W_2(1 + P_2P_3)\omega_2^2 = 0 \tag{2.38}$$

Substituting the terms in equation (2.34) into equations (2.36, 2.38) respectively, we determine the solvability conditions as:
At $e^{i\omega_1 T_0}$

$$\begin{aligned} &A_1'(i\omega_1)L_{11} + A_1(L_{121}i + L_{122} + L_{123}A_1^2 + L_{124}A_2^2) \\ &+ A_2(L_{131}i + L_{132})e^{2i\sigma_1 T_1} + L_{14}(iE_1 + E2)^3 e^{3i\sigma_1 T_1} = 0 \\ &\Longrightarrow A_1' = A_1(-J_{121} + i(J_{122} + J_{123}A_1^2 + J_{124}A_2^2)) \\ &+ A_2(-J_{131} + iJ_{132})e^{2i\sigma_1 T_1} + iJ_{14}(iE_1 + E2)^3 e^{3i\sigma_1 T_1} = 0 \end{aligned} \tag{2.39}$$

At $e^{i\omega_2 T_0}$

$$\begin{aligned} &A_2'(i\omega_2)L_{21} + A_2(L_{221}i + L_{222} + L_{223}A_1^2 + L_{224}A_2^2) + A_1(L_{231}i + L_{232})e^{-2i\sigma_1 T_1} = 0 \\ &\Longrightarrow A_2' = A_2(-J_{221} + i(J_{222} + J_{223}A_1^2 + J_{224}A_2^2)) + A_1(-J_{231} + iJ_{232})e^{-2i\sigma_1 T_1} = 0 \end{aligned} \tag{2.40}$$

where the terms $L_{11}, J_{121}, L_{21}, J_{221}, ...$ are derived from equations (2.36, 2.38), respectively and are given in Appendix A. Introducing the polar notation $A_n = a_n e^{ib_n}$ and using in equations (2.39-2.40), we get

$$\begin{aligned} a_1' &= -J_{121}a_1 + a_2(-J_{131}\cos\gamma - J_{132}\sin\gamma) - J_{151}\cos\delta - J_{152}\sin\delta \\ b_1' &= J_{122} + J_{123}a_1^2 + J_{124}a_2^2 + \frac{a_2(-J_{131}\sin\gamma + J_{132}\cos\gamma)}{a_1} + \frac{-J_{151}\sin\delta + J_{152}\cos\delta}{a_1} \\ a_2' &= -J_{221}a_1 + a_1(-J_{231}\cos\gamma + J_{232}\sin\gamma) \end{aligned}$$

$$b_2^{'} = J_{222} + J_{223}a_1^2 + J_{224}a_2^2 + \frac{a_1(J_{231}\sin\gamma + J_{332}\cos\gamma)}{a_2} \tag{2.41}$$

where $\delta = 3\sigma_1 T_1 - b_1$ and $\gamma = 2\sigma_1 T_1 + b_2 - b_1$. Modifying coordinates, using $x = a_1\cos\delta$, $y = a_1\sin\delta$, $z = a_2\cos(\delta-\gamma)$ and $w = a_2\sin(\delta-\gamma)$, we have the final set of four slow flow equations given by

$$\begin{aligned}
\dot{x} &= -J_{121}x - (3\sigma_1 - J_{122})y + y(J_{123}(x^2+y^2) + J_{124}(z^2+w^2)) \\
&+ J_{13}(-2E_1E_2z + (E_2^2 - E_1^2)w) - J_{14}E_1(3E_2^2 - E_1^2) \\
\dot{y} &= -J_{121}y + (3\sigma_1 - J_{122})x - x(J_{123}(x^2+y^2) + J_{124}(z^2+w^2)) \\
&+ J_{13}(-2E_1E_2w - (E_2^2 - E_1^2)z) - J_{14}E_2(E_2^2 - 3E_1^2) \\
\dot{z} &= -J_{221}z - (\sigma_1 - J_{222})w + w(J_{223}(x^2+y^2) + J_{224}(z^2+w^2)) \\
&+ J_{23}(2E_1E_2x + (E_2^2 - E_1^2)y) \\
\dot{w} &= -J_{221}w + (\sigma_1 - J_{222})z - z(J_{223}(x^2+y^2) + J_{224}(z^2+w^2)) \\
&+ J_{23}(2E_1E_2y - (E_2^2 - E_1^2)x)
\end{aligned} \tag{2.42}$$

The equations (2.42) represent the slow flow equations and are the solvability conditions for the original equation (2.9) to have a bounded solution.

Application of MMS to model based control

We now apply MMS to the equations of the 2R robot driven by model based control. The equations of motion are given by equation (2.18). For the application of MMS, after ordering as done in the case for PD control, we have

$$\begin{aligned}
&[P_1 + 1 + P_2 + 2P_2P_3\left(1 - \frac{\theta_2^2}{2}\right)]\theta_1'' + [1 + P_2P_3\left(1 - \frac{\theta_2^2}{2}\right)]\theta_1'' - P_2P_3\theta_2[2\theta_1' + \theta_2']\theta_2' \\
&= -(\alpha_1 + 2\alpha_2)K_{pn}\theta_1 - (\alpha_3 + \alpha_2)K_{pn}\theta_2 - \epsilon^2[(\alpha_1 + 2\alpha_2)K_{vn}\theta_1' + (\alpha_3 + \alpha_2)K_{vn}\theta_2'] \\
&+ \epsilon[(\alpha_1 + 2\alpha_2)A_{f_1} + (\alpha_3 + \alpha_2)A_{f_2}]((iE_1 + E_2)e^{i\tau} + (-iE_1 + E_2)e^{-i\tau}) \\
&+ \alpha_2\left(\theta_2^2\frac{K_{pn}}{2}(2\theta_1 + \theta_2) - \theta_2\theta_2'[2\theta_1' + \theta_2']\right) + i\frac{\alpha}{2}(2A_{f_1} + A_{f_2})(e^{i\tau} - e^{-i\tau})\theta_2^2
\end{aligned} \tag{2.43}$$

$$\begin{aligned}
&[1 + P_2P_3\left(1 - \frac{\theta_2^2}{2}\right)]\theta_1'' + \theta_2'' + P_2P_3\theta_2\theta_1'^2 = -(\alpha_3 + \alpha_2)K_{pn}\theta_1 - \alpha_3K_{pn}\theta_2 \\
&+ \epsilon[(\alpha_3 + \alpha_2)A_{f_1} + \alpha_3A_{f_2}]((iE_1 + E_2)e^{i\tau} + (-iE_1 + E_2)e^{-i\tau})
\end{aligned}$$

$$-\epsilon^2[(\alpha_3+\alpha_2)K_{vn}\theta_1' + \alpha_3 K_{vn}\theta_2'] + \alpha_2\left(\frac{K_{pn}}{2}\theta_1\theta_2^2 + \theta_2\theta_1'^2 + i\frac{A_{f_1}}{2}(e^{i\tau}-e^{-i\tau})\right)$$

We follow the same procedure as was done in the case of PD control (from equation (2.23) onwards) and obtain the slow flow equations as

$$\begin{aligned}
\dot{x} &= -J_{121}x - (3\sigma_1 - J_{122})y + y(J_{123}(x^2+y^2) + J_{124}(z^2+w^2)) - J_{a1}z + J_{a2}w - J_{a3}\\
\dot{y} &= -J_{121}y + (3\sigma_1 - J_{122})x - x(J_{123}(x^2+y^2) + J_{124}(z^2+w^2)) - J_{a1}w - J_{a2}z - J_{a4}\\
\dot{z} &= -J_{221}z - (\sigma_1 - J_{222})w + w(J_{223}(x^2+y^2) + J_{224}(z^2+w^2)) - J_{a5}x + J_{a6}y \qquad (2.44)\\
\dot{w} &= -J_{221}w + (\sigma_1 - J_{222})z - z(J_{223}(x^2+y^2) + J_{224}(z^2+w^2)) - J_{a5}y - J_{a6}x
\end{aligned}$$

where σ_1 is the detuning parameter of the same form (although numerically different) as given by equation (2.30) for PD control. The terms $J_{121}, J_{122}, ...$ are different from those in the slow flow equations (2.42) for PD control and are given in Appendix A.

2.4 Asymptotic Stability Analysis

In this section, we derive the analytical conditions for the asymptotic stability for the system given by equations (2.42), (2.44) for the PD and model-based controllers respectively, at the fixed point of the both the systems. Equations (2.42), (2.44) are autonomous systems having nine fixed points. Although these fixed points cannot be explicitly given, we can compute them numerically. We discuss the stability of these systems at one of those fixed points, say $f_s = (x_s, y_s, z_s, w_s)$ – f is different for equations (2.42) and (2.44). To analyze the asymptotic stability of equation (2.42), (2.44), we use the Routh-Hurwitz criterion [57,58], the central idea of which is that in order for any system of equations to be asymptotically stable, all eigenvalues of it's Jacobian must have negative real parts. We apply the Routh-Hurwitz criterion by following the sequence of steps:

STEP 1 - Compute the Jacobian of equations (2.42, 2.44) at fixed point f_s

$$J_f = \begin{bmatrix} \frac{\partial f_1}{\partial x} & \frac{\partial f_1}{\partial y} & \frac{\partial f_1}{\partial z} & \frac{\partial f_1}{\partial w} \\ \frac{\partial f_2}{\partial x} & \frac{\partial f_2}{\partial y} & \frac{\partial f_2}{\partial z} & \frac{\partial f_2}{\partial w} \\ \frac{\partial f_3}{\partial x} & \frac{\partial f_3}{\partial y} & \frac{\partial f_3}{\partial z} & \frac{\partial f_3}{\partial w} \\ \frac{\partial f_4}{\partial x} & \frac{\partial f_4}{\partial y} & \frac{\partial f_4}{\partial z} & \frac{\partial f_4}{\partial w} \end{bmatrix}_{(x,y,z,w)=(x_s,y_s,z_s,w_s)} \tag{2.45}$$

STEP 2 - Compute the characteristic equation of the Jacobian J_f as

$$F_c = |J_f - \lambda I| = 0 \tag{2.46}$$

where I is 4×4 identity matrix. The characteristic equation of (2.46) is of the form

$$F_c = a_4\lambda^4 + a_3\lambda^3 + a_2\lambda^2 + a_1\lambda + a_0 \tag{2.47}$$

To apply the Routh-Hurwitz criterion, we write the Hurwitz matrix [57] which for the above fourth-order system is given by

$$\begin{bmatrix} a_3 & a_4 & 0 & 0 \\ a_1 & a_2 & a_3 & a_4 \\ 0 & a_0 & a_1 & a_2 \\ 0 & 0 & 0 & a_0 \end{bmatrix} \tag{2.48}$$

The principal diagonal minors $\Delta_i,\ i = 1, .., 4$ of the Hurwitz matrix are

$$\Delta_1 = a_3, \Delta_2 = \begin{bmatrix} a_3 & a_4 \\ a_1 & a_2 \end{bmatrix}, \Delta_3 = \begin{bmatrix} a_3 & a_4 & 0 \\ a_1 & a_2 & a_3 \\ 0 & a_0 & a_1 \end{bmatrix}, \Delta_4 = a_0\Delta_3 \tag{2.49}$$

From the Routh-Hurwitz criterion, the conditions for asymptotic stability require that all of the principal diagonal minors $\Delta_i,\ i = 1, .., 4$ to be positive provided $a_4 > 0$ [57,58], i.e., we need

$$a_4 > 0,\ \Delta_1 = a_3 > 0,\ \Delta_2 = a_2a_3 - a_4a_1 > 0$$

$$\Delta_3 = a_1 a_2 a_3 - a_4 a_1^2 - a_3^2 a_0 > 0,\ \Delta_4 = a_0 > 0 \tag{2.50}$$

Simplifying the inequalities, the local asymptotic stability of the system at the fixed point f_s is guaranteed iff

$$\begin{aligned} &h_1 = a_i > 0 \ \ \forall i = 0, .., 4, \quad h_2 = a_2 a_3 - a_4 a_1 > 0, \\ &h_3 = a_1 a_2 a_3 - a_4 a_1^2 - a_3^2 a_0 > 0 \end{aligned} \tag{2.51}$$

We can make the following comments from (2.51):

- If all of $h_1, h_2, h_3 > 0$, then the system is **asymptotically stable** – all roots of the characteristic polynomial in equation (2.47) lie in the left half plane.
- If any of $h_1, h_2, h_3 < 0$, then the system is **unstable** and at least one root of the polynomial in (2.47) lies in the right half plane. This case is not considered as the feedback controlled planar 2R robot is known to have simple stability for trajectory following [54].
- If Δ_1, Δ_2, Δ_3 are positive, but $\Delta_4 = 0$, then the system is at the boundary of stability. Since $\Delta_4 = a_0 \Delta_3$, then either $a_0 = 0$ or $\Delta_3 = 0$. If $a_0 = 0$, then one of the roots of the characteristic equation is zero and the system is on the *boundary* of aperiodic stability. If $\Delta_3 = 0$, then the system has two complex conjugate imaginary roots and the system is on the *boundary* of oscillatory stability [95]. The condition of $\Delta_4 = 0$ is termed as **marginal stability** or **indeterminacy**, and we cannot conclude on asymptotic stability.

In the next section, we compute numerically the values of controller gains K_p and K_v where the slow flow equations of the 2R robot driven by PD and model based controllers are asymptotically stable, i.e., the conditions in equation (2.51) are satisfied. The values and ranges of controller gains where equation (2.51) results in indeterminacy are computed and, in the next section, we discuss the approach to resolve the indeterminacy.

2.5 Numerical Simulation Results

In this section, we present the numerical simulation results for the asymptotic stability analysis described in the previous section. To perform the numerical study, we choose

the physical parameters of an existing robot used in reference [55]. These are as given in Table 1.

Table 2.1: Parameters of the 2R planar robot

Parameter	Link 1	Link 2
Mass (kg)	20.15	8.25
Length (m)	0.5	0.4
C.G. (m)	0.18	0.26
Inertia ($\text{kg} - \text{m}^2$)	6.3	1.64

For purposes of numerical simulation, we use $A_{f_1} = (\pi/2)$ rad, $A_{f_2} = (\pi/4)$ rad. The simulations were performed in MATLAB 2012*Rb* using in-built *ode*45 solver. The relative and absolute tolerances were kept at 10^{-6} and 10^{-9}, respectively. The results were checked for convergence using for lower values of tolerances. We briefly describe the procedure for computing the results shown in this section as follows

- Following STEP 1 and 2 in the previous section we compute the ranges of controller gains K_p and K_v at which the slow flow equations given by equation (2.42) for the PD controller and equation (2.44) for the model based controller are asymptotically stable. This is done by checking for the satisfaction of the conditions given by equation (2.51). The values of (K_p, K_v) at which we get asymptotic stability or indeterminacy are plotted in the (K_p, K_v) space.

- In the event that the Routh-Hurwitz condition given by equation (2.51) are not satisfied, we get indeterminacy. To resolve indeterminacy, we compute the Lyapunov exponents [32] on the slow flow equations of the PD and model based controller. Thus, amongst the indeterminate regions, we get chaotic and non-chaotic regions. The non-chaotic regions are asymptotically stable. The values for asymptotic stability derived from equation (2.51), and the chaotic and non-chaotic (and hence asymptotically stable) values are plotted using different markers in the same plots.

- To verify whether the controller gains in the chaotic and non-chaotic regions do indeed demonstrate chaos and asymptotic stability respectively, we pick some values of K_p and K_v in the chaos map in both chaotic and asymptotically stable regions.

We then use these (K_p, K_v) values in the original differential equations (2.9) and (2.18) for the PD and model based controller and compute the Lyapunov exponents for the said (K_p, K_v) values. A positive Lyapunov exponent would indicate chaos and the lack of one would indicate asymptotic stability.

We first present the results and observations for the simulation of the slow flow equations of the PD controller given in equation (2.42) and then present the same for the slow flow equations of the model based computed torque controller given in equation (2.44).

Simulation results for PD control

Figure 2.3 represent the plots of controller gains (K_p, K_v) at various values of forcing frequency (Ω). In the figures, the small light blue dots represent asymptotic stability as determined by the Routh-Hurwitz criterion given by equation (2.51). The red dots represent asymptotically stable regions derived by computing the spectra of Lyapunov exponents at these (K_p, K_v) values in the slow flow equations – at these points the largest Lyapunov exponent is negative. The black dots in the plots represent chaotic regions characterized by a largest positive Lyapunov exponent. We can conclude from the plots that the ranges of controller gains (K_p, K_v) for which the 2R robot driven by PD control is asymptotically stable are those in the non-black regions.

To verify whether the results presented above are accurate, we pick two points in (K_p, K_v) space – one in the black (chaotic) region and one in the non-black (asymptotically stable) region (as shown in figure 2.3 (b)) and substitute these values of controller gains (K_p, K_v) in the original equations of the 2R robot driven by PD control (equation (2.9)). We compute the Lyapunov exponents for these (K_p, K_v) values. Figure 2.5 shows that the largest Lyapunov exponent corresponding to $(K_p, K_v) = (54, 1)$ (black region in the chaos map) is positive indicating chaos (absence of asymptotic stability), whereas the largest Lyapunov exponent corresponding to $(K_p, K_v) = (54, 4)$ (non-black region in the chaos map) is negative indicating asymptotic stability. We have performed similar tests for other points in the black and non-black regions.

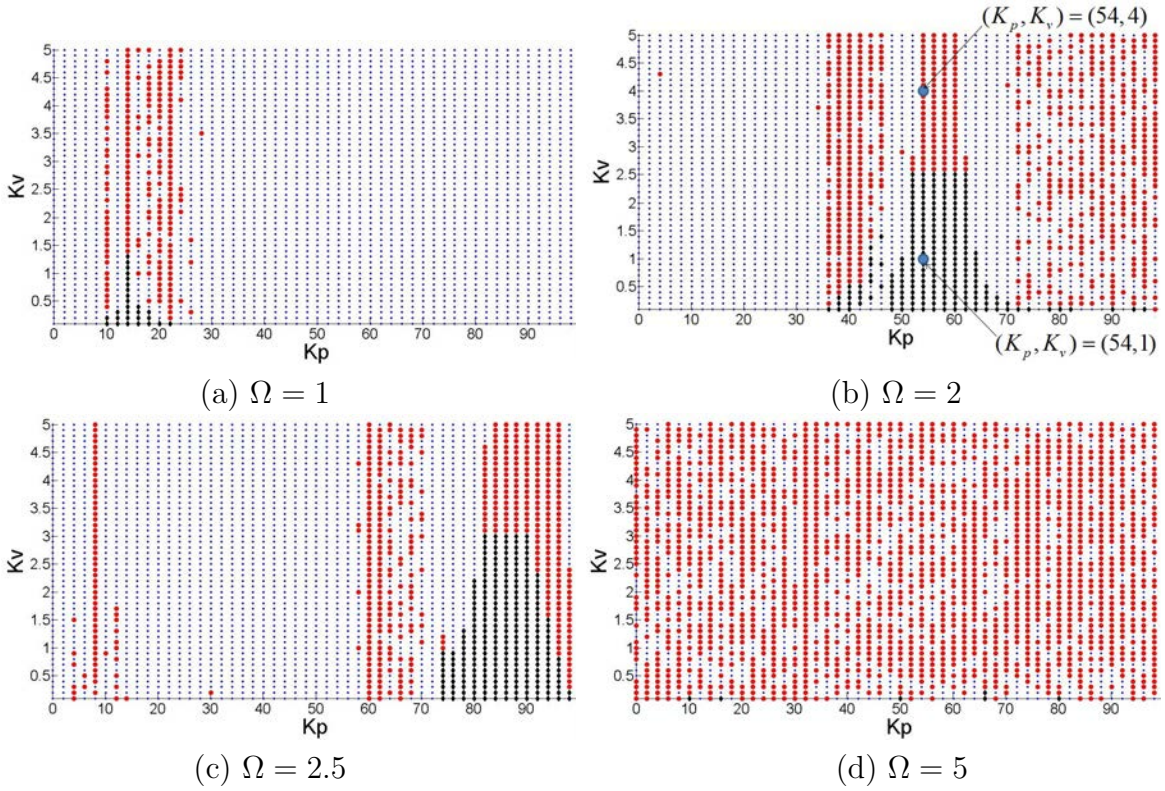

(a) $\Omega = 1$ (b) $\Omega = 2$

(c) $\Omega = 2.5$ (d) $\Omega = 5$

Figure 2.3: Chaos maps in (K_p, K_v) space for PD control for various values of forcing frequency Ω

Observations

From the extensive numerical simulation results performed, we can make the following observations on the asymptotic stability of 2R planar robot driven by PD control.

- For high values of K_p *and* K_v, the 2R robot is asymptotically stable, irrespective of the forcing frequency.
- For low values of K_p *and* K_v, the 2R robot is asymptotically stable for higher values of forcing frequency Ω, but is chaotic for lower values of Ω.
- For low values of K_p and high values of K_v, the 2R robot is asymptotically stable, irrespective of the forcing frequency
- For low values of K_v and high values of K_p, it's asymptotic stability depends on Ω.
- For lower values of Ω, for mid-range K_p $(30 < K_p < 75)$ and low K_v, the motion of the 2R robot is chaotic. But for extremely high values of K_p $(K_p > 100)$, the

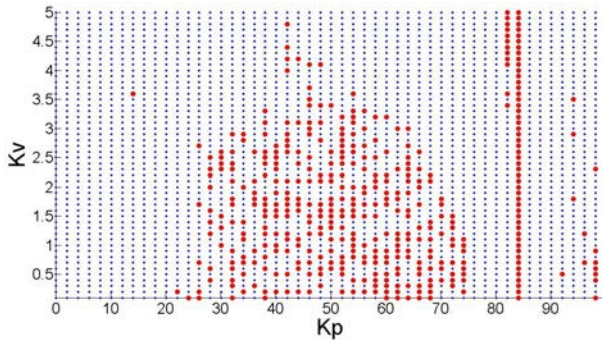

Figure 2.4: Chaos maps in (K_p, K_v) space for PD control – $\Omega = 8$

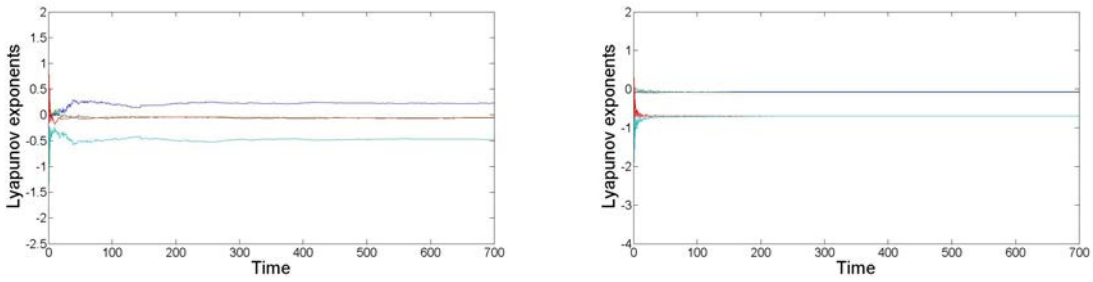

(a) (b)

Figure 2.5: Spectra of Lyapunov exponents of the 2R robot equations (2.9) – (a) $(K_p, K_v) = (54, 1)$ – chaotic (b) $(K_p, K_v) = (54, 4)$ – asymptotically stable

PD controller is stable even for lower values of K_v

- For higher values of Ω, i.e. for $\Omega >= 8$, the PD controller of the 2R robot is asymptotically stable for all values of K_p and K_v.
- It must also be pointed out that range of all K_p, K_v values in the plot is kept less than the values for critical damping. The critical damping of a 2R planar robot is given by $K_v = 2\sqrt{K_p}$. Hence, if we consider K_p values from 0 to 100, then critical damping is given by $K_v = 20$ and we consider K_v values from 0 to 20. The values for outside this range was not obtained as it is intuitively well known that over damped systems ($K_v > 2\sqrt{K_p}$) are not chaotic.

Simulation results for model based control

For the simulation of the slow flow equations of the model based controller, we assume a forcing frequency $\Omega = 2$ (rad/sec).

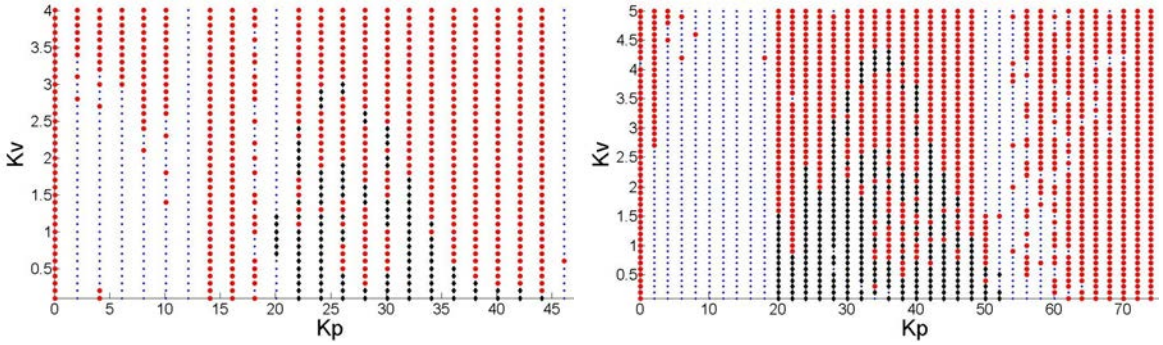

(a) $e = -0.8$ (b) $e = -0.85$

Figure 2.6: Chaos maps in (K_p, K_v) space for model based control

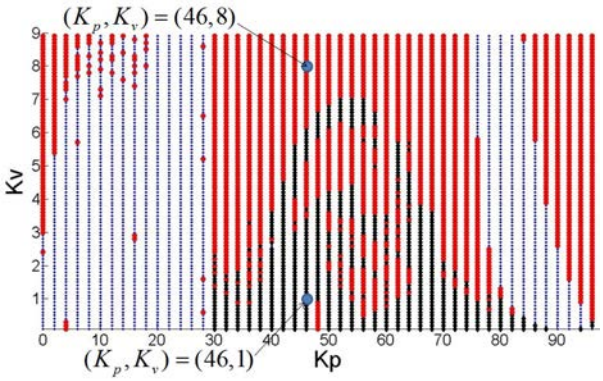

Figure 2.7: Chaos maps in (K_p, K_v) space for model based control – $e = -0.9$

Figures (2.6-2.7) represent the plots of controller gains (K_p, K_v) at various values of mismatch parameter e. As in the case of PD control, the small light blue dots represent asymptotic stability as determined by the Routh-Hurwitz criterion given by equation (2.51). The red dots represent asymptotic stability and the black dots represent chaos as determined by the computation of Lyapunov exponents in the slow flow equations of the model based controller. Thus, the black regions represent chaos whereas the non-black regions (blue or red) represent asymptotic stability.

To verify the above results, we again pick two points in (K_p, K_v) space– one in the black (chaotic) region and one in the non-black (asymptotically stable) region (as shown in figure 2.7) and substitute these values of controller gains (K_p, K_v) in the original equations of the 2R robot driven by model based control (equation (2.18)). Figure 2.8 shows that the largest Lyapunov exponent corresponding to $(K_p, K_v) = (46, 1)$ (black region in the chaos map) is positive indicating chaos, whereas the largest Lyapunov

exponent corresponding to $(K_p, K_v) = (46, 8)$ (non-black region in the chaos map) is negative indicating asymptotic stability.

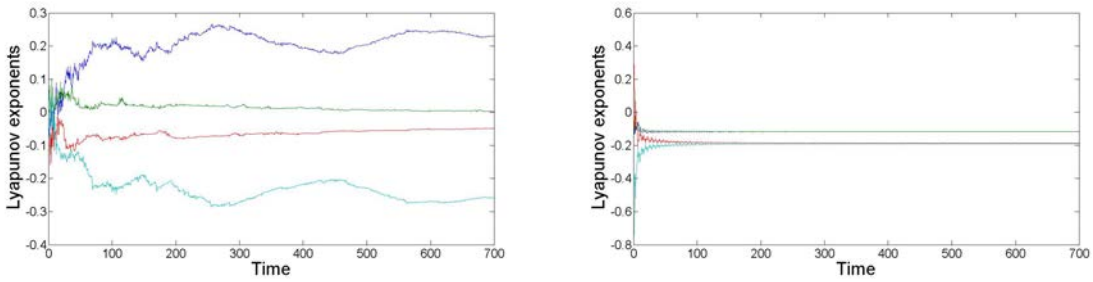

(a) (b)

Figure 2.8: Spectra of Lyapunov exponents of the 2R robot equations (2.18) – (a) $(K_p, K_v) = (46, 1)$ – chaotic (b) $(K_p, K_v) = (46, 8)$ – asymptotically stable

Observations

From the extensive numerical simulation results performed, we make the following observations on the asymptotic stability of 2R planar robot driven by model based computed torque control scheme.

- Chaos exists for greater underestimation ($e < -0.6$) of the model of the 2R robot.
- The controller is asymptotically stable for $e > -0.6$.
- Ranges of K_p and K_v for asymptotic stability vary with the degree of underestimation in the model. For larger underestimation, the ranges of K_p and K_v for asymptotic stability are smaller. For smaller underestimation, the ranges of K_p and K_v for asymptotic stability are larger.
- Chaos exists for mid-range to higher values of K_p (depending upon mismatch parameter e) and lower values of K_v. But unlike PD control, chaos exists even for very high values of K_p.
- The range of all K_p, K_v values in the plot is kept within the range of critical damping.

2.6 Concluding Remarks

In this chapter, the nonlinear dynamical equations of a 2R planar robot driven by PD control and model-based computed torque control following a desired trajectory was analyzed. An semi-analytical method is proposed and the range of controller gains for which the 2R robot is chaotic or asymptotically stable was obtained. The non-dimensional nonlinear ordinary differential equations were analyzed at different time scales by using the method of multiple scales and four slow flow equations were derived. The Routh-Hurwitz criterion was used on the slow flow equations, at a fixed point, to derive analytical conditions for asymptotic stability. The conditions for asymptotic stability were used to compute the ranges of controller gains at which the 2R robot is asymptotically stable or indeterminate. As the use of Routh-Hurwitz criterion can also result in indeterminacy for certain controller gain values, the slow flow equations were further analyzed for the possibility of chaos using Lyapunov exponents. The values of gains, in the indeterminate regions, for which one of the Lyapunov exponent is positive results in chaotic motion and hence for such gain values, the planar 2R robot cannot follow a desired trajectory and be asymptotically stable. The results obtained in this work imply that results related to asymptotic stability of robots following a desired trajectory, available in literature, needs to be re-looked.

The approach of using the method of multiple scales and Routh-Hurwitz criterion is not limited to a planar 2R robot. The number of slow flow equations and the dimension of the Jacobian matrix in n degree-of-freedom robot manipulators would be $2n$ and $2n \times 2n$ respectively. This increase in the number of equations and the dimension of the Jacobian matrix would however make the task of obtaining controller gains for asymptotic stability or chaos more difficult.

Chapter 3

Chaotic Dynamics of a Rotating Flexible Link

The study of the dynamics of flexible manipulators has been an important subject in the field of robotics for the past two decades. Most of the work done on flexible manipulators assume small deformation and use a linear strain-displacement relationship via the linear beam theory [96–98]. However, it has been shown that a linear beam theory approximation is inadequate for fast moving flexible structures [99]. Moreover, it has also been shown that the linear approximation results in the loss of stiffness due to the partial transfer of centrifugal force to the bending equation [100]. Accurate mathematical modeling of flexible manipulators therefore must consider large deformations and thus can only be developed by considering nonlinear elastic deformation in the flexible manipulators. Nonlinearities arising out of large deformations are called geometric nonlinearities [101, 102].

There is very little literature on the dynamics of flexible beams with geometric nonlinearities involving chaotic motion [103–105]. Moreover, the application of the method of multiple scales, as presented in Chapter 1, was done mostly to two or three dimensional systems. In Chapter 1, we pointed out the very little literature that was available for the application of MMS to the study of four-dimensional systems. The simplest model of the dynamics of a flexible beam, subjected to large deformation and geometric nonlinearity, leads to a four-dimensional system [60]. In this Chapter, we study the dynamics of this four-dimensional system using MMS.

In an earlier work [60], a flexible link manipulator with geometric nonlinearities was modeled using a finite element technique to yield four governing ODEs. The four ODEs were written in a non-dimensionalized form using two characteristic velocities, namely the speed of sound and a velocity associated with the transverse bending vibrations of the beam. In this Chapter, we analyze these four ODEs and show that for certain ranges of values of these characteristic velocities the system of equations representing the rotating beam can exhibit chaotic motions. We further show that these values of characteristic velocities are possible to obtain in a rotating blade of a wind turbine (modeled as a beam) or in a flexible link manipulator. Further, we analyze the effect of the presence of damping (Rayleigh damping) on the equations of the flexible manipulator and demonstrate that chaotic motion observed is of a very different nature in damped system as opposed to the undamped system.

This Chapter is organized as follows: In section 3.1, we briefly describe the rotating flexible beam and present the nonlinear ODEs used to model the undamped and damped rotating beam undergoing large deformation and present the non-dimensional form of the equations derived using the two characteristic velocities. In section 3.2, we present a multiple scales analysis of the system of four ODEs to derive the slow flow equations and analyze the system of equations for the undamped and damped case. In section 3.3, we analyze the nature of the system and compute the fixed points of the system. In section 3.4, we examine the results obtained from numerical simulations to obtain better insight as to the range of characteristic velocities for which the system can exhibit chaos. In section 3.5, we present conclusions of this chapter.

3.1 Description of the Rotating Flexible Beam

The modeling of a rotating flexible beam, undergoing large deformation and the derivation of equations of motion in a non-dimensional form is presented in reference [60]. These are presented in brief in this section.

The rotating link was schematically shown in Chapter 1 and the figure is reproduced in figure 3.1 below for convenience. The link is discretized into a finite number of beam elements, with all its nodal variables as described in figure 3.2, defined in the body-fixed

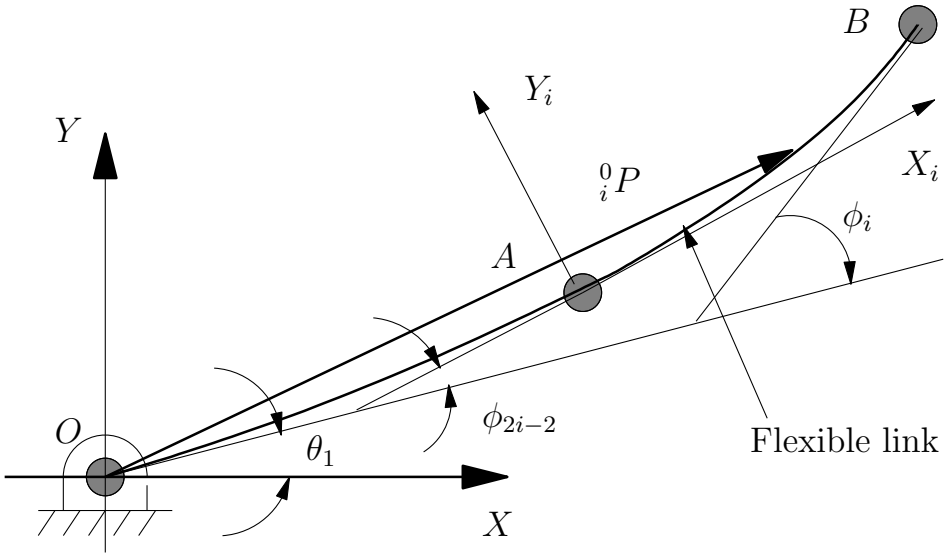

Figure 3.1: Flexible rotating beam

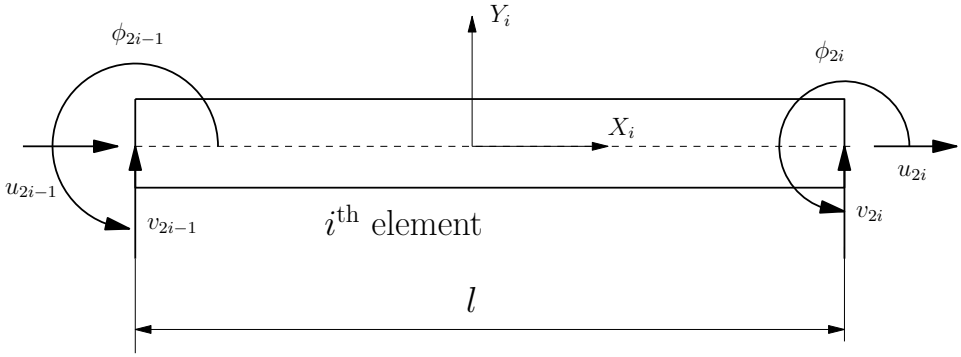

Figure 3.2: A planar beam element

co-ordinate system $O_iX_iY_i$ with O_iX_i along the tangent at the $(2i-2)^{\text{th}}$ node of the system. The co-ordinate system OXY is the global co-ordinate system as shown in figure 3.1 and an arbitrary point on the flexible link, in the global coordinate system, is denoted by ${}^0\mathbf{P}_i$. The rotating flexible link is assumed to have constant cross-sectional area and uniform material properties and is assumed to undergo axial elongation in addition to transverse bending. From the figures (3.1, 3.2), it can be observed that θ_1 is the global variable and $(u_{2i-1}, v_{2i-1}, \phi_{2i-1}, ..., u_{2i}, v_{2i}, \phi_{2i})$ are the nodal variables of the system. The index i refers to the ith discretized element (in figure 3.1, OA is the first element, OB is the second element and so on) of the beam, whereas the total number of such elements of the beam is given by N. In our work, we consider only one element, hence $N = 1$. The beam is assumed to undergo large deformations hence a nonlinear

strain-displacement relationship needs to be used to describe the relation between the strain and the displacements. Following the development in reference [60], we can write

$$\epsilon_{xx} = \frac{\partial u_x}{\partial x} - y\frac{\partial^2 u_y}{\partial x^2} + \frac{1}{2}\left(\frac{\partial u_y}{\partial x}\right)^2 \tag{3.1}$$

where ϵ_{xx} denotes the normal strain, and u_y and u_x denote the longitudinal and transverse displacement at axis $y = 0$ (see figure 3.2) respectively. The above strain-displacement equation can be used to obtain the strain energy of the system as

$$U = \frac{EA}{2}\int_0^l \left(\frac{\partial u_x}{\partial x}\right)^2 dx + \frac{EI}{2}\int_0^l \left(\frac{\partial^2 u_y}{\partial x^2}\right)^2 dx + \frac{EA}{2}\int_0^l \left(\frac{\partial u_x}{\partial x}\right)\left(\frac{\partial u_y}{\partial x}\right)^2 dx \tag{3.2}$$

where E, A, I, l denote the Young's modulus, cross-sectional area, moment of inertia of cross-section and length of the beam, respectively. It can be observed from equation (3.2), that the nonlinearity is quadratic and represents the geometric nonlinearity associated with transverse bending and axial deformation.

Following the development in reference [60], the total kinetic energy of the beam can be obtained from the time derivative of the vector ${}^0\mathbf{P}_i$ and integration. It can be expressed as

$$T = \frac{1}{2}\dot{Q}^T[M]\dot{Q} \tag{3.3}$$

where $[M]$ is the mass matrix and Q is the vector of generalized coordinates given by $(\theta_1, S)^T$ with S denoting the vector of nodal variables given by $(u_1, v_1, \phi_1, ..., u_{2N}, v_{2N}, \phi_{2N})$ (see figure 3.2).

The total potential energy of the beam can be obtained from equation (3.2), and can be written as

$$V = \frac{1}{2}S^T([K] + [\Delta K(S)])S \tag{3.4}$$

where $[K]$ is the conventional stiffness matrix and $[\Delta K(S)]$ is the geometric stiffness matrix. From the potential and kinetic energy given by equations (3.3) and (3.4), the equations of motion can be derived using a Lagrangian formulation. The nonlinear differential equations can be schematically written as

$$[M(Q)]\{\ddot{Q}\} + ([K] + [\Delta K(Q_f)])\{Q_f\} + h(Q, \dot{Q}) = \{\tau\} \tag{3.5}$$

where $h(Q, \dot{Q})$ is the vector of Coriolis and centripetal terms, $\{\tau\} = [\Gamma, 0, 0, 0]^T$ is a vector of input torques and $Q_f = (0, u_2, v_2, \phi_2)^T$ is a vector of flexible variables. Equation (3.5) represents a set of four second-order ordinary differential equations.

The equations of motion (3.5) can be non-dimensionalized [60] using two characteristic velocities

$$U_g = \frac{1}{L}\sqrt{\frac{EI}{\rho A}}, \quad U_a = \sqrt{\frac{E}{\rho}}, \quad T = t/(L/U_g) \tag{3.6}$$

where U_a is the speed of sound and U_g is a characteristic speed associated with bending vibration and T is a non-dimensional time. The quantity U_g is dependent on geometric and material properties of the beam whereas U_a is purely a material property. For a circular cross-section beam of radius R and length L, we can relate U_g and U_a as

$$U_g = \frac{1}{L} \cdot \sqrt{\frac{EI}{\rho A}} = \frac{1}{L} \cdot \sqrt{\frac{E}{\rho}} \cdot \sqrt{\frac{\pi R^4/2}{\pi R^2}} = \frac{U_a R}{L\sqrt{2}} \tag{3.7}$$

The above equation indicate that U_g *decreases* with larger L and smaller R, i.e., U_g is small for thinner and longer beams.

The equations of motion in the non-dimensional form can be written as

$$[\mathcal{M}(Q_f)]\ \{Q^{''}\} + \left(\mathcal{K} + \Delta\mathcal{K}(Q_f, \frac{U_a}{U_g})\right)\{Q\} + \mathcal{C}\{Q'\} + \{\mathcal{H}(Q, Q^{'})\} = \frac{\{\tau\}}{\rho A L U_g^2} \tag{3.8}$$

where $(\cdot)^{'}, (\cdot)^{''}$ represent the first and the second derivative with respect to non-dimensional time T, $\mathcal{M}$ is the 4×4 non-dimensional mass matrix, $\mathcal{K}$ and $\Delta\mathcal{K}$ are the 4×4 non-dimensional conventional and geometric stiffness matrices respectively, $\mathcal{H}$ is the 4×1

vector of non-dimensional centripetal and Coriolis terms, $\{\tau\} = [F\sin(\frac{\Omega L}{U_g}T), 0, 0, 0]^T$ with F and Ω denoting the amplitude and the frequency of forcing term (see Appendix B for details of the terms in equation (3.8)) and $\mathcal{C}\{Q'\}$ represents an added Rayleigh damping term of the form $\alpha[\mathcal{M}] + \beta[\mathcal{K}]$.

In this work we focus on U_g and show that for certain ranges of U_g, the system of four ODEs in equation (3.8) can exhibit chaos. For numerical simulations in section 3.4, we will use the values given in Table 3.1 and we assume the value of amplitude of forcing $F = \pi/2$ and the values of the Rayleigh damping coefficients as $\alpha = 0.02$ and $\beta = 0.02$. The reason for choosing the particular values of damping co-efficients α and β is that high damping increases stability and hence there is no chance of chaotic motion. Hence, we choose low values of α and β as given above to enable the possibility of exploring chaotic motion. It may be noted that the ρ and E values given in Table 3.1 are of E-glass which is used to make wind turbine blades and the value of L is for a 50 kW wind turbine made by Endurance Wind Power Ltd. [106]. The value of Ω is the operating angular speed of the wind turbine blade.

It maybe noted that the blade cross-section in not uniform in a wind turbine and the

Table 3.1: Parameters of the rotating flexible beam

Parameter	Numerical Value
Material	E-Glass
ρ	2550 kg/m^3
E	80 (GPa)
U_a	$\sqrt{\frac{E}{\rho}} = 5601$ m/s
L	9 (m)
Ω	42 (rpm)

U_g value is not known. In section 3.4, we show that if the blade is assumed to have a uniform circular cross-section, then for certain values of U_g (and resulting value of the circular cross-section), the system of equations modeling the rotating blade can exhibit chaos.

3.2 The Method of Multiple Scales

In this section, we apply MMS to the equation (3.8) with and without damping. To apply MMS, we use the same procedure described in Chapter 1. We seek a uniform expansion for the solution of equations (3.8) in the form

$$x(t;\epsilon) = \epsilon x_{10}(T_0, T_1) + \epsilon^2 x_{11}(T_0, T_1) \tag{3.9}$$

where, ϵ is a small dimensionless measure of x which can be any of the variables (θ_1, U_2, V_2, ϕ_2), $T_0 = t$ is the fast scale associated with changes occurring at the forcing frequencies Ω and the natural frequencies ω_n, and $T_1 = \epsilon t$ is the slow scale associated with the modulations of the amplitudes and phases due to nonlinearities and resonances. Equation (3.9) ensures that the nonlinear effects in equations (3.8) appear at the second-order. Ordering the damping and excitation effects so as to appear at the second-order, we can rewrite the set of equations as:

$$[\mathcal{M}(Q_f)]\ \{Q^{''}\} + \left(\mathcal{K} + \Delta\mathcal{K}(Q_f, \frac{U_a}{U_g})\right)\{Q\} + \epsilon\left(\mathcal{C}\{Q^{'}\}\right) + \{\mathcal{H}(Q, Q^{'})\} = \epsilon\left(\frac{\{\tau\}}{\rho A L U_g^2}\right) \tag{3.10}$$

We perform a multiple scales analysis on equation (3.10) – the results for the undamped case can be obtained by setting the damping to zero. Substituting equations (3.9) into equation (3.10) and equating coefficients of like powers of ϵ, we obtain

Order ϵ

$$\begin{aligned}
&\frac{1}{3}D_0^2\theta_{10} + \frac{7}{20}D_0^2V_{20} - \frac{1}{20}D_0^2\phi_{20} = 0\\
&\frac{1}{3}D_0^2U_{20} + \frac{U_a^2}{U_g^2}U_{20} = 0\\
&\frac{7}{20}D_0^2\theta_{10} + 12V_{20} + \frac{13}{35}D_0^2V_{20} - 6\phi_{20} - \frac{11}{210}D_0^2\phi_{20} = 0\\
&-\frac{1}{20}D_0^2\theta_{10} - 6V_{20} - \frac{11}{210}D_0^2V_{20} + 4\phi_{20} + \frac{1}{105}D_0^2\phi_{20} = 0
\end{aligned} \tag{3.11}$$

where $D_n^2 = (\partial^2/\partial T_n^2)$. The solution of equations (3.11) is of the form

$$\theta_{10} = A_3 e^{i\omega_3 T_0} + A_4 e^{i\omega_4 T_0} + c.c.$$

$$
\begin{aligned}
U_{20} &= A_2 e^{i\omega_2 T_0} + c.c. \\
V_{20} &= C_{33}(A_3 e^{i\omega_3 T_0}) + C_{34}(A_4 e^{i\omega_4 T_0}) + c.c. \\
\phi_{20} &= C_{43}(A_3 e^{i\omega_3 T_0}) + C_{44}(A_4 e^{i\omega_4 T_0}) + c.c.
\end{aligned} \tag{3.12}
$$

where $c.c$ stands for complex conjugate and the derivation of equation (3.12) is given in Appendix B. The above equations are used for obtaining **Order** ϵ^2 equations next.

Order ϵ^2

$$
\begin{aligned}
&\frac{1}{3}D_0^2\theta_{11} + \frac{7}{20}D_0^2V_{21} - \frac{1}{20}D_0^2\phi_{21} = -\frac{2}{3}D_0D_1\theta_{10} + \alpha\left(-\frac{1}{3}D_0\theta_{10} - \frac{7}{20}D_0V_{20} + \frac{1}{20}D_0\phi_{20}\right) \\
&- \frac{2}{3}U_{20}D_0^2\theta_{10} + \left(\frac{7}{20}V_{20} - \frac{\phi_{20}}{20}\right)D_0^2U_{20} - \frac{7}{10}D_0D_1V_{20} + \frac{1}{10}D_0D_1\phi_{20} \\
&+ U_{20}\left(\frac{D_0^2\phi_{20}}{20} - \frac{7D_0^2V_{20}}{20}\right) - \frac{2}{3}D_0U_{20}D_0\theta_{10}
\end{aligned}
$$

$$
\begin{aligned}
&\frac{1}{3}D_0^2U_{21} + \frac{U_a^2}{U_g^2}U_{21} = -\frac{\alpha}{3}D_0U_{20} - \frac{2}{3}D_0D_1U_{20} + \left(\frac{7D_0V_{20}}{10} + \frac{D_0\theta_{10}}{3}\right)D_0\theta_{10} \\
&- \frac{U_a^2}{U_g^2}\left(\frac{3}{5}V_{20}^2 + \frac{\phi_{20}^2}{15} - \frac{V_{20}\phi_{20}}{10}\right) + \left(\frac{7V_{20}}{20} - \frac{\phi_{20}}{20}\right)D_0^2\theta_{10}
\end{aligned} \tag{3.13}
$$

$$
\begin{aligned}
&\frac{7}{20}D_0^2\theta_{11} + 12V_{21} + \frac{13}{35}D_0^2V_{21} - 6\phi_{21} - \frac{11}{210}D_0^2\phi_{21} = -\frac{7\alpha}{20}D_0\theta_{10} - \left(\frac{13\alpha}{35} + 12\beta\right)D_0V_{20} \\
&- \frac{26}{35}D_0D_1V_{20} + \left(\frac{11\alpha}{210} + 6\beta\right)D_0\phi_{20} + \frac{11}{105}D_0D_1\phi_{20} - \frac{7}{10}D_0U_{20}D_0\theta_{10} - \frac{7}{20}U_{20}D_0^2\theta_{10} \\
&- \frac{U_a^2}{U_g^2}\left(\frac{6}{5}V_{20} + \frac{\phi_{20}}{10}\right)U_{20} - \frac{7}{10}D_0D_1\theta_{10}
\end{aligned}
$$

$$
\begin{aligned}
&- \frac{1}{20}D_0^2\theta_{11} - 6V_{21} - \frac{11}{210}D_0^2V_{21} + 4\phi_{21} + \frac{1}{105}D_0^2\phi_{21} = \frac{\alpha}{20}D_0\theta_{10} + \frac{11}{105}D_0D_1V_{20} \\
&- \left(\frac{11\alpha}{210} + 6\beta\right)D_0V_{20} - \left(\frac{\alpha}{105} + 4\beta\right)D_0\phi_{20} - \frac{2}{105}D_0D_1\phi_{20} + \frac{1}{10}D_0U_{20}D_0\theta_{10} \\
&- \frac{1}{20}U_{20}D_0^2\theta_{10} - \frac{U_a^2}{U_g^2}\left(-\frac{V_{20}}{10} + \frac{2\phi_{20}}{15}\right)U_{20} + \frac{1}{10}D_0D_1\theta_{10}
\end{aligned}
$$

It is important to note that there are infinite number of eigenvalues and modes for

a continuum. For nonlinear systems, the linearized mode that is directly excited by an external excitation or indirectly excited by an internal resonance with one of the natural frequencies will survive and all other modes would decay in time. In this case, we consider an internal resonance between the second and third mode and a combination external resonance with third mode. In order to separate the secular terms, we introduce a detuning parameter as follows:

$$\omega_2 = 2\omega_3 + \epsilon\sigma_1, \quad \Omega = \omega_3 + \epsilon\sigma_2 \tag{3.14}$$

To determine the solvability conditions, we seek a particular solution free of secular terms corresponding to the terms proportional to $e^{i\omega_n T_0}$, in the form

$$\begin{aligned} \theta_{11} &= \sum_{i=1}^{4} P_i(T_1)e^{i\omega_i T_0}, \quad U_{21} = \sum_{i=1}^{4} Q_i(T_1)e^{i\omega_i T_0} \\ V_{21} &= \sum_{i=1}^{4} R_i(T_1)e^{i\omega_i T_0}, \quad \phi_{21} = \sum_{i=1}^{4} S_i(T_1)e^{i\omega_i T_0} \end{aligned} \tag{3.15}$$

Substituting equation (3.15) on the left-hand side of equation (3.13) and equations (3.12), (3.14) on the right hand side of equation (3.13), and equating the coefficients of the powers of $e^{i\omega_2 T_0}$ and $e^{i\omega_3 T_0}$, we can determine the solvability conditions, thus eliminating the secular terms. Since we have considered resonance between the second and the third modes, we shall consider only the second and third modes in (3.13) at powers $e^{i\omega_2 T_0}$ and $e^{i\omega_3 T_0}$.

At $e^{i\omega_2 T_0}$

$$\begin{aligned} &-\frac{1}{3}\omega_2^2 P_2 - \frac{7}{20}\omega_2^2 R_2 + \frac{1}{20}\omega_2^2 S_2 = 0 \\ &\left(\frac{U_a^2}{U_g^2} - \frac{\omega_2^2}{3}\right) Q_2 = Y_2 \\ &-\frac{7}{20}\omega_2^2 P_2 + (12 - \frac{13}{35}\omega_2^2)R_2 + (\frac{11}{210}\omega_2^2 - 6)S_2 = 0 \\ &\frac{1}{20}\omega_2^2 P_2 + (\frac{11}{210}\omega_2^2 - 6)R_2 + (4 - \frac{1}{105}\omega_2^2)S_2 = 0 \end{aligned} \tag{3.16}$$

At $e^{i\omega_3 T_0}$

$$
\begin{aligned}
&-\frac{1}{3}\omega_3^2 P_3 - \frac{7}{20}\omega_3^2 R_3 + \frac{1}{20}\omega_3^2 S_3 = Z_1 \\
&\left(\frac{U_a^2}{U_g^2} - \frac{\omega_3^2}{3}\right) Q_3 = Z_2 \\
&-\frac{7}{20}\omega_3^2 P_3 + (12 - \frac{13}{35}\omega_3^2) R_3 + (\frac{11}{210}\omega_3^2 - 6) S_3 = Z_3 \\
&\frac{1}{20}\omega_3^2 P_3 + (\frac{11}{210}\omega_3^2 - 6) R_3 + (4 - \frac{1}{105}\omega_3^2) S_3 = Z_4
\end{aligned}
\tag{3.17}
$$

where

$$
\begin{aligned}
Y_2 &= -\frac{2}{3}A_2^{'}(i\omega_2) + J_{22}A_3^2 e^{-i\sigma_1 T_1} - A_2(i\omega_2)\frac{\alpha}{3} \\
Z_1 &= A_3^{'}(i\omega_3)Z_{11} + A_3(i\omega_3)Z_{d1} + A_2\overline{A}_3 e^{i\sigma_1 T_1} Z_{12} - \frac{Fi}{2}e^{i\sigma_2 T_1} \\
Z_2 &= 0 \\
Z_3 &= A_3^{'}(i\omega_3)Z_{31} + A_3(i\omega_3)Z_{d3} + A_2\overline{A}_3 e^{i\sigma_1 T_1} Z_{32} \\
Z_4 &= A_3^{'}(i\omega_3)Z_{41} + A_3(i\omega_3)Z_{d4} + A_2\overline{A}_3 e^{i\sigma_1 T_1} Z_{42}
\end{aligned}
\tag{3.18}
$$

The terms used in the above equation such as J_2, Z_{11}, Z_{12}, ... are given in Appendix B.

Equations (3.16) and (3.17) are a system of four inhomogeneous equations for P_n, Q_n, R_n, S_n. Considering equation (3.16), the homogeneous parts have a non-trivial solution because the determinant of the co-efficient matrix is

$$
\begin{vmatrix}
-\frac{1}{3}\omega_2^2 & 0 & -\frac{7}{20}\omega_2^2 & \frac{1}{20}\omega_2^2 \\
0 & \frac{U_a^2}{U_g^2} - \frac{\omega_2^2}{3} & 0 & 0 \\
-\frac{7}{20}\omega_2^2 & 0 & \left(12 - \frac{13}{35}\omega_2^2\right) & \left(\frac{11}{210}\omega_2^2 - 6\right) \\
\frac{1}{20}\omega_2^2 & 0 & \left(\frac{11}{210}\omega_2^2 - 6\right) & \left(4 - \frac{1}{105}\omega_2^2\right)
\end{vmatrix} = 0
\tag{3.19}
$$

Equation (3.19) represents the determinant matrix of equation (3.16). Hence the non-trivial solution or the solvability conditions can be determined [35] by replacing the first column in equation (3.19) by the column on the right-hand side of equation (3.16). This

gives

$$\begin{vmatrix} 0 & 0 & -\frac{7}{20}\omega_2^2 & \frac{1}{20}\omega_2^2 \\ Y_2 & \frac{U_a^2}{U_g^2}-\frac{\omega_2^2}{3} & 0 & 0 \\ 0 & 0 & \left(12-\frac{13}{35}\omega_2^2\right) & \left(\frac{11}{210}\omega_2^2-6\right) \\ 0 & 0 & \left(\frac{11}{210}\omega_2^2-6\right) & \left(4-\frac{1}{105}\omega_2^2\right) \end{vmatrix} = 0 \tag{3.20}$$

The above condition yields,

$$\begin{aligned} & Y_2 = -\frac{2}{3}A_2'(i\omega_2) + J_{22}A_3^2 e^{-i\sigma_1 T_1} - A_2(i\omega_2)\frac{\alpha}{3} = 0 \\ & \implies iA_2' = -A_2\frac{\alpha}{2} + \frac{3J_{22}}{2\omega_2}A_3^2 e^{-i\sigma_1 T_1} \\ & \implies iA_2' = -A_2\frac{\alpha}{2} + J_2 A_3^2 e^{-i\sigma_1 T_1} \end{aligned} \tag{3.21}$$

The above equations represent amplitude modulation equations at $e^{i\omega_2 T_0}$. We consider the same analysis as above for equation (3.17). The determinant of the coefficient matrix of equation (3.17) is set to zero and we can write

$$\begin{vmatrix} -\frac{1}{3}\omega_3^2 & 0 & -\frac{7}{20}\omega_3^2 & \frac{1}{20}\omega_3^2 \\ 0 & \frac{U_a^2}{U_g^2}-\frac{\omega_3^2}{3} & 0 & 0 \\ -\frac{7}{20}\omega_3^2 & 0 & \left(12-\frac{13}{35}\omega_3^2\right) & \left(\frac{11}{210}\omega_3^2-6\right) \\ \frac{1}{20}\omega_3^2 & 0 & \left(\frac{11}{210}\omega_3^2-6\right) & \left(4-\frac{1}{105}\omega_3^2\right) \end{vmatrix} = 0 \tag{3.22}$$

Hence, by the same logic used to derive solvability matrix at $e^{i\omega_2 T_0}$ given by equation (3.20), we derive the solvability matrix at $e^{i\omega_3 T_0}$ from equation (3.22) as

$$\begin{vmatrix} Z_1 & 0 & -\frac{7}{20}\omega_3^2 & \frac{1}{20}\omega_3^2 \\ Z_2 & \frac{U_a^2}{U_g^2}-\frac{\omega_3^2}{3} & 0 & 0 \\ Z_3 & 0 & \left(12-\frac{13}{35}\omega_3^2\right) & \left(\frac{11}{210}\omega_3^2-6\right) \\ Z_4 & 0 & \left(\frac{11}{210}\omega_3^2-6\right) & \left(4-\frac{1}{105}\omega_3^2\right) \end{vmatrix} = 0 \tag{3.23}$$

Substituting the values of Z_1, Z_2, Z_3 and Z_4 from equation (3.18) in the above equation (3.23), we derive the solvability conditions as

$$\begin{aligned}
&A_3^{'}(i\omega_3)\{Z_{11}Z_{w1} + Z_{31}Z_{w3} + Z_{41}Z_{w4}\} \\
&+ A_3(i\omega_3)(Z_{d1}Z_{w1} + Z_{d3}Z_{w3} + Z_{d4}Z_{w4}) \\
&+ A_2\overline{A}_3 e^{i\sigma_1 T_1}\{Z_{12}Z_{w1} + Z_{32}Z_{w3} + Z_{42}Z_{w4}\} - \frac{Fi}{2}e^{i\sigma_2 T_1}Z_{w1} = 0 \\
&\implies A_3^{'}(i\omega_3)L_1 + A_3(i\omega_3)Z_{d1} + A_2\overline{A}_3 e^{i\sigma_1 T_1}L_2 - \frac{Fi}{2}e^{i\sigma_2 T_1}Z_{w1} = 0 \\
&\implies A_3^{'} = -A_3 J_{3d} + J_{31}e^{i\sigma_2 T_1} + J_{32}iA_2\overline{A}_3 e^{i\sigma_1 T_1}
\end{aligned} \tag{3.24}$$

where $J_{3d} = (L_{3d}/L_1)$, $J_{31} = (FZ_{w1}/2\omega_3 L_1)$,$J_{32} = (L_2/\omega_3 L_1)$ and the values of $Z_{11}, Z_{31}, ...$ are given in Appendix B. The final amplitude modulation equations are given by (3.21, 3.24). We club them together as

$$\begin{aligned}
iA_2^{'} &= -A_2\frac{\alpha}{2} + J_2 A_3^2 e^{-i\sigma_1 T_1} \\
A_3^{'} &= -A_3 J_{3d} + J_{31}e^{i\sigma_2 T_1} + J_{32}iA_2\overline{A}_3 e^{i\sigma_1 T_1}
\end{aligned} \tag{3.25}$$

Introducing the polar notation $A_n = a_n e^{ib_n}$ and inserting it into the above equation (3.25), we get

$$\begin{aligned}
a_2^{'} &= -\frac{\alpha}{2}a_2 - J_2 a_3^2 \sin\gamma \\
b_2^{'} &= -J_2\frac{a_3^2}{a_2}\cos\gamma \\
a_3^{'} &= -J_{3d}a_3 + J_{31}\cos\delta - J_{32}a_2 a_3 \sin\gamma \\
b_3^{'} &= \frac{1}{a_3}J_{31}\sin\delta + J_{32}a_2\cos\gamma
\end{aligned} \tag{3.26}$$

where $\delta = \sigma_2 T_1 - b_3$, $\gamma = \sigma_1 T_1 + b_2 - 2b_3$ and a_2, b_2, a_3, b_3 represent the polar coordinates (amplitude and phase) of A_2 and A_3 respectively. Modifying coordinates using $x = a_2\cos\gamma$, $y = a_2\sin\gamma$, $z = a_3\cos\delta$ and $w = a_3\sin\delta$, we have the final set of four slow flow equations given by

$$\begin{aligned}
\dot{x} &= -\frac{\alpha}{2}x - \sigma_1 y + 2J_{32}xy + 2J_{31}\frac{yw}{z^2+w^2} \\
\dot{y} &= -\frac{\alpha}{2}y + \sigma_1 x - J_2(z^2+w^2) - 2J_{32}x^2 - 2J_{31}\frac{xw}{z^2+w^2}
\end{aligned} \tag{3.27}$$

$$\dot{z} = -J_{3d}z - \sigma_2 w + J_{31} + J_{32}(xw - yz)$$
$$\dot{w} = -J_{3d}w + \sigma_2 z - J_{32}(yw + xz)$$

In the above equations representing the damped slow flow equations of the beam, J_{3d} is dependent on the Rayleigh damping parameters α and β. For the undamped slow flow equations, we set $\alpha = 0$ and $\beta = 0$ in the above equations, and, as a result, the terms α and J_{3d} will vanish. For the purpose of this Chapter, we call equation (3.27) with non-zero (α, β) as the damped slow flow equations. If $\alpha = \beta = 0$, we call equation (3.27) as the undamped slow flow equations.

3.3 Analysis of the Slow Flow Equations

Before numerically simulating the equations (3.27), we try to understand the nature of these equations. We can observe that

- The first two equations contain a factor $\frac{w}{z^2 + w^2}$. This factor arises from using $z = a_3 \cos\delta$ and $w = a_3 \sin\delta$ in equation (3.26) and, as shown in simulation results, the behavior of $x(t)$ and $y(t)$ is very different than the behavior of $z(t)$ and $w(t)$. It can be seen that x, y depend upon γ, whereas z, w depend upon δ. Additionally from equation (3.26), γ is a function of b_2, b_3, whereas δ is only a function of b_3.

- The relationship between x, y, z, w to the original variables, θ_{10}, U_{20}, V_{20} and ϕ_{20} of the flexible beam is given by equation (3.12) and one can infer the behavior of the original rotating flexible link from the behavior of x, y, z and w. As will be shown in Chapter 4 (section 4.2), z, w go to zero and this implies that V_2 and ϕ_2 (see figure 3.2) also go to zero.

To check if the system given by equation (3.27) is dissipative or not, we calculate the gradient of the volume enclosed by the system. As discussed in Chapter 1, this is given by

$$\text{div } V = \frac{\partial f_1}{\partial x} + \frac{\partial f_2}{\partial y} + \frac{\partial f_3}{\partial z} + \frac{\partial f_4}{\partial w} \tag{3.28}$$

where f_1, f_2, f_3, f_4 respectively, denote the four equations in (3.27). Substituting equation (3.27) into equation (3.28), we have

$$\text{div } V = 2J_{32}y - \alpha + 0 - J_{32}y - J_{32}y - 2J_{3d} = -(\alpha + 2J_{3d}) \tag{3.29}$$

From equation (3.29), we can observe that the divergence is nonzero *iff* $\alpha + 2J_{3d} > 0$, i.e., the system is dissipative and the volume enclosed by the system is not preserved for all values of parameter U_g. Hence, the system of equations can have chaotic attractors or repellors. For an undamped system, α and J_{3d} are zero, and hence the gradient for an undamped system, as given by equation (3.29), can be seen to be zero. This implies that the undamped system is conservative and the volume enclosed by such a system is preserved for all U_g. Such a system cannot have chaotic attractors and repellors.

Fixed points

The fixed points of the slow flow equations given by equations (3.27) are obtained by setting $\dot{x} = \dot{y} = \dot{z} = \dot{w} = 0$. We first consider the undamped slow flow equations obtained by setting α and J_{3d} as zero in equation (3.27). After simplification, the fixed point of the system are obtained as $(x_{e_1}, 0, 0, w_{e_1})$ where (x_{e_1}, w_{e_1}) are given by

$$\begin{aligned} x_{e_1} &= \frac{N^{1/3}}{6J_{32}(\sigma_1 - 2\sigma_2)} + \frac{2\sigma_2^2(\sigma_1 - 2\sigma_2)}{3J_{32}N^{1/3}} + \frac{2\sigma_2}{3J_{32}} \\ w_{e_1} &= \frac{J_{31}}{\sigma_2 - J_{32}xe_1} \end{aligned} \tag{3.30}$$

where

$$\begin{aligned} N &= (\sigma_1 - 2\sigma_2)^2 \times \\ &\{8\sigma_2^3\sigma_1 + 16\sigma_2^4 + 108J_{32}J_{22}J_{31}^2 \\ &+ 12J_{31}J_{32}\sqrt{\frac{3J_{22}(-4\sigma_2^3\sigma_1 + 8\sigma_2^4 + 27J_{32}J_{22}J_{31}^2)}{J_{32}}}\} \end{aligned} \tag{3.31}$$

The fixed points of the undamped slow flow equations for different values of U_g can be computed from equation (3.30) and (3.31). The fixed points for representative U_g values are given in Table 3.2 below. The damped slow flow equations given by equations (3.27), where $\alpha \neq 0$, $J_{3d} \neq 0$, have *no fixed points* although the damped slow flow equations

Table 3.2: Fixed points of undamped slow flow equations

U_g	Fixed points
250	(-67.8988,0,0,-4.0000 +58.1750i), (-67.8988,0,0,-4.0000 -58.1750i), (0,0,0,2)
150	(0,0,0,0), (-24.3996,0,0,-0.5000 +77.6724i), (-24.3996,0,0,-0.5000 -77.6724i)
100	(0,0,0,0.1250), (-10.8228,0,0,-122.75-0.06199i), (-10.8228,0,0,123.5+0.06199i)
50	(0,0,0,0), (-2.6902,0,0,-27.5044 + 0.0004i), (-2.6902,0,0,27.5058 - 0.0004i)

show the existence of an attractor. Since there are no fixed points, the attractor can be an attracting limit cycle.

3.4 Numerical Simulation

We now present the numerical simulation of the damped and undamped slow flow equations of the flexible beam given by equation (3.27). We check the equations for the existence of chaos by considering as parameter the non-dimensional characteristic velocity U_g. For this purpose, we use phase plots, Poincaré maps and Lyapunov exponents described in Chapter 1. To perform the numerical study of the system in equation (3.27), we use the parameters given in Table 3.1. All simulations were done using MATLAB 2012Rb [17] and $ode15s$ solver was used to solve the differential equations. The relative and absolute tolerances were kept at 10^{-6} and 10^{-9} respectively. The results were verified to converge to those shown in this section for lower values of tolerances.

Figures (3.3-3.4) show the numerical simulation results of the undamped slow flow equations given by setting α and J_{3d} as zero in equation (3.27). Figure 3.3 show the Poincaré maps of the undamped slow flow system. All the maps shown in figure 3.3 are magnified. Figure 3.3 (a) shows the formation of nonlinear resonance islands at $U_g = 250$. The resonance islands can be observed as elliptic formations, and the appearance of

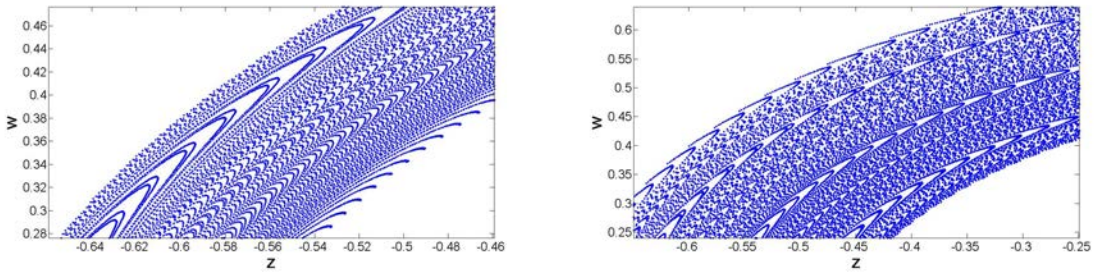

(a) $U_g = 250$ (b) $U_g = 150$

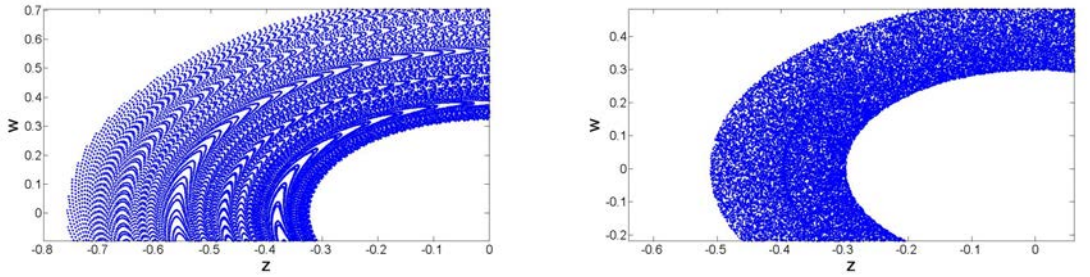

(c) $U_g = 100$ (d) $U_g = 50$ – Chaos

Figure 3.3: Poincaré maps for the undamped slow flow equations

'straight lines' in between the islands, known as invariant tori [107, 108]. Figures 3.3 (b,c) show the Poincaré maps at $U_g = 150$ and $U_g = 100$. We can see that with the decrease in the value of the parameter U_g, the islands are slowly destroyed, implying that nonlinear resonances overlap to break the tori and produce chaotic motion as shown in figure 3.3 (d) with the map filled with chaotic trajectories as shown.

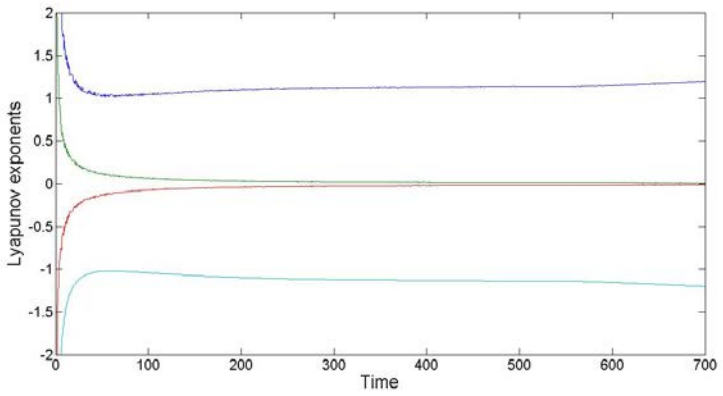

Figure 3.4: Plot of Lyapunov exponents at $U_g = 50$ – undamped case

To confirm chaos, we compute the largest Lyapunov exponent. In figure 3.4, the spectrum of Lyapunov exponents is shown for $U_g = 50$. It can be easily observed from this figure, that the largest Lyapunov exponent is positive, and hence chaos exists at $U_g = 50$.

Figures (3.5-3.6) show the numerical simulation of equation (3.27), representing the damped slow flow equations. The map shown in figure 3.5 (c) is magnified and one can observe the dissipative motion of the system towards the attractor and with the curves winding up on a attractor.

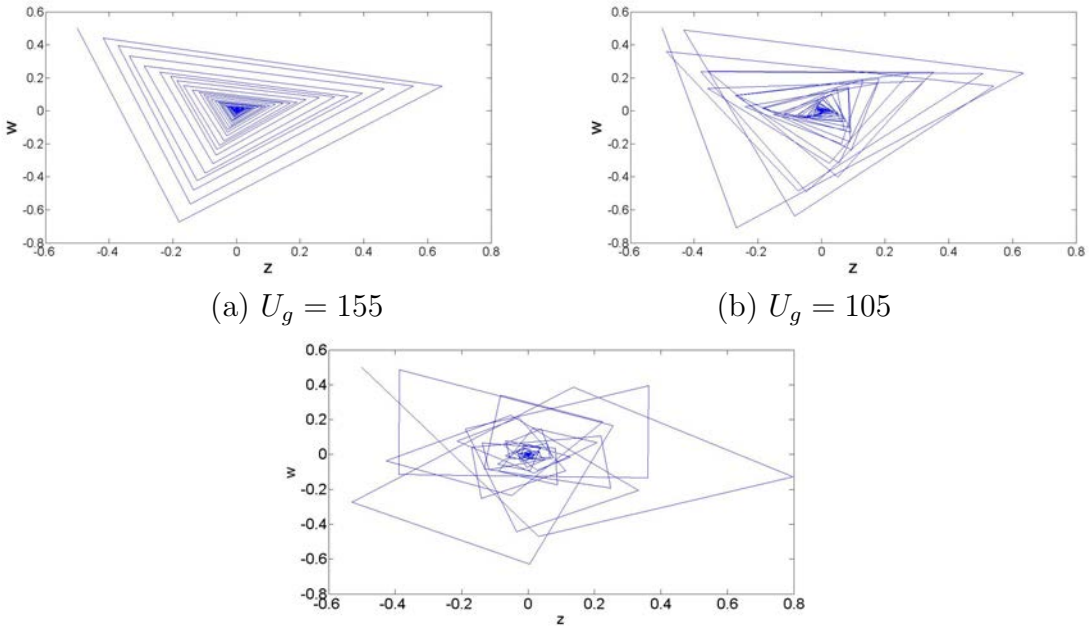

(a) $U_g = 155$ (b) $U_g = 105$

(c) $U_g = 50$

Figure 3.5: Phase plots for the damped slow flow equations

In figure 3.6, the spectrum of Lyapunov exponents is shown for $U_g = 105$. It can be observed from this figure, that the largest Lyapunov exponent is positive, and hence chaos exists at $U_g = 105$ and the attractors shown in the phase plots for $U_g \leq 105$ are chaotic attractors.

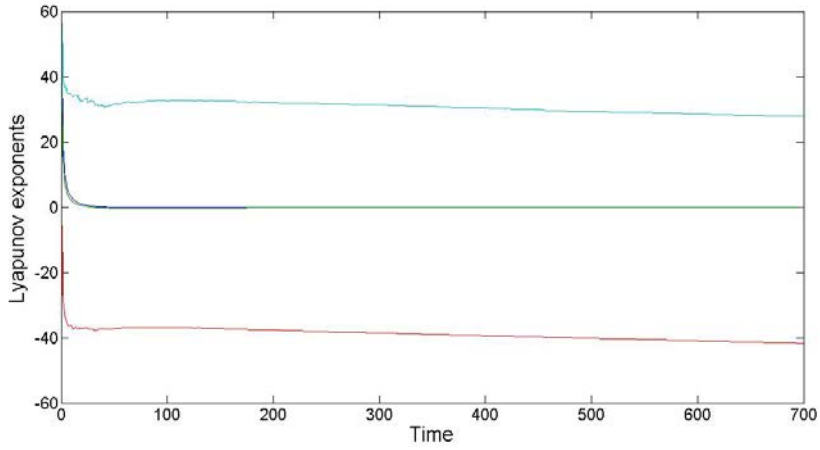

Figure 3.6: Spectra of Lyapunov exponents at $U_g = 105$ – damped case

Observations

From the results presented, it can be observed that in the undamped system of equations chaos occurs by the breaking up of tori by the overlap of nonlinear resonances. For the damped system, however, chaos occurred by the motion settling onto an attractor. The reason for this different routes to chaos is due to the fact that the damped system of equations, as shown in section 3.3, are dissipative. Thus the volume of the system in state space reduces until it settles onto an attractor. On the other hand, the undamped equations are conservative, i.e., the volume of the system in state space is conserved for all values of system parameter U_g. Chaos in conservative systems occurs by the mixing of nonlinear resonances to break the tori as described earlier.

From the numerical simulation results, it can be also seen that the chaotic motion for the undamped slow flow equations appears at $U_g = 50$ and for the damped slow flow equations at $U_g = 105$. From extensive simulations, it was observed that for U_g greater than 150, there is no chaos for the undamped slow flow equations. If we assume that the rotating wind turbine blade has a uniform circular cross-section, using the parameter values in Table 3.1 and from equation (3.7) we obtain that an U_g value of 150 corresponds to $R \approx 34.08$ cm. Hence, to avoid chaotic motion, the radius of the blade must be more than 34.08 cm. Likewise, for the damped slow flow equations, for an U_g value greater than 200, no chaos is observed in simulations. Using equation (3.7), the corresponding radius of the blade is $R \approx 45.44$ cm and hence, in order to avoid chaotic motion, the

radius of the blade must be more than 45.44 cm. It may be noted that a rotating wind turbine blade will be subjected to torsion as well as bending and in that sense, the U_g and corresponding R values are only indicative. Nevertheless, the chaotic dynamic analysis presented in this work can be used in the initial design of the wind turbine blades.

3.5 Concluding Remarks

This Chapter dealt with the chaotic dynamics of a flexible rotating beam with large deformation and geometric nonlinearities. The equations of motion were obtained as a set of four ordinary differential equations and were non-dimensionalized using two characteristic velocities representing the speed of sound (U_a) and speed of transverse vibrations (U_g). A perturbation analysis was done to study the nonlinear system at a slower time scale and the slow flow equations were derived from the original nonlinear ordinary differential equations by the method of multiple scales. Both the undamped and damped system of equations were obtained and analyzed. The slow flow equations were simulated numerically to investigate the existence of chaos. From the numerical simulation results, it can be concluded that in both undamped and damped cases chaos is obtained below certain values of U_g. The practical application of this analysis would be in the initial design of a rotating wind turbine blades where the radius of the blade could be chosen to avoid possible chaotic motion.

Chapter 4

Synchronization of Chaos in a Rotating Flexible Link

In the previous Chapter, we analyzed the chaotic motion of a flexible rotating link, modeled as a one link flexible beam. We performed a multiple scales analysis on the equations of motion of the beam and derived four first-order autonomous equations, also known as slow flow equations, of the system which represent the solvability conditions for the beam's equations to have a solution. The slow flow equations were shown to be chaotic. In this Chapter, we develop a method for controlling chaos using a technique known as chaos synchronization.

In the recent past, chaos synchronization has received significant attention after the work of Pecora et al. [69, 70]. The idea behind chaos synchronization is as follows. Any chaotic system, by definition, is sensitive to initial conditions. The same chaotic system, when simulated with one set of initial conditions shows one particular kind of behavior. But when the initial conditions are altered, even slightly, the behavior of the system radically changes. Chaos synchronization is a technique by which the behavior of the chaotic system at *different initial conditions* is *synchronized*, i.e., irrespective of the initial conditions of the system, the behavior of the system, after synchronization, does not change. The implication of this is that the core feature of chaos, which is sensitivity to initial conditions, is nullified.

We consider a chaotic system-known as the *drive system*, which we operate at one set of initial conditions. We then consider an identical system to the drive system-known

as the *response system*, which we operate at a different set of initial conditions. In the absence of a controller, the behavior of the drive and response systems after some period of time, will diverge due to the property of chaotic systems, i.e., sensitivity to initial conditions. The central idea of synchronization is to design a controller such that the response system asymptotically tracks the drive system. This means the behavior of both the systems will converge, thus nullifying the property of sensitivity to initial conditions.

The chaos synchronization approach is conceptual. More work needs to be done to implement this on a physical system and such an implementation or its details (real-time, measurement of states and its relationship to the actual variables of the rotating link, output of the controller etc.) is outside the scope of this work. To describe chaos synchronization conceptually, consider

$$\begin{aligned} \dot{X}_d &= f(X_d) && \text{Drive System} \\ \dot{X}_r &= f(X_r) + U && \text{Response System} \end{aligned} \tag{4.1}$$

where X_d, X_r are the vectors of state variables of the drive and response systems respectively, while U is the vector of controllers. The idea of chaos synchronization is to design U such that X_r tracks X_d and the error between the two goes to zero. To implement the controller, we follow the scheme as shown in Figure 4.1.

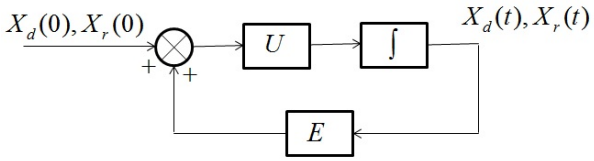

Figure 4.1: Schematic of Controller for Chaos Synchronization

In figure 4.1, the inputs are the vectors of initial conditions $X_d(0), X_r(0)$ of the drive and response systems respectively. The difference between the two will be the initial error vector $E(0)$. The initial error vector and the initial response vector will be used to compute the control law U. The control law is then substituted into the second part of equation (4.1), which in turn is integrated to calculate the response vector $X_r(t)$. The drive vector $X_d(t)$ is computed by integrating the first part of equation (4.1). Now the error vector is computed as $E = X_d(t) - X_r(t)$. This error is resubstituted to compute the control law U.

A number of approaches for chaos synchronization already exist in literature and were presented in Chapter 1. Apart from those mentioned in Chapter 1, global chaos synchronization was studied using sliding mode control [109, 110] on the Li-Wu and the Zhu systems, respectively. Chaos Synchronization of chaotic chua system with cubic nonlinearity in complex coupled networks [111] and modified projective synchronization of different order chaotic systems with adaptive scaling factor [112] were also studied.

In this Chapter, we perform the chaos synchronization of the equations of a flexible rotating link studied in the previous Chapter. In Chapter 3, we studied the chaotic dynamics of a flexible link modeled as a beam, which for practical purposes, we considered as representing a rotating power generating wind turbine blade. We then derived (using MMS) four first-order autonomous slow flow equations (equation (3.27)). In this Chapter, we reintroduce those equations and explain the nature of chaos in those those equations. Then we develop an active nonlinear control scheme, using Lyapunov stability theory, to synchronize the chaotic slow flow equations represented by equation (3.27).

4.1 Chaos Synchronization of a rotating flexible link

The slow flow equations (3.27) of the flexible rotating link developed in Chapter 3 using MMS are given by

$$\begin{aligned}
\dot{x} &= -\frac{\alpha}{2}x - \sigma_1 y + 2J_{32}xy + 2J_{31}\frac{yw}{z^2+w^2} \\
\dot{y} &= -\frac{\alpha}{2}y + \sigma_1 x - J_2(z^2+w^2) - 2J_{32}x^2 - 2J_{31}\frac{xw}{z^2+w^2} \\
\dot{z} &= -J_{3d}z - \sigma_2 w + J_{31} + J_{32}(xw - yz) \\
\dot{w} &= -J_{3d}w + \sigma_2 z - J_{32}(yw + xz)
\end{aligned} \tag{4.2}$$

The above equations are chaotic as demonstrated in Chapter 3 and owing to the property of chaotic systems of being sensitive to initial conditions, that prediction of state output of equation (4.2) is nearly impossible after some time. Our task is to construct a controller to ensure that irrespective of the particular initial conditions, the system given by equation (4.2) gives a predictable output, i.e., the behavior of the state output remains the same. We attempt to do this by constructing a nonlinear controller

using Lyapunov stability theory. First we construct the drive and response systems, as described in the first part of this Chapter, identical to equation (4.2). The drive and the response systems are given by

$$\begin{aligned}
\dot{x_d} &= -\frac{\alpha x_d}{2} - \sigma_1 y_d + 2J_{32} x_d y_d + 2J_{31}\frac{y_d w_d}{{z_d}^2 + {w_d}^2} \\
\dot{y_d} &= -\frac{\alpha y_d}{2} + \sigma_1 x_d - J_2({z_d}^2 + {w_d}^2) - 2J_{32}{x_d}^2 - 2J_{31}\frac{x_d w_d}{{z_d}^2 + {w_d}^2} \\
\dot{z_d} &= -J_{3d} z_d - \sigma_2 w_d + J_{31} + J_{32}(x_d w_d - y_d z_d) \\
\dot{w_d} &= -J_{3d} w_d + \sigma_2 z_d - J_{32}(y_d w_d + x_d z_d)
\end{aligned} \tag{4.3}$$

and

$$\begin{aligned}
\dot{x_r} &= -\frac{\alpha x_r}{2} - \sigma_1 y_r + 2J_{32} x_r y_r + 2J_{31}\frac{y_r w_r}{{z_r}^2 + {w_r}^2} + u_1 \\
\dot{y_r} &= -\frac{\alpha y_r}{2} + \sigma_1 x_r - J_2({z_r}^2 + {w_r}^2) - 2J_{32}{x_r}^2 - 2J_{31}\frac{x_r w_r}{{z_r}^2 + {w_r}^2} + u_2 \\
\dot{z_r} &= -J_{3d} z_r - \sigma_2 w_r + J_{31} + J_{32}(x_r w_r - y_r z_r) + u_3 \\
\dot{w_r} &= -J_{3d} w_r + \sigma_2 z_r - J_{32}(y_r w_r + x_r z_r) + u_4
\end{aligned} \tag{4.4}$$

where the lower subscript d and r stand for drive and response system respectively, and $u_i,\ i = 1, 2, 3, 4$ are the control which synchronizes the two chaotic systems. The two systems given by equations (4.3, 4.4) shall be operated at different initial conditions, hence producing different state outputs both of which are unpredictable owing to their chaotic nature. Under active control (u_i), if the error between the drive and response systems given by equation (4.3) and equation (4.4) respectively, goes to *zero*, then the two systems stand synchronized and our goal shall be deemed to have been achieved. For that, we consider the error between the equations of the drive and response systems as

$$\begin{aligned}
\dot{e_1} &= -\frac{\alpha e_1}{2} - \sigma_1 e_2 + 2J_{32}(x_r e_2 + y_r e_1 - e_1 e_2) + 2J_{31}\frac{y_r w_r}{{z_r}^2 + {w_r}^2} \\
&- 2J_{31}\frac{(y_r - e_2)(w_r - e_4)}{(z_r - e_3)^2 + (w_r - e_4)^2} + u_1 \\
\dot{e_2} &= -\frac{\alpha e_2}{2} + \sigma_1 e_1 - J_2(e_3(2z_r - e_3) + e_4(2w_r - e_4)) \\
&- 2J_{32}(e_1(2x_r - e_1)) - 2J_{31}\frac{x_r w_r}{{z_r}^2 + {w_r}^2} + 2J_{31}\frac{(x_r - e_1)(w_r - e_4)}{(z_r - e_3)^2 + (w_r - e_4)^2} + u_2
\end{aligned}$$

$$\begin{aligned}
\dot{e_3} &= -J_{3d}e_3 - \sigma_2 e_4 + J_{31} \\
&+ J_{32}(x_r e_4 + w_r e_1 - e_1 e_4 - y_r e_3 - z_r e_2 + e_2 e_3) + u_3 \\
\dot{e_4} &= -J_{3d}e_4 + \sigma_2 e_3 - J_{32}(x_r e_3 + z_r e_1 - e_1 e_3 + y_r e_4 + w_r e_2 - e_2 e_4) + u_4
\end{aligned} \tag{4.5}$$

where $e_1 = x_r - x_d$, $e_2 = y_r - y_d$, $e_3 = z_r - z_d$ and $e_4 = w_r - w_d$ represent the errors of the four state variables of the drive and response systems respectively. If these error states go asymptotically to zero, then the drive and the response system will be synchronized. For this end, we must propose the use of a control input $u = [u_1, u_2, u_3, u_4]^T$ which makes the error states asymptotically go to zero. Using the Lyapunov second method for stability, consider the candidate Lyapunov function

$$V = (1/2)({e_1}^2 + {e_2}^2 + {e_3}^2 + {e_4}^2) \tag{4.6}$$

The differential of the Lyapunov function along the trajectory of the system is

$$\dot{V} = e_1\dot{e_1} + e_2\dot{e_2} + e_3\dot{e_3} + e_4\dot{e_4} \tag{4.7}$$

Substituting equation (4.5) in equation (4.7), we get

$$\begin{aligned}
\dot{V} &= -\frac{\alpha}{2}{e_1}^2 - \frac{\alpha}{2}{e_2}^2 - J_{3d}{e_3}^2 - J_{3d}{e_4}^2 \\
&+ J_{32}(y_r(2{e_1}^2 - {e_3}^2 - {e_4}^2) - 2x_r e_1 e_2) + (J_{32} + J_2)e_2({e_3}^2 + {e_4}^2) \\
&- z_r(e_2 e_3(J_{32} + J_2) + J_{32}e_1 e_4) + w_r(e_1 e_3 J_{32} - (J_{32} + J_2)e_2 e_4) \\
&+ 2J_{31}(x_r e_2 - y_r e_1)Q_1 + u_1 e_1 + u_2 e_2 + u_3 e_3 + u_4 e_4
\end{aligned} \tag{4.8}$$

For asymptotic stability according to the Lyapunov second method, we must have $V > 0$ and $\dot{V} < 0$. It can be seen from equation (4.6) that $V > 0$. To ensure $\dot{V} < 0$, the control input $u = [u_1, u_2, u_3, u_4]^T$ in equation (4.8) must be designed accordingly. Hence, we propose the following control law,

$$\begin{aligned}
u_1 &= \left(\frac{\alpha}{2} - 1\right)e_1 + J_{32}(2e_2 x_r - 2e_1 y_r + e_4 z_r - e_3 w_r) + 2J_{31}y_r Q_1 \\
u_2 &= \left(\frac{\alpha}{2} - 1\right)e_2 - (J_{32} + J_2)({e_3}^2 + {e_4}^2) \\
&+ (J_{32} + 2J_2)(e_3 z_r + e_4 w_r) - 2J_{31}x_r Q_1 \\
u_3 &= (J_{3d} - 1)e_3 + J_{32}y_r e_3, \qquad u_4 = (J_{3d} - 1)e_4 + J_{32}y_r e_4
\end{aligned} \tag{4.9}$$

where

$$Q_1 = \left(\frac{w_r - e_4}{(z_r - e_3)^2 + (w_r - e_4)^2} - \frac{w_r}{(z_r)^2 + (w_r)^2} \right) \tag{4.10}$$

Substituting (4.9) into (4.8), we have

$$\dot{V} = -{e_1}^2 - {e_2}^2 - {e_3}^2 - {e_4}^2 < 0 \tag{4.11}$$

and we can obtain asymptotic stability in the sense of Lyapunov.

The above analysis shows that the chaotic systems (4.3) and (4.4) are synchronized for any initial conditions with the use of the control law (4.9). In the next section, we present numerical simulation results illustrating synchronization.

4.2 Numerical Simulation

In this section we verify the effectiveness of the control law proposed in section 4.1. We numerically simulate equations (4.3), (4.4), and (4.5) from section 4.1. To perform the numerical simulation, we use the parameters given in Table 3.1 for the power generating wind turbine blade. All simulations are done in MATLAB 2012Rb [17] and *ode*15*s* solver was used to solve the differential equations. The relative and absolute tolerances were kept at 10^{-6} and 10^{-9} respectively. We verified that the results converged to those presented in this section for lower values of tolerances. For both the undamped and damped slow flow equations, we have used $U_g = 50$ in the numerical simulations.

For numerical simulations in this section, we use the MATLAB command *randi* to generate random initial conditions and consider these as the initial conditions for the *drive system* given by equation (4.3). Since equation (4.3) is chaotic (sensitive to initial conditions) for particular values of system parameter U_g, we slightly perturb the above initial conditions, and consider them as the initial conditions for the response system given by equation (4.4).

$$\begin{aligned} (x_d(0), y_d(0), z_d(0), w_d(0)) &= (-0.3538, -1.5771, 0.2820, -1.3337) \quad \text{Drive System} \\ (x_r(0), y_r(0), z_r(0), w_r(0)) &= (-0.34, -1.5771, 0.2820, -1.3337) \quad \text{Response System} \end{aligned} \tag{4.12}$$

Using the above initial conditions, we plot the time responses of the damped slow flow equations for two state variables (x, y) of the drive and response systems with and without control (figure 4.2).

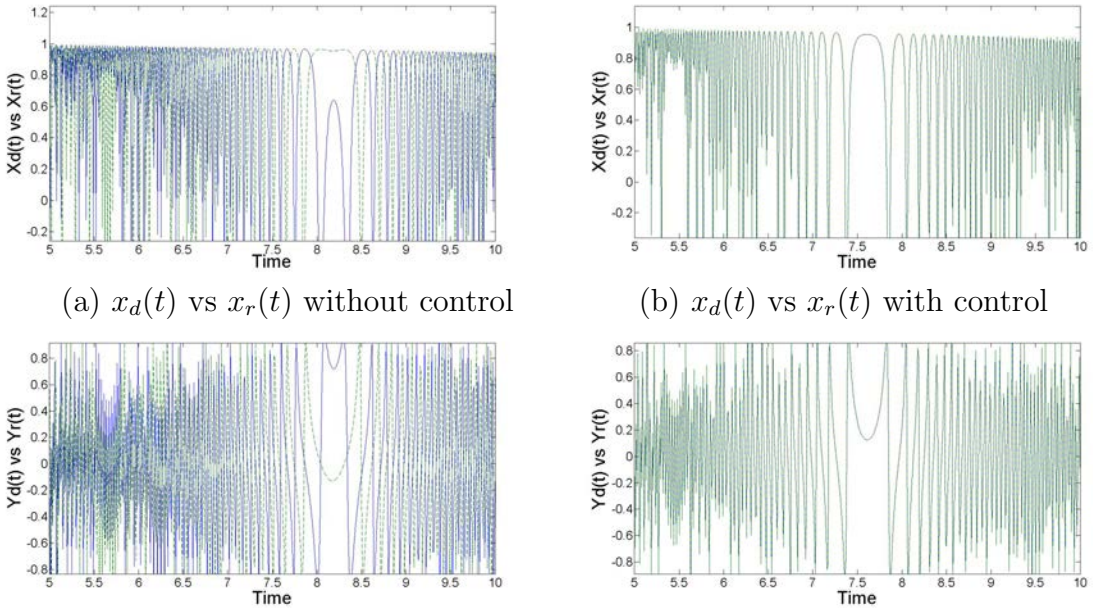

(a) $x_d(t)$ vs $x_r(t)$ without control

(b) $x_d(t)$ vs $x_r(t)$ with control

(c) $y_d(t)$ vs $y_r(t)$ without control

(d) $y_d(t)$ vs $y_r(t)$ with control

Figure 4.2: Magnified image of time series of state variables (x, y) of the damped slow flow equations with and without control

The figures have been magnified for clarity with the solid lines representing the drive system, whereas the dashed lines represent the response system. As seen from the figure 4.2, the motions of response system and the drive system are different when no controller is present and there is divergence in the drive and response systems. Whereas in the presence of the controller, the response system asymptotically tracks the drive system – the dashed lines are not visible as they lie on top of the solid lines implyingg asymptotic tracking of the response system with the drive system. The asymptotic tracking is more evident in figures (4.3, 4.4) where the error, given in equations (4.5), between the drive and response system is plotted for the damped and undamped equations respectively. It can be clearly seen that the controller drives the error to zero.

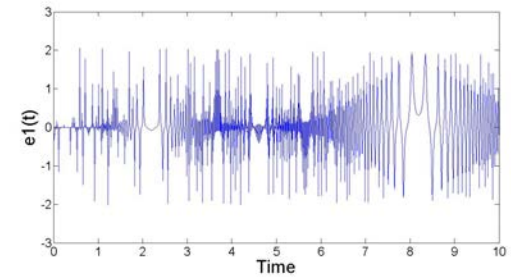

(a) $e_1(t)$ vs time (without control)

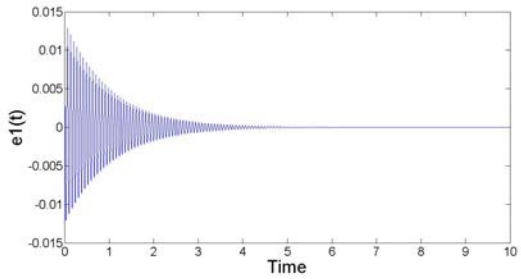

(b) $e_1(t)$ vs time (with control)

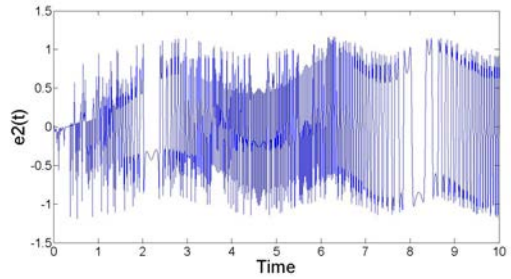

(c) $e_2(t)$ vs time (without control)

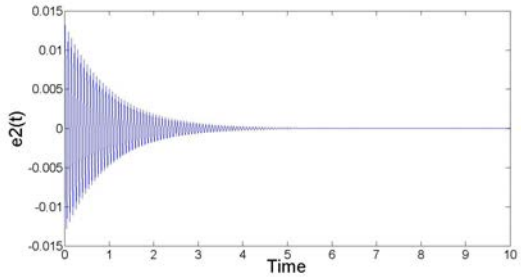

(d) $e_2(t)$ vs time (with control)

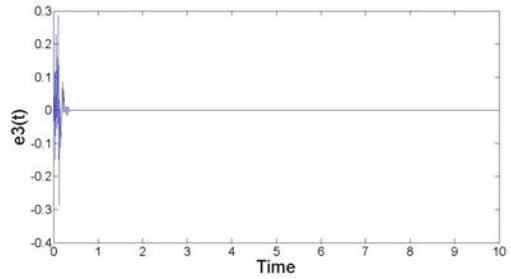

(e) $e_3(t)$ vs time (without control)

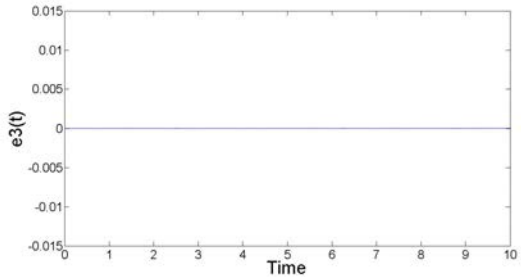

(f) $e_3(t)$ vs time (with control)

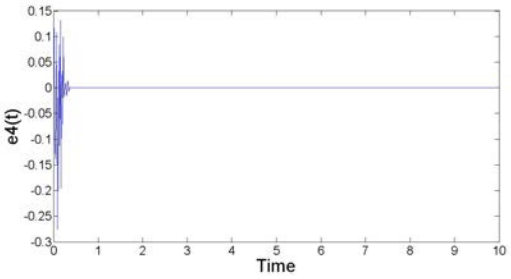

(g) $e_4(t)$ vs time (without control)

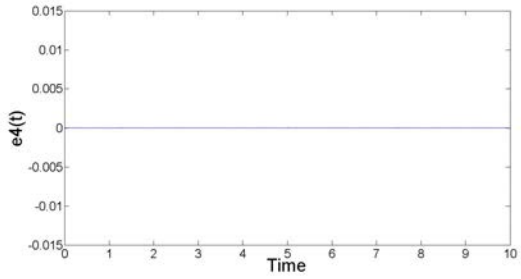

(h) $e_4(t)$ vs time (with control)

Figure 4.3: Plots of the error of the damped slow flow equations with respect to time with and without control

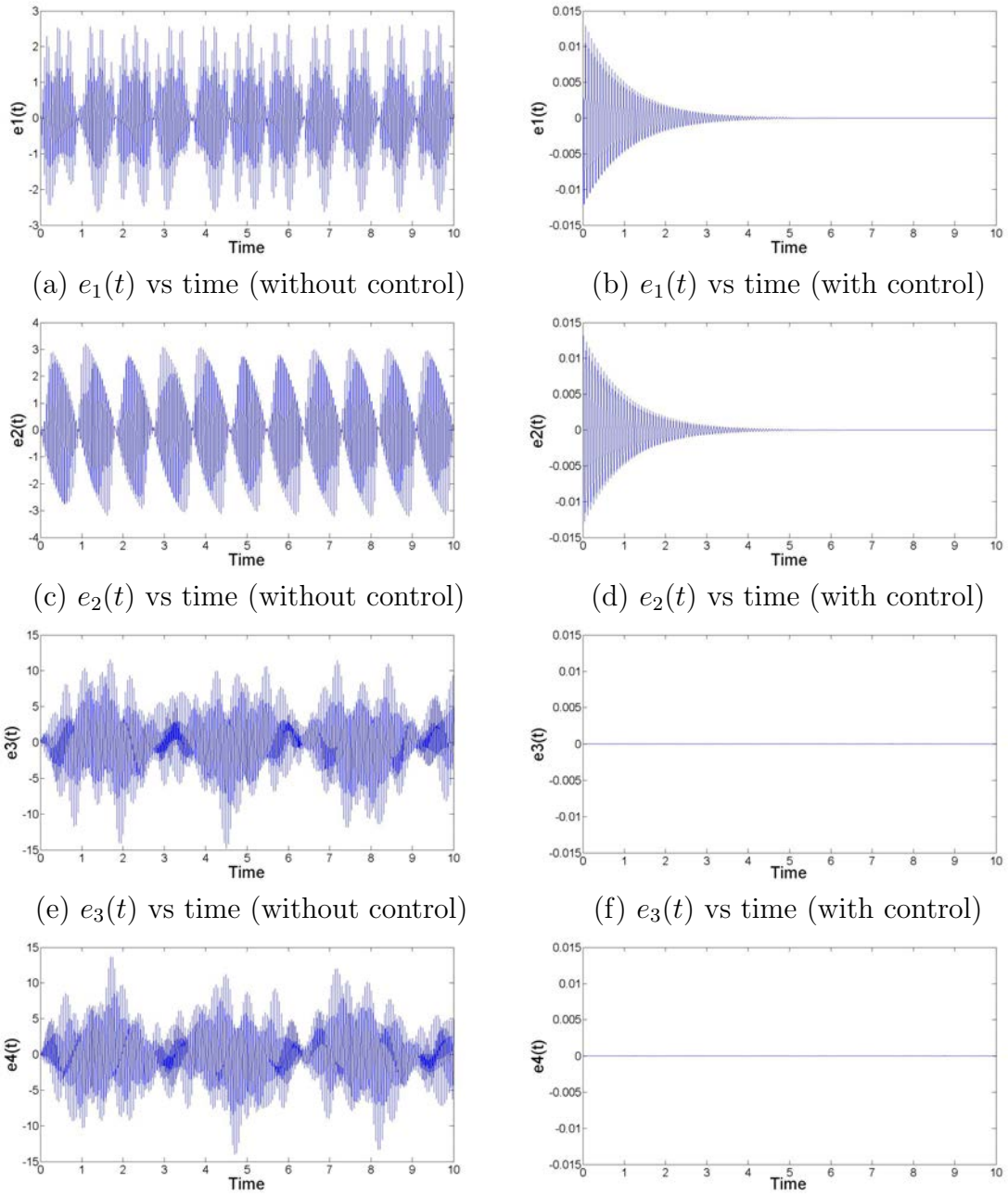

(a) $e_1(t)$ vs time (without control)

(b) $e_1(t)$ vs time (with control)

(c) $e_2(t)$ vs time (without control)

(d) $e_2(t)$ vs time (with control)

(e) $e_3(t)$ vs time (without control)

(f) $e_3(t)$ vs time (with control)

(g) $e_4(t)$ vs time (without control)

(h) $e_4(t)$ vs time (with control)

Figure 4.4: Plots of the error of the undamped slow flow equations with respect to time with and without control

Observations

From the results presented, it can be observed that the control law given by equation (4.9) is successful in forcing the response system (equation (4.4)) to track the drive system (equation (4.3)). The error state variables given by equation (4.5) are plotted with and without the use of the controller. Figures (4.3, 4.4) show the plots of the damped and undamped slow flow equations with and without control. It can be observed that in the absence of the controller, the errors are large, whereas in the presence of the controller the errors asymptotically go to zero. Thus the response system with the controller asymptotically tracks the drive system and chaos synchronization has been achieved.

It is interesting to observe that for the damped slow flow equations, the errors $e_3(t)$ and $e_4(t)$ (related to $z(t)$ and $w(t)$) go to zero even without the controller (see figure 4.3 (e) and (g)). This can be more clearly seen from the phase plots for the damped slow flow equations (shown in Chapter 3) where we can see that the state variables z and w go to zero in both the chaotic case and the non-chaotic case. Figure 4.5 shows illustration of this, where irrespective of the chaoticity, the two state variables z, w tend to zero – the spiral trajectory in the $z - w$ plane can be clearly seen in figure 4.5.

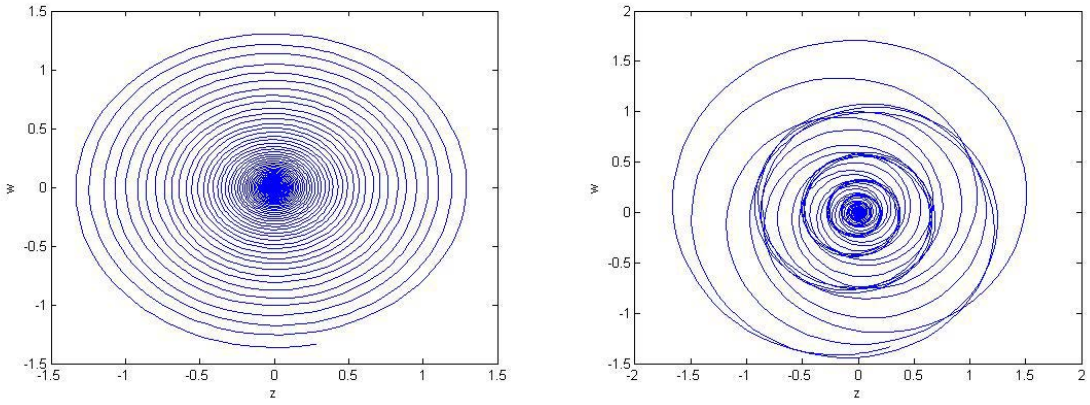

(a) $U_g = 400$ – non-chaotic case (b) $U_g = 100$ – chaotic case

Figure 4.5: Phase plots for the damped slow flow equations

4.3 Concluding Remarks

In this Chapter, we investigate the synchronization of chaos in a flexible rotating beam, whose equations were developed in Chapter 3. A nonlinear control law for asymptotic chaos synchronization was proposed. The nonlinear control law is derived using Lyapunov stability theory and numerical simulations demonstrated the effectiveness of the control law with the response system asymptotically tracking the drive system.

Chapter 5

Conclusions and Future Work

5.1 Conclusions

In this Chapter, we summarize the work presented in this thesis and present some of the scope for future work in this research area.

The two problems studied in this thesis had a common theme binding them, i.e., the presence of chaotic motion in their governing equations. The study of chaotic equations has had a long history with several interesting problems. One such problem was considered in Chapter 2, with the demonstration of the ranges of parameter gain values of asymptotic stability of a 2R planar robot driven by PD and model based control (absence of chaos implies asymptotic stability). Results in literature had demonstrated a numerical way of deriving such ranges of parameter gains. In Chapter 2, we demonstrated an analytical approach of deriving such ranges using the Routh-Hurwitz criterion. Numerical simulations were done to compute these ranges which are also known as chaos maps. The asymptotically stable regions of parameter gains were examined with variation in the forcing frequency (in the case of PD control), whereas they were examined with respect to the model mismatch parameter in the case of model based control. The results verified the numerical approaches used in literature.

In Chapter 3, we demonstrated the chaotic motion of a one link flexible beam, whose equations were derived from a finite element model of the beam. We considered a single element in the modeling. We also found out various values of parameter U_g (characteristic

velocity associated with bending) for which the equations show chaos. We assumed the equations represented a model of a power generating wind turbine blade with uniform circular cross section. Numerical simulations verified the existence of chaotic motion. The flexible beam, however showed two different types of chaotic motion depending upon whether damping (in the form of Rayleigh damping) was present or absent. If damping was present, the beam system became dissipative in nature and the motion of the beam wound up on an attractor. In the absence of damping, the beam system showed conservation of volume in state space and the route to chaos was by the breaking up to tori due to the *chaotic mixing* of nonlinear resonances.

In Chapter 4, we demonstrated the synchronization of chaotic motion of the equations of the flexible beam developed in Chapter 3. To this effect, we used active nonlinear control and Lyapunov stability theory. The use of active nonlinear control is justified by its simplicity of usage. Numerical simulations verified the control law proposed for chaos synchronization.

The core method used in the two problems solved in this thesis is the method of multiple scales. The problems were shown to be bounded by using the method of multiple scales, which was represented by the presence of *solvability conditions* as a result of performing the analysis at various time scales. The method of multiple scales (MMS) is useful for two reasons:

- Numerical integration at slower time scales is faster than that of the full original system of equations. Studies of the effects of various parameters on the system can be conducted more effectively and extensively.

- MMS converts equations that are non-autonomous (forced equations given by the equations of both the system we considered in the thesis) into autonomous equations (solvability conditions or slow flow equations), making it easier to analyze.

The full range of engineering problem solvable by MMS is yet to be seen. We close by the concluding remark that there exists a variety of problems yet to be explored and solved by classical method of multiple scales.

5.2 Scope for Future Work

In Chapter 2, we derived an analytical approach for testing the asymptotic stability of a 2R planar robot for trajectory tracking. In the analytical procedure, the Routh-Hurwitz criterion was used, according to which if the co-efficients of the characteristic equation derived from the jacobian of the slow flow equations (see Chapter 2) satisfied particular conditions, then the 2R robot system was asymptotically stable. However the success was only partial. This is due to the fact that if any of the co-efficients were zero, then asymptotic stability was indeterminate. This means that although we could determine ranges of asymptotic stability at some values of parameter gains, the ranges where the Routh-Hurwitz criterion did not show asymptotic stability could not be concluded as *asymptotically unstable* – they could also be indeterminate. We resolved the indeterminacy, but we used a numerical approach for doing so. One problem for the future work could be to attempt find a complete analytical procedure for deriving such ranges of asymptotic stability.

In Chapter 3, we studied chaotic motions in a rotating flexible beam. We assumed that the equations of the beam represented a model of a power generating wind turbine blade with uniform circular cross section. It is not clear if the same method used for studying the beam's dynamics is applicable for models where the cross-section is not uniform. We also considered the beam to be a single element in the finite element model used to derive the beam's equations. The applicability of the method where the model consists of more than one element in the finite element model is possible area of future work.

In Chapter 4, we developed an active nonlinear controller using Lyapunov stability theory for synchronization the chaotic slow flow equations of the flexible beam developed in Chapter 3. Such control procedures are used for their simplicity and the same method has been used in literature of chaos synchronization for many systems. However, these exists almost no method of *unified* chaos synchronization of any system, let alone a class of systems. The only proposal so far known was given by Wu et al. [114] where the authors demonstrated chaos synchronization for a class of unified Lorenz systems. However, its applicability to a system of higher dimension in not known and could be one problem for the future work.

Appendix A

Derivation of equations (2.24)

In section 2.3, we performed a multiple scales analysis on the equations of a 2R planar robot. At order ϵ, two equations, given by equations (2.23) were obtained. The solution to those equations was given by equation (2.24). This section presents the derivation of equation (2.24).

From equation (2.23), we get a system of coupled differential equations with constant coefficients whose solutions can be obtained by letting

$$\theta_{10} = c_1 e^{i\omega T_0}, \quad \theta_{20} = c_2 e^{i\omega T_0} \tag{A-1}$$

Substituting equation (A-1) into equation (2.23), we get

$$\begin{aligned}
&[(K_{pn} - (P_1 + 1 + P_2 + 2P_2P_3)\omega^2)c_1 - (1 + P_2P_3)\omega^2 c_2]e^{i\omega T_0} = \\
&A_{f_1}((iE_1 + E_2)e^{iT_0} + (-iE_1 + E_2)e^{-iT_0}) \\
&[-(1 + P_2P_3)\omega^2 c_1 + (K_{pn} - \omega^2)c_2]e^{i\omega T_0} = A_{f_2}((iE_1 + E_2)e^{iT_0} + (-iE_1 + E_2)e^{-iT_0})
\end{aligned} \tag{A-2}$$

In equation (A-2), the left-hand side is a multiple of $e^{i\omega T_0}$, whereas the right-hand side is a multiple of e^{iT_0}. To compute the solution of equation (A-2), we first equate terms proportional to $e^{i\omega T_0}$ (by putting the right-hand side to zero) and compute c_1 and c_2. Then we put $\omega = 1$ and recompute the values of c_1 and c_2 by equating terms proportional to e^{iT_0}. Putting the right-hand side equal to zero, we get

$$[(K_{pn} - (P_1 + 1 + P_2 + 2P_2P_3)\omega^2)c_1 - (1 + P_2P_3)\omega^2 c_2]e^{i\omega T_0} = 0$$

$$[-(1+P_2P_3)\omega^2 c_1 + (K_{pn}-\omega^2)c_2]e^{i\omega T_0} = 0 \tag{A-3}$$

For a non-trivial solution, the determinant matrix must be zero, i.e., we have

$$\begin{vmatrix} K_{pn}-(P_1+1+P_2+2P_2P_3)\omega^2 & -(1+P_2P_3)\omega^2 \\ -(1+P_2P_3)\omega^2 & K_{pn}-\omega^2 \end{vmatrix} = 0 \tag{A-4}$$

The values of ω thus calculated are,

$$\omega_1 = \sqrt{\frac{K_{pn}(L_{q2}+\sqrt{L_{q1}})}{2L_{q3}}}, \qquad \omega_2 = \sqrt{\frac{K_{pn}(L_{q2}-\sqrt{L_{q1}})}{2L_{q3}}} \tag{A-5}$$

where

$$\begin{aligned} L_{q1} &= 4+8P_2P_3+4P_1P_2P_3+(P_1+P_2)^2+4P_2^2P_3+8P_2^2P_3^2 \\ L_{q2} &= 2+P_1+P_2+2P_2P_3 \\ L_{q3} &= P_1+P_2-P2^2P_3^2 \end{aligned} \tag{A-6}$$

Substituting the values of ω in the second equation in (A-3), we have

$$\begin{aligned} &\text{When } \omega=\omega_1,\ c_{11}=1, c_{21}=\frac{K_{pn}-\omega_1^2}{(1+P_2P_3)\omega_1^2} \\ &\text{When } \omega=\omega_2,\ c_{12}=1, c_{22}=\frac{K_{pn}-\omega_2^2}{(1+P_2P_3)\omega_2^2} \end{aligned} \tag{A-7}$$

The general solution of equation (2.13) can be written as,

$$\begin{bmatrix}\theta_{10}\\ \theta_{20}\end{bmatrix} = A_1 e^{i\omega_1 T_0}\begin{bmatrix}c_{11}\\ c_{21}\end{bmatrix} + A_2 e^{i\omega_2 T_0}\begin{bmatrix}c_{12}\\ c_{22}\end{bmatrix} \tag{A-8}$$

Now, in equation (A-2), we substitute $\omega = 1$ and equate terms proportional to e^{iT_0}. We get

$$\begin{bmatrix} K_{pn}-(P_1+1+P_2+2P_2P_3) & -(1+P_2P_3) \\ -(1+P_2P_3) & K_{pn}-1 \end{bmatrix}\begin{bmatrix}c_1\\ c_2\end{bmatrix} = \begin{bmatrix} A_{f_1}((iE_1+E_2)e^{iT_0}+(-iE_1+E_2)e^{-iT_0}) \\ A_{f_2}((iE_1+E_2)e^{iT_0}+(-iE_1+E_2)e^{-iT_0}) \end{bmatrix} \tag{A-9}$$

Solving for c_1 and c_2, we get

$$\begin{aligned} c_1 &= F_1(iE_1 + E_2)e^{iT_0} + F_1(-iE_1 + E_2)e^{-iT_0} \\ c_2 &= F_2(iE_1 + E_2)e^{iT_0} + F_2(-iE_1 + E_2)e^{-iT_0} \end{aligned} \tag{A-10}$$

where

$$\begin{aligned} F_1 &= \frac{(K_{pn} - 1)A_{f_1} + (1 + P_2P_3)A_{f_2}}{E_f} \\ F_2 &= \frac{(1 + P_2P_3)A_{f_1} + (K_{pn} - (P_1 + 1 + P_2 + 2P_2P_3))A_{f_2}}{E_f} \\ E_f &= (K_{pn} - 1)(K_{pn} - (P_1 + 1 + P_2 + 2P_2P_3)) - (1 + P_2P_3)^2 \end{aligned} \tag{A-11}$$

Combining equation (A-8) and (A-10), we get

$$\begin{aligned} \theta_{10} &= A_1e^{i\omega_1T_0} + A_2e^{i\omega_2T_0} + F_1(iE_1 + E_2)e^{iT_0} + F_1(-iE_1 + E2)e^{-iT_0} + c.c. \\ \theta_{20} &= c_{21}A_1e^{i\omega_1T_0} + c_{22}A_2e^{i\omega_2T_0} + F_2(iE_1 + E_2)e^{iT_0} + F_2(-iE_1 + E2)e^{-iT_0} + c.c. \end{aligned} \tag{A-12}$$

The equation (A-12) is identical to the equation (2.24) in section 2.3.

Terms in equation (2.34)

$$\begin{aligned} &R_{11} = -2(P_1 + 1 + P_2 + 2P_2P_3 + (1 + P_2P_3)c_{21}), \quad R_{121} = -K_{vn}\omega_1 \\ &R_{122} = -P_2P_3F_2^2\omega_1^2(2 + c_{21})(E_2^2 + E_1^2), \; R_{124} = -P_2P_3c_{22}^2\omega_1^2(2 + c_{21}) \\ &R_{123} = \frac{-P_2P_3c_{21}^2\omega_1^2(2 + c_{21})}{2}, \quad R_{14} = \frac{-3P_2P_3F_2^2(2F_1 + F_2)}{2} \\ &R_{13} = -P_2P_3(\omega_2 + 2)\left(\frac{F_2^2(2 + c_{22})\omega_2}{2} + c_{22}F_2(2F_1 + F_2)\right) \\ &S_{11} = -2(P_1 + 1 + P_2 + 2P_2P_3 + (1 + P_2P_3)c_{22}), \quad S_{121} = -K_{vn}\omega_2 \\ &S_{122} = -P_2P_3F_2^2\omega_2^2(2 + c_{22})(E_2^2 + E_1^2), \; S_{123} = -P_2P_3c_{21}^2\omega_2^2(2 + c_{22}) \\ &S_{13} = P_2P_3(\omega_1 - 2)\left(\frac{-F_2^2(2 + c_{21})\omega_1}{2} + c_{21}F_2(2F_1 + F_2)\right) \\ &R_{21} = -2(1 + P_2P_3 + c_{21}), \; R_{221} = -K_{vn}\omega_1c_{21}, \quad S_{124} = \frac{-P_2P_3c_{22}^2\omega_2^2(2 + c_{22})}{2} \\ &R_{223} = \frac{-P_2P_3c_{21}\omega_1^2(2 + 3c_{21})}{2}, \; R_{24} = \frac{-P_2P_3F_1F_2(2F_1 - F_2)}{2} \end{aligned} \tag{A-13}$$

$$R_{222} = -P_2P_3(E_2^2 + E_1^2)(c_{21}F_1(2F_1 + F_2) + F_2(c_{21}F_1 + F_2\omega_1^2))$$
$$R_{224} = -P_2P_3(c_{21}\omega_2^2(2 + c_{22}) + c_{22}(c_{21}\omega_2^2 + c_{22}\omega_1^2))$$
$$R_{23} = P_2P_3\left(\frac{F_1c_{22}(2F_1 - F_2)}{2} + F_2(2F_1\omega_2 - \frac{c_{22}F_1 + F_2\omega_2^2}{2})\right)$$
$$S_{21} = -2(1 + P_2P_3 + c_{22}),\ S_{221} = -K_{vn}\omega_2c_{22},\ \ S_{224} = \frac{-P_2P_3c_{22}\omega_2^2(2 + 3c_{22})}{2}$$
$$S_{222} = -P_2P_3(E_2^2 + E_1^2)(c_{22}F_1(2F_1 + F_2) + F_2(c_{22}F_1 + F_2\omega_2^2))$$
$$S_{223} = -P_2P_3(c_{22}\omega_1^2(2 + c_{21}) + c_{21}(c_{21}\omega_2^2 + c_{22}\omega_1^2))$$
$$S_{23} = P_2P_3\left(\frac{F_1c_{21}(2F_1 - F_2)}{2} + F_2(-2F_1\omega_1 - \frac{c_{21}F_1 + F_2\omega_1^2}{2})\right)$$

Terms in equations (2.39, 2.40)

$$L_{11} = R_{11}(K_{pn} - \omega_1^2) + R_{21}(1 + P_2P_3)\omega_1^2,\ \ L_{13} = R_{13}(K_{pn} - \omega_1^2) + R_{23}(1 + P_2P_3)\omega_1^2$$
$$L_{121} = R_{121}(K_{pn} - \omega_1^2) + R_{221}(1 + P_2P_3)\omega_1^2$$
$$L_{122} = R_{122}(K_{pn} - \omega_1^2) + R_{222}(1 + P_2P_3)\omega_1^2$$
$$L_{123} = R_{123}(K_{pn} - \omega_1^2) + R_{223}(1 + P_2P_3)\omega_1^2$$
$$L_{124} = R_{124}(K_{pn} - \omega_1^2) + R_{224}(1 + P_2P_3)\omega_1^2$$
$$L_{14} = R_{14}(K_{pn} - \omega_1^2) + R_{24}(1 + P_2P_3)\omega_1^2$$
$$L_{21} = S_{11}(K_{pn} - \omega_2^2) + S_{21}(1 + P_2P_3)\omega_2^2,\ \ L_{23} = S_{13}(K_{pn} - \omega_2^2) + S_{23}(1 + P_2P_3)\omega_2^2$$
$$L_{221} = S_{121}(K_{pn} - \omega_2^2) + S_{221}(1 + P_2P_3)\omega_2^2$$
$$L_{222} = S_{122}(K_{pn} - \omega_2^2) + S_{222}(1 + P_2P_3)\omega_2^2 \qquad \text{(A-14)}$$
$$L_{223} = S_{123}(K_{pn} - \omega_2^2) + S_{223}(1 + P_2P_3)\omega_2^2$$
$$L_{224} = S_{124}(K_{pn} - \omega_2^2) + S_{224}(1 + P_2P_3)\omega_2^2$$
$$J_{121} = \frac{L_{121}}{\omega_1L_{11}},\ J_{122} = \frac{L_{122}}{\omega_1L_{11}},\ J_{123} = \frac{L_{123}}{\omega_1L_{11}},\ J_{124} = \frac{L_{124}}{\omega_1L_{11}},\ J_{13} = \frac{L_{13}}{\omega_1L_{11}},\ J_{14} = \frac{L_{14}}{\omega_1L_{11}}$$
$$J_{221} = \frac{L_{221}}{\omega_2L_{21}},\ \ J_{222} = \frac{L_{222}}{\omega_2L_{21}},\ \ J_{223} = \frac{L_{223}}{\omega_2L_{21}},\ \ J_{224} = \frac{L_{224}}{\omega_2L_{21}},\ \ J_{23} = \frac{L_{23}}{\omega_2L_{21}}$$

Terms in equations (2.44)

Considering the following terms

$$D_{11} = K_{pn}\alpha_3 - \omega_1^2, \qquad D_{12} = (1 + P_2P_3)\omega_1^2 - K_{pn}(\alpha_3 + \alpha_2), \qquad E_1 = \frac{1 - K_{pn}}{2}$$

$$D_{21} = K_{pn}\alpha_3 - \omega_2^2, \quad D_{22} = (1 + P_2P_3)\omega_2^2 - K_{pn}(\alpha_3 + \alpha_2), \quad E_2 = \frac{K_{vn}}{2}$$

we have

$$J_{a1} = 2J_{13}E_1E_2 - J_{15}E_2, \quad J_{a2} = J_{13}(E_2^2 - E_1^2) + J_{15}E_1$$
$$J_{a3} = J_{14}E_1(3E_2^2 - E_1^2) - J_{16}(E_2^2 - E_1^2), \; J_{a4} = J_{14}E_2(E_2^2 - 3E_1^2) + 2J_{16}E_1E_2$$
$$J_{a5} = 2J_{23}E_1E_2 - J_{25}E_2, \quad J_{a6} = J_{23}(E_2^2 - E_1^2) + J_{25}E_1$$

where

$$J_{12k} = \frac{L_{12k}}{\omega_1 L_{11}} \quad \forall k = 1,2,3,4, \qquad J_{1k} = \frac{L_{1k}}{\omega_1 L_{11}} \quad \forall k = 3,4,5,6$$
$$J_{22k} = \frac{L_{22k}}{\omega_2 L_{21}} \quad \forall k = 1,2,3,4, \qquad J_{2k} = \frac{L_{2k}}{\omega_2 L_{21}} \quad \forall k = 3,5$$

where

$$\omega_1 = \sqrt{\frac{K_{pn}(L_{q1} + \sqrt{L_{q2}})}{L_{q3}}}, \qquad \omega_2 = \sqrt{\frac{K_{pn}(L_{q1} - \sqrt{L_{q2}})}{L_{q3}}}$$

where $L_{q1} = \alpha_1 + \alpha_3(P_1 + P_2 - 1) - 2P_2P_3\alpha 2, \quad L_{q3} = P_1 + P_2 - P_2^2P_3^2$

$L_{q3} = P_1^2\alpha_3^2 4P_1P_2P_3\alpha_2\alpha_3 - 2P_1P_2\alpha_3^2 - 2P_1\alpha_1\alpha_3 + 4P_1\alpha_2^2 + 2P_1\alpha_3^2 + 4P_2^2P_3^2\alpha_1\alpha_3$
$- 4P_2^2P_3^2\alpha_3^2 - 4P_2^2P_3\alpha_2\alpha_3 + P_2^2\alpha_3^2 - 4P_2P_3\alpha_1\alpha_2 + 4P_2P_3\alpha_2\alpha_3 - 2P_2\alpha_1\alpha_3 + 4P_2\alpha_2^2$
$+ 2P_2\alpha_3^2 + \alpha_1^2 - 2\alpha_1\alpha_3 + \alpha_3^2$

and $L_{1k} = Q_{1k}D_{11} + Q_{2k}D_{12} \;\; \forall k = 1,3,4,5,6, \quad L_{2k} = R_{1k}D_{21} + R_{2k}D_{22} \;\; \forall k = 1,3,5$

$L_{12k} = Q_{12k}D_{11} + Q_{22k}D_{12}, \qquad L_{22k} = R_{12k}D_{21} + R_{22k}D_{22} \qquad \forall k = 1,2,3,4$

where

$Q_{11} = -2(P_1 + 1 + P_2 + 2P_2P_3 + C_{21}(1 + P_2P_3)), \; Q_{15} = \alpha_2(2A_{f_1} + A_{f_2})E_1C_{22}F_2$
$Q_{121} = -K_{vn}\omega_1(\alpha_1 + (2 + C_{21})\alpha_2 + C_{21}\alpha_3), R_{121} = -K_{vn}\omega_2(\alpha_1 + (2 + C_{22})\alpha_2 + C_{22}\alpha_3)$
$Q_{14} = F_2^2(2F_1 + F_2)\left(\frac{\alpha_2(2 + K_{pn}) - 3P_2P_3}{2}\right), \; Q_{16} = \alpha_2(2A_{f_1} + A_{f_2})E_1\frac{F_2^2}{2}$
$Q_{122} = (E_2^2 + E_1^2)(P_2P_3(-F_2^2\omega_1^2(2 + C_{21}) - 2C_{21}F_2(2F_1 + F_2))$
$+ (P_2P_3 - \alpha_2)(2C_{21}F_2(2F_1 + F_2))) - 2\alpha_2C_{21}E_1^2F_2(2A_{f_1} + A_{f_2})$

$$+ K_{pn}\alpha_2(2F_2^2(2+C_{21}) + 4C_{21}F_2(2F_1+F_2))\left(\frac{E_2^2+E_1^2}{2}\right)$$

$$Q_{123} = P_2P_3\left(\frac{-3C_{21}^2\omega_1^2(2+C_{21})}{2}\right) + (P_2P_3-\alpha_2)(C_{21}^2\omega_1^2(2+C_{21}))$$

$$+ K_{pn}\alpha_2\left(\frac{3C_{21}^2(2+C_{21})}{2}\right),\quad Q_{124} = -P_2P_3C_{22}^2\omega_1^2(2+C_{21}) - 2\alpha_2C_{21}C_{22}\omega_2^2(2+C_{22})$$

$$+ K_{pn}\alpha_2\left(\frac{2C_{22}^2(2+C_{21}) + 4C_{21}C_{22}(2+C_{22})}{2}\right),\quad Q_{15} = \alpha_2(2A_{f_1}+A_{f_2})E_1C_{22}F_2$$

$$R_{11} = -2(P_1+1+P_2+2P_2P_3+C_{22}(1+P_2P_3)),\ R_{15} = \alpha_2(2A_{f_1}+A_{f_2})E_1C_{21}F_2$$

$$R_{122} = (E_2^2+E_1^2)(P_2P_3(-F_2^2\omega_2^2(2+C_{22}) - 2C_{22}F_2(2F_1+F_2))$$

$$+ (P_2P_3-\alpha_2)(2C_{22}F_2(2F_1+F_2))) - 2\alpha_2C_{22}E_1^2F_2(2A_{f_1}+A_{f_2})$$

$$+ K_{pn}\alpha_2(2F_2^2(2+C_{22}) + 4C_{22}F_2(2F_1+F_2))\left(\frac{E_2^2+E_1^2}{2}\right)$$

$$R_{124} = P_2P_3\left(\frac{-3C_{22}^2\omega_2^2(2+C_{22})}{2}\right) + (P_2P_3-\alpha_2)(C_{22}^2\omega_2^2(2+C_{22}))$$

$$+ K_{pn}\alpha_2\left(\frac{3C_{22}^2(2+C_{22})}{2}\right),\quad R_{123} = -P_2P_3C_{21}^2\omega_2^2(2+C_{22}) - 2\alpha_2C_{21}C_{22}\omega_1^2(2+C_{21})$$

$$+ K_{pn}\alpha_2\left(\frac{2C_{21}^2(2+C_{22}) + 4C_{21}C_{22}(2+C_{21})}{2}\right)$$

$$Q_{13} = -P_2P_3\left(\frac{F_2^2\omega_2^2(2+C_{22})}{2} + C_{22}F_2(2F_1+F_2)\right)$$

$$- (P_2P_3-\alpha_2)(F_2^2\omega_2(2+C_{22}) + (\omega_2+1)C_{22}F_2(2F_1+F_2))$$

$$+ K_{pn}\alpha_2F_2\left(\frac{F_2(2+C_{22}) + 2C_{22}(2F_1+F_2)}{2}\right),\ Q_{21} = -2(1+P_2P_3+C_{21})$$

$$R_{13} = -P_2P_3\left(\frac{F_2^2\omega_1^2(2+C_{21})}{2} + C_{21}F_2(2F_1+F_2)\right)$$

$$+ (P_2P_3-\alpha_2)(F_2^2\omega_1(2+C_{21}) + (\omega_1-1)C_{21}F_2(2F_1+F_2))$$

$$+ K_{pn}\alpha_2F_2\left(\frac{F_2(2+C_{21}) + 2C_{21}(2F_1+F_2)}{2}\right),\ R_{21} = -2(1+P_2P_3+C_{22})$$

$$Q_{25} = \alpha_2A_{f_1}E_1C_{22}F_2,\ R_{25} = \alpha_2A_{f_1}E_1C_{21}F_2,\ Q_{26} = \alpha_2A_{f_1}E_1\frac{F_2^2}{2}$$

$$Q_{221} = -K_{vn}\omega_1(\alpha_3+\alpha_2+C_{21}\alpha_3),\ R_{221} = -K_{vn}\omega_2(\alpha_3+\alpha_2+C_{22}\alpha_3)$$

$$Q_{222} = -2\alpha_2C_{21}E_1^2F_2A_{f1} + (-P_2P_3(F_2^2\omega_1^2 - 2C_{21}F_1F_2) + \frac{K_{pn}\alpha_2}{2}(2F_2^2 + 4C_{21}F_1F_2)$$

$$+ 2(\alpha_2-P_2P_3)C_{21}F_1^2)(E_2^2+E_1^2),\ R_{222} = (\frac{K_{pn}\alpha_2}{2}(2F_2^2 + 4C_{22}F_1F_2)$$

$$- P_2P_3(F_2^2\omega_2^2 - 2C_{22}F_1F_2) + 2(\alpha_2-P_2P_3)C_{22}F_1^2)(E_2^2+E_1^2) - 2\alpha_2C_{22}E_1^2F_2A_{f_1}$$

$$Q_{223} = -3P_2P_3C_{21}^2\frac{\omega_1^2}{2} + (\alpha_2 - P_2P_3)C_{21}\omega_1^2 + 3K_{pn}\alpha_2\frac{C_{21}^2}{2}$$
$$Q_{24} = \frac{F_1F_2}{2}(F_1(P_2P_3 - 2\alpha_2) + F_2K_{pn}\alpha_2)$$
$$Q_{224} = K_{pn}\alpha_2C_{22}(C_{22} + 2C_{21}) - P_2P_3(C_{22}^2\omega_1^2 + 2C_{21}C_{22}\omega_2^2) - 2(\alpha_2 - P_2P_3)C_{21}\omega_2^2$$
$$R_{223} = K_{pn}\alpha_2C_{21}(C_{21} + 2C_{22}) - P_2P_3(C_{21}^2\omega_2^2 + 2C_{21}C_{22}\omega_1^2) - 2(\alpha_2 - P_2P_3)C_{22}\omega_1^2$$
$$R_{224} = -3P_2P_3C_{22}^2\frac{\omega_2^2}{2} + (\alpha_2 - P_2P_3)C_{22}\omega_2^2 + 3K_{pn}\alpha_2\frac{C_{22}^2}{2}$$

where

$$C_{21} = \frac{\omega_1^2(1 + P_2P_3) - K_{pn}(\alpha_3 + \alpha_2)}{(K_{pn}\alpha_3 - \omega_1^2)}, \quad C_{22} = \frac{\omega_2^2(1 + P_2P_3) - K_{pn}(\alpha_3 + \alpha_2)}{(K_{pn}\alpha_3 - \omega_2^2)}$$
$$F_1 = \frac{1}{E_f}((K_{pn}\alpha_3 - 1)(A_{f_1}\alpha_1 + A_{f_2}\alpha_3 + \alpha_2(2A_{f_1} + A_{f_2}))$$
$$+ (1 + P_2P_3 - K_{pn}(\alpha_3 + \alpha_2))(A_{f_1}(\alpha_3 + \alpha_2) + A_{f_2}\alpha_3))$$
$$F_2 = \frac{1}{E_f}((1 + P_2P_3 - K_{pn}(\alpha_3 + \alpha_2))(A_{f_1}\alpha_1 + A_{f_2}\alpha_3 + \alpha_2(2A_{f1} + A_{f2}))$$
$$+ (K_{pn}(\alpha_1 + 2\alpha_2) - (P_1 + 1 + P_2 + 2P_2P_3))(A_{f_1}(\alpha_3 + \alpha_2) + A_{f_2}\alpha_3))$$

where

$$E_f = (K_{pn}\alpha_3 - 1)(K_{pn}(\alpha_1 + 2\alpha_2) - (P_1 + 1 + P_2 + 2P_2P_3))$$
$$- (1 + P_2P_3 - K_{pn}(\alpha_3 + \alpha_2))^2$$

Non-dimensional parameters K_{pn} and K_{vn} are

$$K_{pn} = \frac{K_p}{\Omega^2}, \qquad K_{vn} = \frac{K_v}{\Omega}$$

Appendix B

The description of the terms given in equation (3.8) is presented in this section. It may be noted that all terms have been computed symbolically using Maple [113].

Table B.1: Description of terms in the equation (3.8)

Term	Description
$[Q_f]_{4\times1}$	Vector of flexible nodal variables U_2, V_2, ϕ_2
$[Q]_{4\times1}$	Vector of all variables $\theta_1, U_2, V_2, \phi_2$
$[\tau]_{4\times1}$	Vector of input torques $[\Gamma, 0, 0, 0]^T$
ρ	Density of the Material (kg/m^3)
A	Area of cross-section (m^2)
L	Length of the beam element (m)
E	Modulus of elasticity of beam element (GPa)
I	Polar moment of inertia of beam element (m^4)
U_a	Speed of sound through the material (m/s)
U_g	Velocity associated with transverse vibration (m/s)
$[M]_{4\times4}$	System mass matrix
$[K]_{4\times4}$	Conventional Stiffness matrix
$[\Delta K]_{4\times4}$	Geometric Stiffness matrix
$[H]_{4\times1}$	Vector of coriolis and centripetal terms

Elements of the mass matrix

In this section, we present the detailed mass matrix, conventional and geometric stiffness matrix and the centrifugal and coriolis effects in their nondimensional form for the rotating flexible link given in figure 3.1. The mass and stiffness matrices are symmetric and hence only the upper triangular part is presented.

$$
\begin{aligned}
M(1,1) &= \frac{1}{3} + \frac{2}{3}U_2 + \frac{1}{3}U_2^2 + \frac{13}{35}V_2^2 - \frac{11}{105}V_2\phi_2 + \frac{1}{105}\phi_2^2 \\
M(1,2) &= -\frac{7}{20}V_2 + \frac{1}{20}\phi_2 \\
M(1,3) &= \frac{7}{20} + \frac{7}{20}U_2 \\
M(1,4) &= -\frac{1}{20} - \frac{1}{20}U_2 \\
M(2,2) &= \frac{1}{3} \\
M(2,3) &= 0 \\
M(2,4) &= 0 \\
M(3,3) &= \frac{13}{35} \\
M(3,4) &= -\frac{11}{210} \\
M(4,4) &= \frac{1}{105}
\end{aligned}
$$

Conventional stiffness matrix

$$
\Big[K\Big] = \begin{bmatrix} 0 & 0 & 0 & 0 \\ 0 & 0 & 0 & 0 \\ 0 & 0 & 12 & -6 \\ 0 & 0 & -6 & 4 \end{bmatrix}
$$

Geometric stiffness matrix

The non-zero elements of the symmetric geometric stiffness matrix are

$$
\begin{aligned}
\Delta\mathcal{K}(2,2) &= \frac{U_a^2}{U_g^2},\ \Delta\mathcal{K}(2,3) = \frac{U_a^2}{U_g^2}\left(\frac{3}{5}V_2 - \frac{1}{20}\phi_2\right) \\
\Delta\mathcal{K}(2,4) &= \frac{U_a^2}{U_g^2}\left(-\frac{1}{20}V_2 + \frac{1}{25}\phi_2\right),\ \Delta\mathcal{K}(3,3) = \frac{U_a^2}{U_g^2}\left(\frac{3}{5}U_2\right) \\
\Delta\mathcal{K}(3,4) &= -\frac{U_a^2}{U_g^2}\left(\frac{1}{20}U_2\right),\ \Delta\mathcal{K}(4,4) = \frac{U_a^2}{U_g^2}\left(\frac{1}{15}U_2\right)
\end{aligned}
$$

Nonlinear terms due to centrifugal and Coriolis effects

$$\begin{aligned}
\mathcal{H}(1,1) &= \frac{2}{3}\dot{U}_2\dot{\theta}_1 \\
\mathcal{H}(1,2) &= -\frac{7}{10}\dot{V}_2\dot{\theta}_1 - \frac{1}{3}\dot{\theta_1}^2 \\
\mathcal{H}(1,3) &= \frac{7}{10}\dot{U}_2\dot{\theta}_1 - \frac{13}{35}V_2\dot{\theta_1}^2 \\
\mathcal{H}(1,4) &= -\frac{1}{10}\dot{U}_2\dot{\theta}_1 + \frac{11}{210}V_2\dot{\theta_1}^2
\end{aligned}$$

Derivation of equations (3.12)

In Chapter 4, we performed a multiple scales analysis of the rotating link. At order ϵ, four equations, given by equations (3.11) were obtained. The solution to those equations was given by equation (3.12). This section presents the derivation of this set of equations.

From equation (3.11), we get a system of coupled differential equations with constant coefficients whose solutions can be obtained by letting

$$\theta_{10} = c_1 e^{i\omega T_0}, U_{20} = c_2 e^{i\omega T_0}, V_{20} = c_3 e^{i\omega T_0}, \phi_{20} = c_4 e^{i\omega T_0} \tag{B-1}$$

Substituting (B-1) into (3.11), we get

$$\begin{aligned}
&-\frac{1}{3}\omega^2 c_1 - \frac{7}{20}\omega^2 c_3 + \frac{1}{20}\omega^2 c_4 = 0 \\
&\left(\frac{U_a^2}{U_g^2} - \frac{\omega^2}{3}\right) c_2 = 0 \\
&-\frac{7}{20}\omega^2 c_1 + \left(12 - \frac{13}{35}\omega^2\right) c_3 + \left(\frac{11}{210}\omega^2 - 6\right) c_4 = 0 \\
&\frac{1}{20}\omega^2 c_1 + \left(\frac{11}{210}\omega^2 - 6\right) c_3 + \left(4 - \frac{1}{105}\omega^2\right) c_4 = 0
\end{aligned} \tag{B-2}$$

For a non-trivial solution, the determinant matrix must be zero, i.e.,

$$\begin{vmatrix} -\frac{1}{3}\omega^2 & 0 & -\frac{7}{20}\omega^2 & \frac{1}{20}\omega^2 \\ 0 & \frac{U_a^2}{U_g^2} - \frac{\omega^2}{3} & 0 & 0 \\ -\frac{7}{20}\omega^2 & 0 & \left(12 - \frac{13}{35}\omega^2\right) & \left(\frac{11}{210}\omega^2 - 6\right) \\ \frac{1}{20}\omega^2 & 0 & \left(\frac{11}{210}\omega^2 - 6\right) & \left(4 - \frac{1}{105}\omega^2\right) \end{vmatrix} = 0 \tag{B-3}$$

The values of ω thus calculated are,

$$\omega_1 = 0, \omega_2 = \frac{\sqrt{3}U_a}{U_g}, \omega_3 = 70.0871, \omega_4 = 17.5444 \tag{B-4}$$

Substituting the values of ω in equation (3.11), we have

$$\text{When } \omega = \omega_1,\ c_{11} = c_{21} = c_{31} = c_{41} = 0 \tag{B-5}$$

$$\text{When } \omega = \omega_2,\ c_{12} = c_{32} = c_{42} = 0, c_{22} = 1 \tag{B-6}$$

$$\text{When } \omega = \omega_3,\ c_{13} = 1, c_{23} = 0, c_{33} = -0.8222, \quad c_{34} = 0.9112 \tag{B-7}$$

$$\text{When } \omega = \omega_4,\ c_{41} = 1, c_{42} = 0, c_{43} = -1.2789, \quad c_{44} = -2.2856 \tag{B-8}$$

The general solution of equation (3.11) can be written as,

$$\begin{aligned} \begin{bmatrix} \theta_{10} \\ U_{20} \\ V_{20} \\ \phi_{20} \end{bmatrix} &= A_1 e^{i\omega_1 T_0} \begin{bmatrix} c_{11} \\ c_{21} \\ c_{31} \\ c_{41} \end{bmatrix} + A_2 e^{i\omega_2 T_0} \begin{bmatrix} c_{12} \\ c_{22} \\ c_{32} \\ c_{42} \end{bmatrix} \\ &+ A_3 e^{i\omega_3 T_0} \begin{bmatrix} c_{13} \\ c_{23} \\ c_{33} \\ c_{43} \end{bmatrix} + A_4 e^{i\omega_4 T_0} \begin{bmatrix} c_{14} \\ c_{24} \\ c_{34} \\ c_{44} \end{bmatrix} \end{aligned} \tag{B-9}$$

which is identical to the form in equation (3.12).

Terms in equation (3.18, 3.24)

$$J_{22} = \frac{1}{20}(c_{43} - 7c_{33})\omega_3^2 - \frac{U_a^2}{U_g^2}\left(\frac{3}{5}c_{33}^2 + \frac{c_{43}^2}{15} - \frac{c_{33}c_{43}}{10}\right)$$
$$- \frac{7}{10}c_{33}\omega_3^2 - \frac{\omega_3^2}{3}, Z_{11} = -\frac{2}{3} - \frac{7c_{33}}{10} + \frac{c_{43}}{10}$$

$$Z_{12} = (\omega_3 - \omega_2)\left(\frac{2}{3}\omega_3 + (\omega_3 + \omega_2)\left(\frac{7c_{33} - c_{43}}{20}\right)\right)$$
$$Z_{31} = -\frac{7}{10} - \frac{26c_{33}}{35} + \frac{11c_{43}}{105}$$

$$Z_{32} = \frac{7\omega_3}{20}(\omega_3 - 2\omega_2) + \frac{U_a^2}{U_g^2}\left(-\frac{6c_{33}}{5} + \frac{c_{43}}{10}\right)$$
$$Z_{41} = \frac{1}{10} + \frac{11c_{33}}{105} - \frac{2c_{43}}{105}, \quad Z_{w1} = \frac{\omega_3^4}{3780} - \frac{34\omega_3^2}{105} + 4$$
$$Z_{42} = \frac{\omega_3}{20}(2\omega_2 - \omega_3) + \frac{U_a^2}{U_g^2}\left(\frac{c_{33}}{10} - \frac{2c_{43}}{15}\right)$$
$$Z_{w3} = \frac{11\omega_3^2}{30} - \frac{\omega_3^4}{4200}, \quad Z_{w4} = \frac{\omega_3^2}{2} + \frac{\omega_3^4}{12600}$$
$$Z_{d1} = \alpha\left(-\frac{1}{3} - \frac{7c_{33}}{20} + \frac{c_{43}}{20}\right)$$
$$Z_{d3} = \left(-\frac{7\alpha}{20} - \left(\frac{13\alpha}{35} + 12\beta\right)c_{33} + \left(\frac{11\alpha}{210} + 6\beta\right)c_{43}\right)$$
$$Z_{d4} = \left(\frac{\alpha}{20} + \left(\frac{11\alpha}{210} + 6\beta\right)c_{33} - \left(\frac{\alpha}{105} + 4\beta\right)c_{43}\right)$$

where c_{33}, c_{43} were calculated in the preceding section of this Appendix.

References

[1] Chen W. C., Nonlinear dynamics and chaos in a fractional-order financial system, *Chaos, Solitons and Fractals*, 36(5), 1305-1314, 2008.

[2] Guegan D., Chaos in economics and finance, *Annual Reviews in Control, International Federation of Automatic Control*, 33(1), 89-93, 2009.

[3] Hilborn R. C., Chaos and Nonlinear Dynamics: An Introduction to Scientists and Engineers, *Oxford University Press*, 2000.

[4] Nikolai A. M. and Sidorov S. V., New Methods for Chaotic Dynamics, *World Scientific Series on Nonlinear Science: Series A*, 2006.

[5] Strogatz S. H., Nonlinear Dynamics and Chaos: With applications to Physics, Biology, Chemistry and Engineering, *Westview Press*, 2007.

[6] Sun J. Q. and Luo A. C. J., Bifurcations and Chaos in Complex Systems, *Edited Series on Advances in Nonlinear Science and Complexity*, Vol. 1, 2006.

[7] Guckenheimer J. and Holmes P., Nonlinear Oscillations, Dynamical Systems, and Bifurcations of Vector Fields, *Applied Mathematical Sciences, Springer-Verlag, New York*, Vol. 42, 1983.

[8] Sathyamoorthy M., Nonlinear Analysis of Structures, *Mechanical and Aerospace Engineering Series, CRC Press, Florida*, 1998.

[9] Fertis D. G., Nonlinear Structural Engineering: With Unique Theories and Methods to Solve Effectively Complex Nonlinear Problems, *Springer Publications*, 2006.

[10] Jones R. M., Deformation Theory of Plasticity, *Bull Ridge Publishing, Virginia*, 2009.

[11] Kong Q., Sensitivity Analysis for Nonlinear Structures, *Doctor of Philosophy Thesis, New Brunswick Rutgers, State University of New Jersey*, 2008.

[12] Ohashi Y. and Kamiya N., On the bending of thin plates of material having a nonlinear stress-strain relation, *International Journal of Mechanical Sciences*, 9(4), 183-193, 1967.

[13] Bian Y. H., Analysis of nonlinear stresses and strains in a thin current-carrying elastic plate, *International Applied Mechanics*, 51(1), 108-120, 2015.

[14] Rasskazov A. O., Trach V. M. and Gupalyuk V. N., Geometrically nonlinear stress-strain state of multilayer shells of revolution with variable geometric parameters, *Strength of Materials*, 32(1), 86-91, 2000.

[15] Schmueser D. W., Nonlinear stress-strain and strength response of axisymmetric bimodulus composite material shells, *AIAA Journal*, 21(12), 1742-1747, 1983.

[16] Kovacic I. and Brennan M. J., The Duffing Equation: Nonlinear Oscillators and Their Behaviour, *1st ed., John Wiley & Sons, Ltd.*, 2011.

[17] MATLAB, *Version 8.0 (R2012b)*, The MathWorks Inc., Natick, Massachusetts, 2012.

[18] Seydel R., Schneider F. W., Kupper T. and Troger H., Bifurcation and Chaos: Analysis, Algorithms, Applications , *International Series of Numerical Mathematics, Birkhauser*, 1991.

[19] Ku Y. H. and Sun X., Chaos in Van der Pol's equation, *Journal of the Franklin Institute*, 327(2), 197-207, 1990.

[20] Jing Z., Deng J. and Yang J., Bifurcations of periodic orbits and chaos in damped and driven morse oscillator, *Chaos, Solitons and Fractals*, 35(3), 486-505, 2008.

[21] Dixon D. D., Cummings F. W. and Kaus P. E., Continuous chaotic dynamics in two dimensions, *Physica D: Nonlinear Phenomena*, 65(1-2), 109-116, 1993.

[22] Rossler O. E., An equation for continuous chaos, *Physics Letters A*, 57(5), 397-398, 1976.

[23] Kennedy M. P., Three steps to chaos. II. A Chua's circuit primer, *Circuits and Systems 1: Fundamental Theory and Applications, IEEE Transactions on*, 40(10), 657-674, 1993.

[24] Arneodo A., Coullet P. and Tresser C., Occurence of strange attractors in three-dimensional Volterra equations, *Physics Letters A*, 79(4), 259-263, 1980.

[25] Lorenz E. N., Deterministic nonperiodic flow, *Journal of Atmospheric Sciences*, 20(2), 130-141, 1963.

[26] Thompson J. M. T. and Stewart H. B., Nonlinear Dynamics and Chaos, *2nd ed., John Wiley & Sons, Chichester*, 2002.

[27] Sparrow C., The Lorenz equations: Bifurcations, chaos and strange attractors, *Applied Mathematical Sciences, Springer-Verlag*, Vol. 41, 1982.

[28] Arneodo A., Coullet P., Peyraud J. and Tresser C., Strange attractors in volterra equations for species in competition, *Journal of Mathematical Biology*, 14(2), 153-157, 1982.

[29] Wang R. and Xiao D., Bifurcations and chaotic dynamics in a 4-dimensional competitive LotkaVolterra system, *Nonlinear Dynamics*, 59(3), 411-422, 2010.

[30] Huang G. Q., Analysis of new four-dimensional chaotic circuits with experimental and numerical methods, *International Journal of Bifurcation and Chaos*, 22(2), 2012.

[31] Kita T., Chaos in a four-dimensional system consisting of fundamental lag elements and the relation to the system eigenvalues, *Chaos, Solitions and Fractals*, 23(4), 1413-1428, 2005.

[32] Parker T. S. and Chua L. O., Practical numerical algorithms for chaotic systems, *Springer Verlag New York Inc.*, 1989.

[33] Tsumoto K., Ueta T., Yoshinaga T. and Kawakami H., Bifurcation analyses of nonlinear dynamical systems: From theory to numerical computations, *Nonlinear theory and its applications IEICE*, 3(4), 458-476, 2012.

[34] Sandri M., Numerical Calculation of Lyapunov Exponents, *The Mathematica Journal, Miller Freeman Publications*, 1996.

[35] Nayfeh A. H., Introduction to Perturbation Techniques, *John Wiley and Sons Inc.*, 1993.

[36] Kevorkian J. and Cole J. D., Multiple scale and singular perturbation methods, *Applied Mathematical Sciences, Springer-Verlag*, Vol. 114, 1996.

[37] Nayfeh A. H. and Balachandran B., Applied Nonlinear Dynamics: Analytical, Computational and Experimental Methods, *Wiley-VCH Verlag GmbH and Co. KGaA*, 2004.

[38] Nayfeh A. H. and Mook D. T., Nonlinear Oscillations, *John Wiley and Sons, Inc.*, 1979.

[39] Cartmell M. P., Ziegler S. W., Khanin R. and Forehand D. I. M., Multiple scales analysis of the dynamics of weakly nonlinear dynamical systems, *Applied Mechanics Reviews*, 56(5), 455-492, 2003.

[40] El-Bassiouny A. F., Response of a three-degree-of-freedom system with cubic nonlinearities to harmonic excitation, *Applied Mathematics and Computation*, 104, 65-84, 1999.

[41] Cao D. X. and Zhang W., Global bifurcations and chaotic dynamics for a string-beam coupled system, *Chaos, Solitons and Fractals*, 37(3), 858-875, 2006.

[42] Jinchen J. and Yushu C., Bifurcation in a parametrically excited two degree of freedom nonlinear oscillating system with 1:2 internal resonance, *Applied Mathematics and Mechanics*, 20(4), 350-359, 1999.

[43] Nayfeh A. H., Chin C. M. and Pratt J., Perturbation methods in nonlinear dynamics-applications to machining dynamics, *ASME Journal of Manufacturing Science and Engineering*, 119(4A), 485-493, 1997.

[44] Ganesan R., Effects of bearing and shaft asymmetries on the instability of rotors operating at near critical speeds, *Mechanism and Machine Theory*, 35, 737-752, 2000.

[45] Ji Z. and Zu J. W., Method of multiple scales for vibration analysis of rotor shaft systems with nonlinear pedestal model, *Journal of Sound and Vibration*, 218(2), 293-305, 1998.

[46] Hu H. Y. and Wang Z. H., Singular perturbation methods for nonlinear dynamic systems with time delay, *Chaos, Solitons and Fractals*, 40, 13-27, 2009.

[47] Das S. L. and Chatterjee A., Multiple scales without center manifold reductions for delay differential equations near Hopf bifurcations, *Nonlinear Dynamics*, 30, 323-335, 2002.

[48] Das S. L. and Chatterjee A., Multiple scales via Galerkin projections: Approximate asymptotics for strongly nonlinear oscillations, *Nonlinear Dynamics*, 32, 161-186, 2003.

[49] Chatterjee A. and Chatterjee D., Analytical investigation of hydrodynamics cavitation control by ultrasonics, *Nonlinear Dynamics*, 46, 179-194, 2006.

[50] Rossikhin, Yu A. and Shitikova M. V., Application of fractional calculus for analysis of nonlinear damped vibrations of suspension bridges, *Jounral of Engineering Mechanics*, 124(9), 1029-1036, 1998.

[51] Balachandran B. and Nayfeh A. H., Cyclic motions near a Hopf bifurcation of a four-dimensional system, *Nonlinear Dynamics*, 3(1), 19-39, 1992.

[52] Wahi P. and Kumawat V., Nonlinear stability analysis of a reduced order model of nuclear reactors: A parametric study relevant to the advanced heavy water reactor, *Nuclear Engineering and Design*, 241, 134-143, 2011.

[53] Ghosal A., Robotics, Fundamental Concepts and Analysis, *Oxford University Press*, 2006.

[54] Asada H., Slotine J. J. E., Robot Analysis and Control, *John Wiley and Sons*, 1986.

[55] Lankalapalli S. and Ghosal A., Chaos in robot control equations, *International Journal of Bifurcation and chaos*, 7(3), 707-720, 1997.

[56] Ravishankar A. S. and Ghosal A., Nonlinear dynamics and chaotic motions in feedback controlled two and three-degree-of-freedom robots, *International Journal of Robotics Research*, 18(1), 93-108, 1999.

[57] H. S. Wall, 1945, "Polynomials whose zeros have negative real parts", *The American Mathematical Monthly*, 52(6), pp. 308-322.

[58] Gupta P. D., Majee N. C. and Roy A. B., Asymptotic stability, orbital stability of Hopf-bifurcating periodic solution of a simple three-neuron artificial neural network with distributed delay, *Nonlinear Analysis: Modeling and Control*, 13(1), 9-30, 2008.

[59] Przemieniecki J. S., Theory of Matrix Structural Analysis, *Mcgraw Hill Book Co.*, 1968.

[60] Chandra Shaker M. and Ghosal, A., Nonlinear modeling of flexible link manipulators using non-dimensional variables, *Trans. ASME, Journal of Computational and Nonlinear Dynamics*, 1(2), 123-134, 2006.

[61] Ott E., Grebogi C. and Yorke, J. A., Controlling chaos, *Physical Review Letters*, 64(11), 1196-1199, 1990.

[62] Francisco Heitor Pereira-Pinto I., Armando Ferreira M. and Marcelo Savi A., Chaos control in a nonlinear pendulum using a semi-continuous method, *Chaos Solitions and Fractals*, 22, 653-668, 2004.

[63] Aline Souza de Paula and Marcelo Amorim Savi, Controlling chaos in a nonlinear pendulum using an extended time-delayed feedback control method, *Chaos, Solitons and Fractals*, 42, 2981-2988, 2009.

[64] Zareiyan Jahromi S. A., Haji A. H. and Mahzoon M., Non-Linear dynamics and chaos control of a physical pendulum with rotating mass, *13th Annual (International) Mechanical Engineering Conference, Isfahan University of Technology, Isfahan, Iran*, 2005.

[65] John Starett and Randall Tagg, Control of a chaotic parametrically driven pendulum, *Physical Review Letters*, 74(11), 1974-1977, 1995.

[66] Pyragas K., Control of chaos via an unstable delayed feedback controller, *Physical Review Letters*, 86(11), 2265-2268, 2001.

[67] Alexander Fradkov L. and Robin Evans J., Control of chaos: Methods and applications in engineering, *Annual Reviews in Control*, 29, 33-56, 2005.

[68] Ruiqi W. and Zhujun J., Chaos control of chaotic pendulum system, *Chaos, Solitons and Fractals*, 21, 201-207, 2004.

[69] Pecora L. M. and Carroll T. L., Synchronization in chaotic systems, *Physical Review Letters*, 64, 821-824, 1990.

[70] Pecora L. M. and Carroll T. L., Synchronizing chaotic circuits, *IEEE Trans. Circuits and Systems*, 38, 453-356, 1991.

[71] Wu X and Lu J., Parameter identification and backstepping control of uncertain Lu system, *Chaos, Solitons and Fractals*, 18, 721-729, 2003.

[72] Yu Y. G., and Zhang S. C., Adaptive backstepping synchronization of uncertain chaotic systems, *Chaos, Solitons and Fractals*, 27, 1369-1375, 2006.

[73] Yau H. T., Design of adaptive sliding mode controller for chaos synchronization with uncertainties, *Chaos, Solitons and Fractals*, 22, 341-347, 2004.

[74] Slotine J.J.E. and Li W., Applied Nonlinear Control, *Prentice Hall Inc., New Jersey*, 1991.

[75] Antonio L., Erjen L. and Henk N., Global asymptotic stability of robot manipulators with linear PID and PI2D control, *SACTA*, 3(2), 138-149, 2000.

[76] Rafael K., A tuning procedure for stable PID control of robot manipulators, *Robotica*, 13(2), 141-148, 1995.

[77] Jose A. H. and Wen Y., A high observer-based PD control for Robot Manipulator, *Proceedings of the American Control Conference, Chicago, Illinois*, 2000.

[78] Ge S. S., Lee T. H. and Zu G., Non-model-based position control of a planar multi-link flexible robot, *Mechanical Systems and Signal Processing*, 11(5), 707-724, 1997.

[79] Amol A.K., Gopinathan L. and Goshaidas R., An adaptive fuzzy controller for trajectory tracking of a robot manipulator, *Intelligent Control and Automation*, 2, 364-370, 2011.

[80] Antonio Y., Victor S. and Javier M. V., Global asymptotic stability of the classical PID controller by considering saturation effects in industrial robots, *International Journal of Advanced Robotic Systems*, 8(4), 34-42, 2011.

[81] Vincente P. G., Suguru A., Yun H.L., Gerhard H., Prasad A., Dynamic sliding PID control for tracking of robot manipulators: Theory and experiments, *IEEE Transaction on Robotics and Automation*, 19(6), 967-976, 2003.

[82] Ruvinda G. and Fathi G., PD Control of closed-chain mechanical systems: An experimental study, *Proc. of the Fifth IFAC Symposium of Robot Control, France*, 1, 79-84, 1997.

[83] Chien H. L., Lyapunov based control of a robot and mass spring system undergoing an impact collision, *Master of Science Thesis*, University of Florida, 2007.

[84] Khalil K. H., 1996, *Nonlinear Systems*, Upper Saddle River, NJ: Prentice Hall, pp. 191-196.

[85] Li K. F., Li L. and Chen Y., Chaotic motion phenomenon in planar 2R robot, *Mechanical Science and Technology*, 29(l), 6-8, 2002.

[86] Yu P. and Bi Q., Analysis of nonlinear dynamics and bifurcations of a double pendulum, *Journal of Sound and Vibration*, 217(4), 691-736, 1988.

[87] Burov, A. A., On the non-existence of a supplementary integral in the problem of a heavy two-link plane pendulum, *Prikl. Matem. Mekhan, USSR*, 50(1), 123-125, 1986.

[88] Lankalapalli S. and Ghosal A., Possible chaotic motion in a feedback controlled 2R robot, In *Proceedings of the 1996 IEEE International Conference on Robotics and Automation, Minneapolis, MN, April, N. Caplan and T. J. Tarn (eds.)*, 1241-1246. IEEE Press, New York, 1996.

[89] Nakamura Y., Suzuki T. and Koinuma M., Nonlinear behavior and control of a non-holonomic free-joint manipulator, *IEEE Transactions on Robotics and Automation*, 13(6), 853-862, 1997.

[90] Mahout V., Lopez P., Carcasss J. P. and Mira C., Complex behaviours of a two-revolute joints robot: Harmonic, subharmonic, higher harmonic, fractional harmonic, chaotic responses, In *Proceedings of the IEEE Systems, Man & Cybernetics '93 Conference, Le Touquet, France*, October 17-20, 201-205, 1993.

[91] Verduzco F. and Alvarez J., Bifurcation analysis of a 2-DOF robot manipulator driven by constant torques, *International Journal of Bifurcation and Chaos*, 9(4), 617-627, 1999.

[92] Yin Z. and Ge X., Chaotic self-motion of a spatial redundant robotic manipulator, *Research Journal of Applied Sciences, Engineering and Technology*, 3(9), 993-999, 2011.

[93] Paden B. and Panja R., Globally asymptotically stable 'PD+' controller for robot manipulators, *International Journal of Control*, 47(6), 1697-1712, 1988.

[94] LaSalle J. and Lefschetz S., Stability by Liapunov's Direct Method with Applications, *Academic Press*, 1961.

[95] M. G. O. Arthur, 1999, *Design and Analysis of Control Systems*, Boca Raton, Florida, USA: CRC Press LLC, pp. 323-332.

[96] Hastings G. and Book W. J., Linear dynamic model for flexible link manipulator, *IEEE Control System Magazine*, 7(1), 61-64, 1987.

[97] Trucic D. A. and Midha A., Generalized equations of motion for dynamic analysis of elastic mechanism, *ASME Journal of Dynamic Systems, Measurement and Control*, 106, 243-248, 1984.

[98] Theodore R. J. and Ghosal A., Comparison of assumed mode and finite element methods for flexible multi-link manipulators, *International Journal of Robotics Research*, 14(2), 91-111, 1995.

[99] Damaren C. and Sharf L., Simulation of flexible-link manipulators with inertia and geometric nonlinearities, *ASME J of Dynamic, Systems, Measurement and Control*, 117, 74-87, 1995.

[100] Simo J. C. and Vu-Quoc L., The role of nonlinear theories in transient dynamic analysis of flexible structures, *Journal of Sound and Vibration*, 119(3), 487-508, 1987.

[101] Li Q., Wang T. and Ma X., Geometric nonlinear effects on the planar dynamics of a pivoted flexible beam encountering a point-surface impact, *Multibody System Dynamics*, 21(3), 249-260, 2009.

[102] Chen Z. Q. and Agar T. J. A., Geometric nonlinear analysis of flexible spatial beam structures, *Computers and structures*, 49(6), 1083-1094, 1993.

[103] Yang X. D. and Chen L. Q., Bifurcation and chaos of an axially accelerating viscoelastic beam, *Chaos, Solitons and Fractals*, 23, 249-258, 2005.

[104] Awrejcewicz J., Krysko A. V., Bochkarev V. V., Babenkova T. V., Papkova I. V. and Mrozowski J., Chaotic vibrations of two-layered beams and plates with geometric physical and design nonlinearities, *Multibody System Dynamics*, 21(3), 249-260, 2009.

[105] Xiang J., Yan Y. and Li D., Recent advance in nonlinear aeroelastic analysis and control of the aircraft, *Chinese Journal of Aeronautics*, 27(1), 12-22, 2014.

[106] Endurance Wind Power Ltd., http://www.endurancewindpower.com/e3120.html (last accessed August 17, 2015)

[107] Morozov D. A., 1998, *Quasi-Conservative Systems: Cycles, Resonances and Chaos*, Farrer Road, Singapore 912805: World Scientific Publishing Co. Pte. Ltd., pp. 69-93.

[108] Lakshmanan M., Rajasekar S., 2003, *Nonlinear Dynamics: Integrability, Chaos and Patterns*, Heidelberg, Berlin: Springer-Verlag, pp. 191-228.

[109] Sundarapandian V., Global chaos synchronisation of identical Li-Wu chaotic systems via sliding mode control, *International Journal of Modelling, Identification and Control*, 22(2), 170-177, 2014.

[110] Sundarapandian V., Sivaperumal S. and Ahmad T. A., Global chaos synchronisation of identical chaotic systems via novel sliding mode control method and its application to Zhu system, *International Journal of Modelling, Identification and Control*, 23(1), 92-100, 2015.

[111] Handa H. and Sharma B. B., Simple synchronisation scheme of chaotic Chua's systems with cubic nonlinearity in complex coupled networks, *International Journal of Applied Nonlinear Science*, 1(4), 300-311, 2014.

[112] Saha P., Ghosh D. and Chowdhury A. R., Modified projective synchronisation of different order chaotic systems with adaptive scaling factor, *International Journal of Applied Nonlinear Science*, 1(3), 230-246, 2014.

[113] Michael B. Monagan, Keith O. Geddes, K. Michael Heal, George Labahn, Stefan M. Vorkoetter, James McCarron and Paul DeMarco., *Maple 14 Programming Guide*, Maplesoft, Waterloo ON, Canada, 2012.

[114] Wu X., Chen G. and Cai J., Chaos synchronization of the masterslave generalized Lorenz systems via linear state error feedback control, *Physica D:Nonlinear Phenomena*, 229(1), 52-80, 2007.

Publications from this thesis

[1] B. Sandeep Reddy, A. Ghosal, Nonlinear Dynamics of a Rotating Flexible Link, *ASME Journal of Computational and Nonlinear Dynamics*, 10(6), 061014, 2015. DOI: 10.1115/1.4028929.

[2] B. Sandeep Reddy, A. Ghosal, Asymptotic stability and chaotic motions in trajectory following feedback controlled robots, *ASME Journal of Computational and Nonlinear Dynamics*, Accepted for Publication, 2015. DOI: 10.1115/1.4032389.

[3] B. Sandeep Reddy, A. Ghosal, Chaotic motion in a flexible rotating beam and synchronization, *International Journal of Applied Nonlinear Science* - Under Review.